A Reproduced Copy

OF

_____

Reproduced for NASA

by the

NASA Scientific and Technical Information Facility
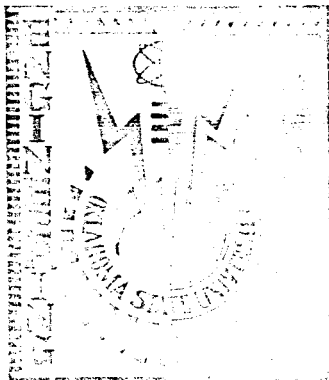
Fluid Power Controls Laboratory
School of Mechanical Engineering
OKLAHOMA STATE UNIVERSITY
Stillwater, Oklahoma

INTERIM REPORT NO. 66-7

STUDY OF FLUID TRANSIENTS IN
CLOSED CONDUITS

Contract: NAS 8 11302

Contractor: Oklahoma State University, Stillwater, Oklahoma

Segment Generating Report: School of Mechanical Engineering
Fluid Power and Controls Laboratory

STUDY OF FLUID TRANSIENTS IN CLOSED CONDUITS

CONTRACT: NAS 8-11302

CONTROL NUMBER: DCN-1-4-50-01153-01(IF)
CPB 02-1209-64

Date:

Prepared for: George C. Marshall Space Flight Center, Huntsville,
Alabama

Prepared by: Hudy C. Hewitt

Approved:

J. D. Parker, Project Director

TABLE OF CONTENTS

APPENDICES

LIST OF TABLES

LIST OF FIGURES

CHAPTER I

INTRODUCTION

The first problem in bubble dynamics was proposed by Besant in 1859. In 1917, Rayleigh gave the first solution to a bubble dynamics problem for one set of boundary conditions. After World War II, interest in boiling heat transfer, cavitation, and fluid pumping directed the attention of many scientific minds to the field of bubble dynamics. This concentrated interest resulted in the development of the theoretical equations governing the bubble dynamics problem.

The theoretical knowledge in the area of bubble dynamics has been experimentally tested only for non-cryogens. The purpose of the present investigation is to extend the knowledge of bubble dynamics into the field of cryogens. To make use of the theoretical work done for non-cryogens, experimental evidence must be available to demonstrate that this theoretical work is valid for cryogens.

Photographic records of vapor bubbles in superheated liquid nitrogen were obtained experimentally in this investigation. The dynamic behavior of these vapor bubbles was measured and compared to the behavior predicted theoretically for non-cryogens. Several investigators have verified this theoretical solution for non-cryogens.

There are two mechanisms causing bubble collapse. One mechanism, inertia controlled, results from the inertia forces of the liquid. The other mechanism, heat transfer controlled, results from the reduction

1

of the vapor pressure inside the vapor bubble due to the reduction of the temperature of the bubble wall by heat transfer to the liquid. Experimental measurements of heat transfer controlled bubble collapse in liquid nitrogen were made in this investigation. The theoretical solutions of the bubble dynamics equations governing heat transfer controlled collapse are presented and possible modifications of these solutions are suggested. The experimental data of this investigation were used to demonstrate that the theoretical equations have not been adequately resolved. A previous experimental investigation of heat transfer controlled collapse, using water and alcohol at zero gravity, aided in this demonstration (1)[1]. A comparison of the data for water and liquid nitrogen is presented.

The equations governing bubble growth with transient liquid pressure were developed and the solution for the case where the change in bubble wall temperature can be neglected is presented. This solution is the solution for inertia controlled collapse or growth. Three nitrogen vapor bubbles were measured for measured liquid pressure variation. These measurements are compared to the theoretical solution for inertia controlled growth and to the theoretical solution for bubble growth in a superheated liquid.

A limited amount of data on the persistence time of vapor bubbles is presented. In this thesis, persistence time is defined as that time, after the apparent bubble collapse, that a bubble has the potential to reappear or rebound. This investigation provided experimental evidence of the persistence time of vapor bubbles in liquid nitrogen

---

[1]Numbers in parentheses indicate references in the Bibliography.

subcooled less than four degrees Rankine. The only other experimental evidence of persistence time is for steam bubbles collapsing by an inertia controlled process (2).

In addition to demonstrating that theories of bubble dynamics may be applied to cryogens, this investigation provided experimental data in three areas where data are lacking: (1) temperature controlled collapse, (2) bubble growth with transient pressure, and (3) the persistence time of vapor bubbles. This data should be valuable in the extension of the theories of bubble dynamics. Several theoretical and experimental studies are recommended to continue the growth of knowledge in the field of bubble dynamics.

CHAPTER II

REVIEW OF PREVIOUS INVESTIGATIONS

The dynamic problem associated with the appearance of a vapor bubble in a liquid was first proposed by Besant (3) in the form:

$$R\ddot{R} + 1.5\dot{R}^2 = -\frac{P_{\infty L}}{\rho_L} \qquad (\text{II-1})$$

where

R = bubble radius

$P_{\infty L}$ = pressure in the liquid away from bubble

ρ_L = liquid density

and dots represent differentiation with respect to time.

Lord Rayleigh (4) gave a solution to Equation (II-1) for the time required for a bubble to collapse. More recently, the equation has been modified to account for the effects of viscosity, surface tension, and vapor pressure inside the bubble. The modified equation was developed from the continuity equation and the equation of motion by Zwick (5). This development is presented in Appendix A along with order of magnitude considerations for liquid nitrogen. The modified Besant-Rayleigh equation is:

$$R\ddot{R} + 1.5\dot{R}^2 + 4\mu\frac{\dot{R}}{R} = \frac{P_v - P_{\infty L}}{\rho_L} - \frac{2\sigma}{R\rho_L} \qquad (\text{II-2})$$

where

μ = viscosity of the liquid (dynamic viscosity)

σ = surface tension

and P_v = vapor pressure inside the bubble.

Equation (II-2) governs both bubble collapse and growth. The boundary conditions for bubble growth result in one type of solution while the boundary conditions for collapse result in another. Therefore, the problem is divided into the classes of bubble growth and bubble collapse.

Bubble Collapse

The theoretical solution for the dynamic behavior of a collapsing bubble has been the subject of many investigations beginning when Lord Rayleigh (4) first gave a solution to Equation (II-1) for the case where $P_{\infty L}$ is a constant. If the viscosity and surface tension terms are neglected in Equation (II-2), it reduces to

$$R\ddot{R} + 1.5\dot{R}^2 = \frac{P_v - P_{\infty L}}{\rho_L}. \qquad (II-3)$$

Rayleigh solved Equation (II-3) for the case where $P_v - P_{\infty L}$ was assumed to be constant. This assumption physically represents inertia controlled collapse. Fritz (6) and McNieto and Smith (7) presented tabular results for the problem considered by Rayleigh.

Plesset and Zwick (8) and (9) recognized that any change in the size of a vapor bubble was accompanied by a change in the liquid temperature in a thin shell around the bubble because of the latent heat of vaporization or condensation requirement. They solved the non-steady heat diffusion problem with moving spherical boundary to obtain the

temperature distribution around the vapor bubble. Their solution for the temperature is

$$T(t) - T_o = \frac{\alpha}{k} \eta(t) - (\frac{\alpha}{\pi})^{\frac{1}{2}} \int_0^t \frac{R^2(x)(\frac{\partial T}{\partial r})_{r=R(x)} dx}{\{\int_x^t R^4(Y)dy\}^{\frac{1}{2}}} \qquad (II-4)$$

where

$T(t)$ = temperature at the bubble wall

T_o = initial temperature of the liquid

x and y = variables of integration

$R(x)$ = bubble wall radius dependent on the integration variable, x

$R(y)$ = bubble wall radius dependent on the integration variable, y

α = thermal diffusivity

k = thermal conductivity

$\eta(t)$ = heat source per unit volume (by radiation)

r = spherical coordinate

and t = time.

This particular solution is valid for the assumptions:

1. The temperature change in the liquid effectively takes place in an infinitely thin boundary layer around the bubble. The first order approximation given here satisfies this assumption.

2. The bubble is stationary with respect to the liquid.

Plesset and Zwick assumed that thermal equilibrium existed inside the vapor bubble. They neglected the motion of the vapor and assumed

that the vapor pressure, P_v, was equal to the equilibrium vapor pressure of the liquid at the temperature of the bubble wall. Equations (II-3) and (II-4) must be solved simultaneously for the collapse of the vapor bubble.

Plesset and Zwick solved these equations numerically for one set of liquid conditions and found that the solution was almost identical to the Rayleigh solution. This should have been expected since the case they chose was for a vapor bubble in water subcooled by 110°R. Inertia controlled collapse is dominant for water subcooled greater than approximately 40°R because the collapse occurs so rapidly that the effect of temperature change is negligible (1). Therefore, the collapse was completely dominated by liquid inertia effects.

Florschuetz and Chao (1) investigated Equations (II-3) and (II-4) to theoretically determine the effect of various fluid conditions on bubble collapse. Their investigation provided information on bubble collapse controlled by heat transfer, bubble collapse controlled by liquid inertia, and bubble collapse where both effects must be considered. Their theoretical solutions predicted that when both liquid inertia and heat transfer must be considered, the resultant bubble motion may be oscillatory. The reason for this was that the energy of condensation increased the temperature of the liquid around the bubble which increased the vapor pressure. The liquid inertia caused compression of the vapor bubble until the pressure inside the bubble became large enough to cause bubble growth and resultant cooling of the liquid. The oscillatory vibration was dampened by the transfer of heat away from the bubble wall into the liquid by conduction and convection.

Hsieh (10) developed the bubble dynamics equations in their most

general form. He then pointed out how Equations (II-3) and (II-4) could be derived from his equations by making various assumptions.

Experimental verification of the validity of Equations (II-3) and (II-4) has been provided by a number of authors. Table I is a summary of the experimental work.

TABLE I

SUMMARY OF BUBBLE COLLAPSE

Reference	Fluid	Radius Range inches	Liquid Pressure	Collapse Type	Subcooling
Knapp and Hollander (2)	water	0.01-0.14	variable	inertia	--
Plesset (11)	water	0.005-0.14	variable	inertia	--
Ellion (12)	water	0.004-0.02	const.	inertia	35-134°F
Gunther (13)	water	0.005-0.03	const.	inertia	60-130°F
Levenspiel (14)	water alcohol	0.02-0.2	const.	inertia heat transfer	1-20°C
Florschuetz and Chao (1)	water	0.01-0.14	const.	inertia heat transfer	5.2-13°C

Plesset (11) and Knapp and Hollander (2) solved Equation (II-3) numerically, predicting the growth and collapse of vapor bubbles formed

in water by the cavitation phenomenon. Various experimental obstacles were placed in a flowing water stream. $P_{\infty L}$ for Equation (II-3) was determined from Bernoulli's equation by the water velocity and the type of obstacle placed in the stream. The theoretical solution for both growth and collapse was obtained by neglecting the effect of the changing temperature of the bubble wall. Therefore, the collapse was inertia controlled. The theoretical solutions gave adequate predictions of the experimental behavior.

Ellion (12) and Gunther (13) generated vapor bubbles by superheating water. They observed inertia controlled collapse after the bubble moved away from the heating surface.

Levenspiel (14) generated bubbles by forcing water vapor into a container of water. Bubble collapse was controlled by both inertia and heat transfer.

Florschuetz and Chao (1) provided some experimental results for bubble collapse controlled primarily by heat transfer.

Bubble Growth

Plesset and Zwick (8) (9) demonstrated that Equations (II-3) and (II-4) were also valid for bubble growth.

Forster (15) solved the heat diffusion problem to obtain a solution very similar to that of Plesset and Zwick. From his analysis,

$$T(t) - T_o = \frac{L \rho_v}{c_L \rho_l (\pi \alpha)^{\frac{1}{2}}} \int_0^t \frac{R(x) \dot{R}(x) \, dx}{R(t) \, (t-x)^{\frac{1}{2}}} \qquad (II-5)$$

where

L = heat of vaporation

c_L = specific heat of the liquid

and ρ_V = density of the vapor.

Forster and Zuber (16) solved Equations (II-3) and (II-5) for bubble growth in a superheated liquid. Their solution for asymptotic bubble growth (bubble growth after R = 0.0015 cm) is

$$R = \frac{\sqrt{\pi} \; \rho_L}{\rho_V} \; \frac{c_L \, \Delta T}{L} \; (\alpha \, t)^{\frac{1}{2}} \qquad (II\text{-}6)$$

where

$$\Delta T = T_\infty - T_{sat}$$

and

$$T_{sat} = \text{saturation temperature at } P_{\infty L}.$$

Plesset and Zwick (9) obtained

$$R = \left(\frac{12}{\pi}\right)^{\frac{1}{2}} \; \frac{\rho_L \; c_L \Delta T}{\rho_V \; L} \; (\alpha \, t)^{\frac{1}{2}}. \qquad (II\text{-}7)$$

Scriven (17), Birkhoff and Horning (18), and Dergarabedian (19) all obtained an equation of the type:

$$R = A(\alpha \, t)^{\frac{1}{2}} \qquad (II\text{-}8)$$

where

A = a constant for a given fluid condition.

Experimental verification for the theoretical bubble growth equation has been provided by several authors. Table II is a summary of the previous work.

TABLE II

SUMMARY OF BUBBLE GROWTH

Reference	Fluid	Radius Range inches	Superheating
Dergarabedian (19) (20)	water carbon tetrachloride benzene ethyl alcohol methyl alcohol	0.001-0.01	1.4-6.3°C
Fareuff McLean and Scherrer (21)	water	0.001-0.01	Selected to fit theory
Semeria (22)	water	0.002-0.05	--
Staniszewski (23)	water ethanol	0.002-0.06	--

Dergarabedian (19) (20), Faneuff, McLean, and Scherrer (21), and Semeria (22) all obtained experimental results indicating that the theoretical solution, $R = A(\alpha t)^{\frac{1}{2}}$, was valid. However, in all experimental work, it is necessary to shift the time axis since the actual time the bubble started to grow is unknown for two reasons: (1) bubbles smaller than 0.001 inches are almost impossible to photograph, (2) the shutter speed of the camera, used in obtaining experimental results, must operate at a finite rate and there is an uncertainty of when the bubble was first observable. Therefore, an exact experimental determination of the constant of proportionality has not yet been completed. Experimental error and the uncertainty of the time when the bubble is

first observable allow the value of A from Equation (II-8) to be determined in such a way that all authors claim agreement between theory and experiment within ten percent.

The experimental work of Staniszwski (23) did not fit the theoretical solution. However, his bubbles were observed while near a heater unit, and Zuber (24) pointed out that a modified equation must be used for this type of experimental data. The temperature of the liquid around the bubbles was higher due to the heating surface.

CHAPTER III

‑ ANALYTICAL APPROACH

The equations governing vapor bubble dynamics were discussed in
Chapter II and are developed in Appendix A. The following assumptions
were made in the development:

1. external body forces neglected

2. constant viscosity

3. irrotational flow

4. incompressible liquid

5. viscous heating neglected

6. liquid velocity at the wall equals bubble wall velocity

7. constant fluid density

8. spherical bubbles

9. Newtonian fluid

10. vapor inertia neglected

11. constant thermal properties

12. uniform temperature in the liquid

13. vapor velocity neglected in comparison to bubble wall velocity

14. surface tension neglected

15. infinite liquid.

The continuity equation, the equation of motion, and the energy equa-
tion were combined and simplified, by the above assumptions, to the
forms:

$$R\ddot{R} + 1.5\dot{R}^2 = \frac{P_v(T_w) - P_{\infty L}(t)}{\rho_L} \qquad \text{(III-1)}$$

and

$$\rho_L c_L\left[\frac{\partial T}{\partial t} + \vec{V}\cdot\nabla T\right] = k\nabla^2 T + \dot{q} \qquad \text{(III-2)}$$

where

$P_v(T_w)$ = the saturation pressure at the bubble wall temperature

$\vec{V}$ = liquid velocity

T = liquid temperature

and

$\dot{q}$ = heat generation rate per unit volume.

The boundary conditions for these equations are:

$$R(t = 0) = R_o, \quad \dot{R}(t = 0) = \dot{R}_o \qquad \text{(III-3)}$$

$$R^2 k \left.\frac{\partial T}{\partial r}\right|_{r=R} = \frac{L}{3}\frac{d(R^3\rho_V)}{dt} \qquad \text{(III-4)}$$

and

$$T(r, t = 0) = T_o. \qquad \text{(III-5)}$$

The vapor pressure, $P_v(T_w)$, of Equation (III-1) depends on the temperature of the bubble wall. The bubble wall temperature comes from the solution of Equation (III-2) with the boundary conditions given. This functional relationship between Equations (III-1) and (III-2) requires that they be solved simultaneously to give the solution to the bubble dynamics problem. Before exploring the possibilities of a simultaneous solution of these equations, it is desirable to solve Equations (III-2), (III-4) and (III-5) for the bubble wall temperature. Then, a

relationship between bubble wall temperature and vapor pressure can be used to reduce the two equations to one.

The solution of the energy equation, Equation (III-2), involves the solution of a heat transfer problem with moving boundaries. No solution in closed form has been obtained for the moving boundary condition. The most prominent approximation to a solution to Equation (III-2) was presented by Plesset and Zwick (9). The essential steps of this solution are presented in Appendix B. The result of this presentation for zero heat generation ($\dot{q} = 0$), neglecting the $\vec{V} \cdot \nabla T$ term, assuming a thin thermal boundary layer around the vapor, and using the boundary condition Equations (III-4) and (III-5), is

$$T(R, t) - T_0 = \frac{-L}{3k} \sqrt{\frac{\alpha}{\pi}} \int_0^t \frac{\frac{d}{dx}(R^3(x)\rho_V) \, dx}{\left\{ \int_x^t R^4(y) dy \right\}^{\frac{1}{2}}} . \qquad \text{(III-6)}$$

The solution of Equations (III-1) and (III-6) simultaneously has not been obtained for the general case. However, the bubble dynamic problem can be solved for four special cases: (1) bubble growth in a superheated liquid, (2) bubble collapse in a highly subcooled liquid, (3) bubble collapse in a slightly subcooled liquid, and (4) bubble growth and collapse under very fast transient pressures in the liquid. The bubble dynamic problem can be solved for bubble growth in a superheated liquid and bubble collapse in a slightly subcooled liquid because the inertia terms can be neglected and only the energy equation remains to be solved. For the other two cases, the effect of temperature can be neglected and only Equation (III-1) remains to be solved. These special cases will be considered in the following paragraphs. The development

of new theoretical solutions was not attempted. The experimental data of this investigation was taken for fluid conditions similar to the special cases.

Bubble Growth in a Superheated Liquid

When no variation in the external pressures occur, asymptotic bubble growth in a superheated liquid is controlled by the heat transfer rate at the bubble wall. Equation (III-1) shows that the potential for bubble growth results from the difference between the pressure inside the bubble and the external pressure of the liquid.

The pressure inside the vapor bubble is determined by the temperature at the bubble wall. This pressure is the saturation pressure at the temperature of the bubble wall. The maximum value of vapor pressure occurs when the bubble wall temperature reaches the liquid temperature, T_o. The bubble wall temperature at which no growth occurs is the saturation temperature, $T_{s\infty}$, associated with the liquid pressure away from the bubble, P_∞.

When the bubble wall temperature is greater than $T_{s\infty}$, the pressure inside the bubble is higher than the external pressure, and the bubble starts to grow. However, evaporation must occur at the bubble wall to provide growth, and the heat of evaporation results in the cooling of the liquid around the bubble to the limiting temperature, $T_{s\infty}$. The asymptotic growth is then controlled by the heat transfer rate to the bubble wall required to provide the heat of vaporization necessary for growth. The temperature solution of Equation (III-6) tends toward

$$T(R, t) - T_o = T_{s\infty} - T_o$$

for asymptotic growth.

The details of the solution of the governing equations are presented in Appendix C. The result of this solution is Equation (C-14),

$$R = \sqrt{\frac{12}{\pi}} \; \frac{k \Delta T}{L \, \rho_v \sqrt{\alpha}} \, (t)^{\frac{1}{2}} = \sqrt{\frac{12}{\pi}} \; \frac{\rho_L \, c_L \Delta T}{\rho_v \, L} \, (\alpha t)^{\frac{1}{2}}. \qquad (III\text{-}7)$$

Equation (III-7) results from the analysis of Plesset and Zwick (9). References (17), (18), and (19) all arrived at the conclusion that

$$R = A (\alpha t)^{\frac{1}{2}}. \qquad (III\text{-}8)$$

The results of Forster and Zuber (16), Equation (II-6), gave a coefficient of $t^{\frac{1}{2}}$ that varied from that of Equation (III-7) by nine percent. The other authors either used a coefficient already determined or left the coefficient in an indeterminant form. The value of the coefficient was determined by the assumptions made in the solution of the energy equation. A discussion of the experimental verification of the theoretically determined coefficient is presented in the results of this investigation.

Bubble Collapse in a Subcooled Liquid

Inertia controlled collapse and temperature controlled collapse are two special cases of bubble collapse that can be solved in an approximate form. In inertia controlled collapse, the initial value of $P_v(T_w) - P_\infty(t)$ of Equation (III-1) is so large that the liquid inertia completely dominates the collapse. The resultant increase in $P_v(T_w)$ with collapse never significantly affects the collapse rate, therefore,

the solution of Equation (III-6) simultaneously with Equation (III-1) is not necessary. The only equation to be solved for inertia controlled collapse is:

$$R \ddot{R} + 1.5 \dot{R}^2 = \frac{P_v(T_w) - P_\infty(t)}{\rho_L}$$

where $P_v(T_w) - P_\infty(t)$ is assumed to be a constant. This constant has been called ΔP in several references. When a change of variables, $\gamma = R/R_o$, is made in the above equation, the equation becomes:

$$\gamma \ddot{\gamma} + 1.5 \dot{\gamma}^2 = \frac{\Delta P}{\rho_L R_o^3} . \tag{III-9}$$

Equation (III-9) is the Rayleigh equation and the solution is easily obtained in the following manner:

$$\frac{1}{2\gamma^2 \dot{\gamma}} \frac{d}{dt} (\gamma^3 \dot{\gamma}^2) = \frac{\Delta P}{\rho_L R_o^3} . \tag{III-10}$$

For inertia controlled collapse, the right side of Equation (III-10) is a constant and one integration of the equation gives

$$\gamma^3 \dot{\gamma}^2 = \frac{2\Delta P}{3\rho_L R_o^2} (\gamma_o^3 - \gamma^3) .$$

Solving for $\dot{\gamma}$ and integrating again gives

$$t = R_o \sqrt{\frac{3 \rho_L}{2 \Delta P}} \int_\gamma^1 \frac{\gamma^{3/2} d\gamma}{\sqrt{1 - \gamma^3}} \tag{III-11}$$

This can be solved for a zero lower limit of integration by gamma

functions. No additional analytical work was done in the area of inertia controlled collapse because all of the experimental data of the present investigation was taken for fluid conditions where bubble collapse was controlled by the bubble wall temperature.

Temperature, or heat transfer, controlled collapse is defined to be collapse governed by Equations (III-1) and (III-6) where the inertia term, $R\ddot{R} + 1.5\dot{R}^2$, is assumed to be zero. If this assumption is applied to Equation (III-1),

$$P_V(T_w) = P_\infty(t). \qquad \text{(III-12)}$$

This requires that

$$T(R, t) = T_{s\infty}.$$

For this condition, Equation (III-6) becomes

$$T_{s\infty} - T_o = \frac{-L}{3k}\sqrt{\frac{\alpha}{\pi}} \int_0^t \frac{\frac{d}{dx}(R^3(x)\,\rho_V)}{\left\{\int_x^t R^4(y)\,dy\right\}^{\frac{1}{2}}}\, dx. \qquad \text{(III-13)}$$

The solution of Equation (III-13) is given in Appendix C. An indication of the fluid conditions under which Equations (III-1) and (III-6) must both be considered for the solution is also given in Appendix C.

The error introduced by neglecting the bubble motion with respect to the fluid is inherent in Equation (III-13) because it was developed by neglecting the effect of this term. A study of the effects of this error on bubble behavior predicted by the above analysis is presented in Chapter VI.

Bubble Dynamics With Transient Liquid Pressure

When a transient pressure occurs in the liquid, the term, $P_v(T_w) - P_\infty(t)$, becomes a variable forcing function in Equation (III-I). The transient pressure is represented by $P_\infty(t)$. If the transient pressure occurs rapidly enough, the heat transfer is small and the vapor pressure inside the bubble is approximately constant. However, when the transient pressure occurs slowly, the effect of a change in the vapor pressure must be considered. The frequency of the transient pressure determines the type of solution that must be made.

The numerical solution of Equation (III-1) presents no problems if the effect of vapor pressure and the corresponding Equation (III-6) may be neglected. A numerical solution using the Runge-Kutta technique is given in Appendix C. This solution was written for a particular transient pressure and neglects the effect of vapor pressure variation. The solution did not converge for increments in time greater than one microsecond.

When the vapor pressure must be considered, Equations (III-1) and (III-6) must be solved simultaneously. This solution may also be accomplished by numerical methods, but Equation (III-6) requires the storage of R and $\dot{R}$ for each step of the numerical process. The same time step was required for convergence and the solution was not included in the present investigation because of the computer time and storage requirement. An extension of the discussion of the problems associated with this solution is given in Chapter VI.

CHAPTER IV

EXPERIMENTAL APPARATUS

The goal of this experimental study was to obtain photographic records of the dynamic behavior of single vapor bubbles in liquid nitrogen under known, controlled conditions of liquid pressure and temperature. Figure 1 is a schematic drawing of the bubble observation chamber constructed to obtain the desired experimental conditions and instrumentation.

Outer Chamber

The outer vacuum jacket of Figure 1 was necessary to prevent frost formation on the liquid nitrogen container windows and to reduce the heat transfer rate to the liquid nitrogen. This vacuum jacket was constructed from fourteen inch diameter carbon steel pipe with welded steel flanges. The window for this chamber was made of one-half inch thick plexiglas. A Viton O-ring was used to seal the window to the steel flange. The force of the vacuum helped to secure the seal without the introduction of severe clamping stresses.

The pressure between the vacuum jacket and the inner chamber measured 10^{-3} mm mercury on a McLeod gauge. The vacuum system was leak checked using a leak detector model MD-140, made by the Vacuum Instruments Corporation. The vacuum pumping system consisted of an oil diffusion pump and a Sargent duo-seal vacuum pump. The pressure between

CHAMBER A

SOLENOID VALVE

VACUUM JACKET

PYREX GLASS
WITH INVAR
HOLDER

FASTAX
CAMERA

PLEXIGLAS
WINDOW

INNER CHAMBER

FILL LINE
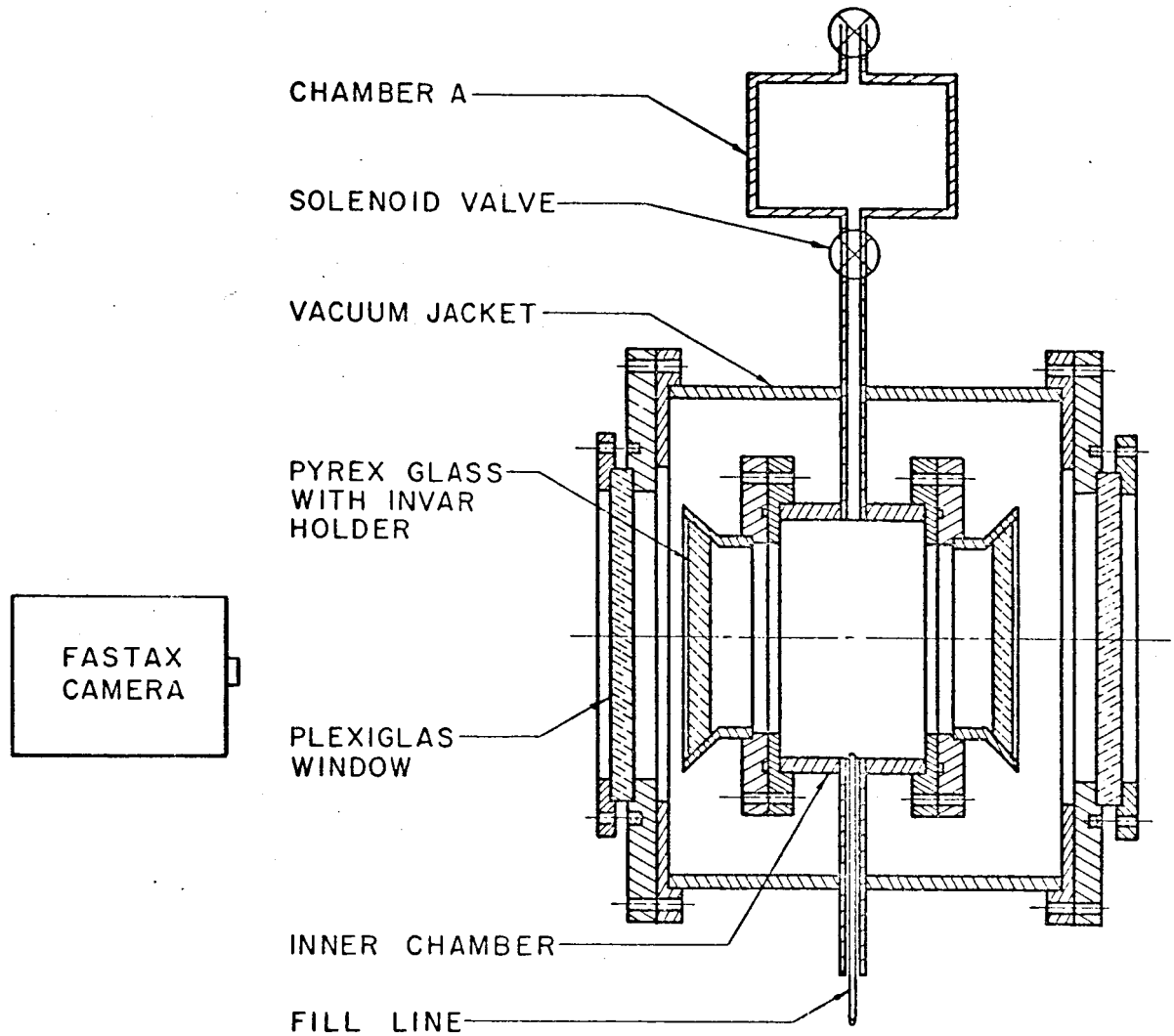
Figure 1. Schematic View of Bubble Observation Chamber

the chambers of 10^{-3} mm of mercury was adequate for the prevention of frost formation on the windows. According to Chelton and Mann (25, page 126) this pressure was not low enough to produce a significant reduction in the heat transfer rate to the liquid nitrogen. However, the duration of an experimental observation was less than five seconds and the heat transfer rate did not cause an observable change in the liquid conditions for this short time. This was checked using the thermocouple readings.

Liquid Nitrogen Container

The inner chamber contained the liquid nitrogen and had the connections necessary to measure the liquid conditions, to control the liquid conditions, and to generate vapor bubbles. It was constructed from six inch diameter stainless steel pipe with welded stainless steel flanges and fittings. All connections to the inner chamber were made of stainless steel to reduce the conduction heat transfer to the liquid nitrogen container by reducing the thermal conductivity. A cooling coil was placed around all connections to the inner chamber and liquid nitrogen was forced through this coil during experimental observations to reduce the conduction heat transfer down the connections by reducing the temperature gradient.

The windows on the inner chamber were made of five-eighths inch thick beveled pyrex glass. The thermal stresses due to the difference in the thermal expansion of pyrex glass and stainless steel required that the pyrex glass be first attached to a holder made of invar metal. The linear expansion of invar is approximately that of pyrex for the temperature range of this investigation. Therefore, the thermal

stresses in the glass were not excessive. The pyrex glass was glued to the invar holder with Armstrong epoxy A-6. The invar holder was then attached to a stainless steel flange with the same epoxy. These two windows were purchased from the CryoVac Company of Columbus, Ohio. A teflon coated metal O-ring was the seal between the stainless steel flange of the window and the flange of the inner chamber.

Figure 2 is a view of the inner chamber. Three of the five copper-constantan thermocouples can be seen in the chamber. Two additional thermocouples were located at the surface and inside the horizontal cylinder shown in this figure. The horizontal cylinder contained a 120 ohm, one-half watt electrical resistance. Armstrong A-6 epoxy was used to hold the resistor in place. Electrical leads connected to an external variable power supply allowed this resistor to be used as a variable electrical heater for the generation of vapor bubbles.

A second method of generating vapor bubbles was provided by the two vertical tubes located in the center at the bottom of the inner chamber. These tubes were connected to a high pressure gaseous nitrogen tank through a valve system including a solenoid valve. A microswitch controlled the solenoid valve allowing pulses of gaseous nitrogen to be forced into the inner chamber.

The third method of generating vapor bubbles was to evacuate chamber B of Figure 3 and open the solenoid valve connecting this chamber to the inner chamber. The connection is shown in schematic form in Figure 1. The pressure drop obtained by this method resulted in a superheated liquid which boiled readily. Chamber A of Figure 3 was used to provide transient increases in the pressure inside the inner chamber. The chamber was charged with pressure from the gaseous
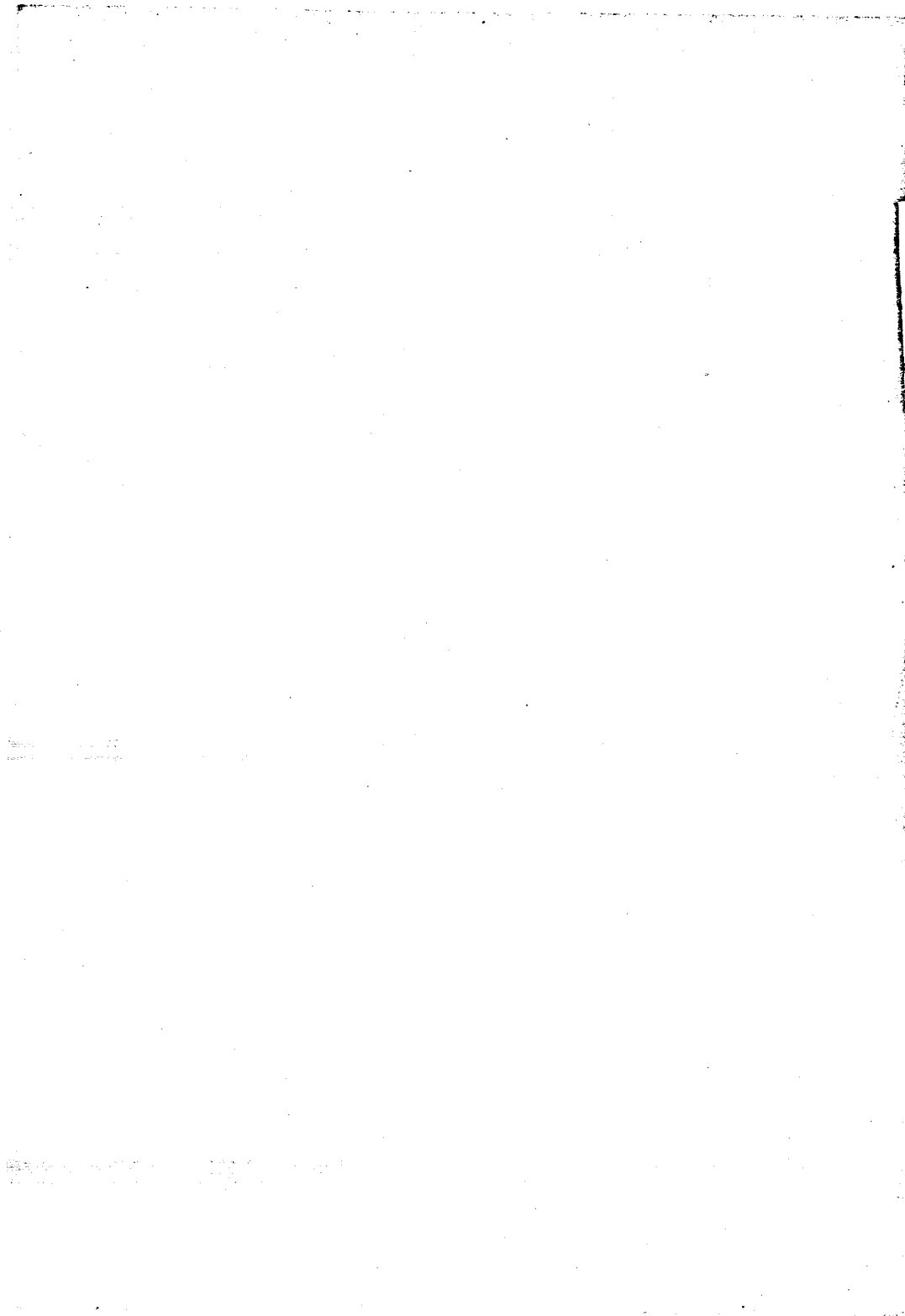
Figure 2. Inside View of Bubble Chamber
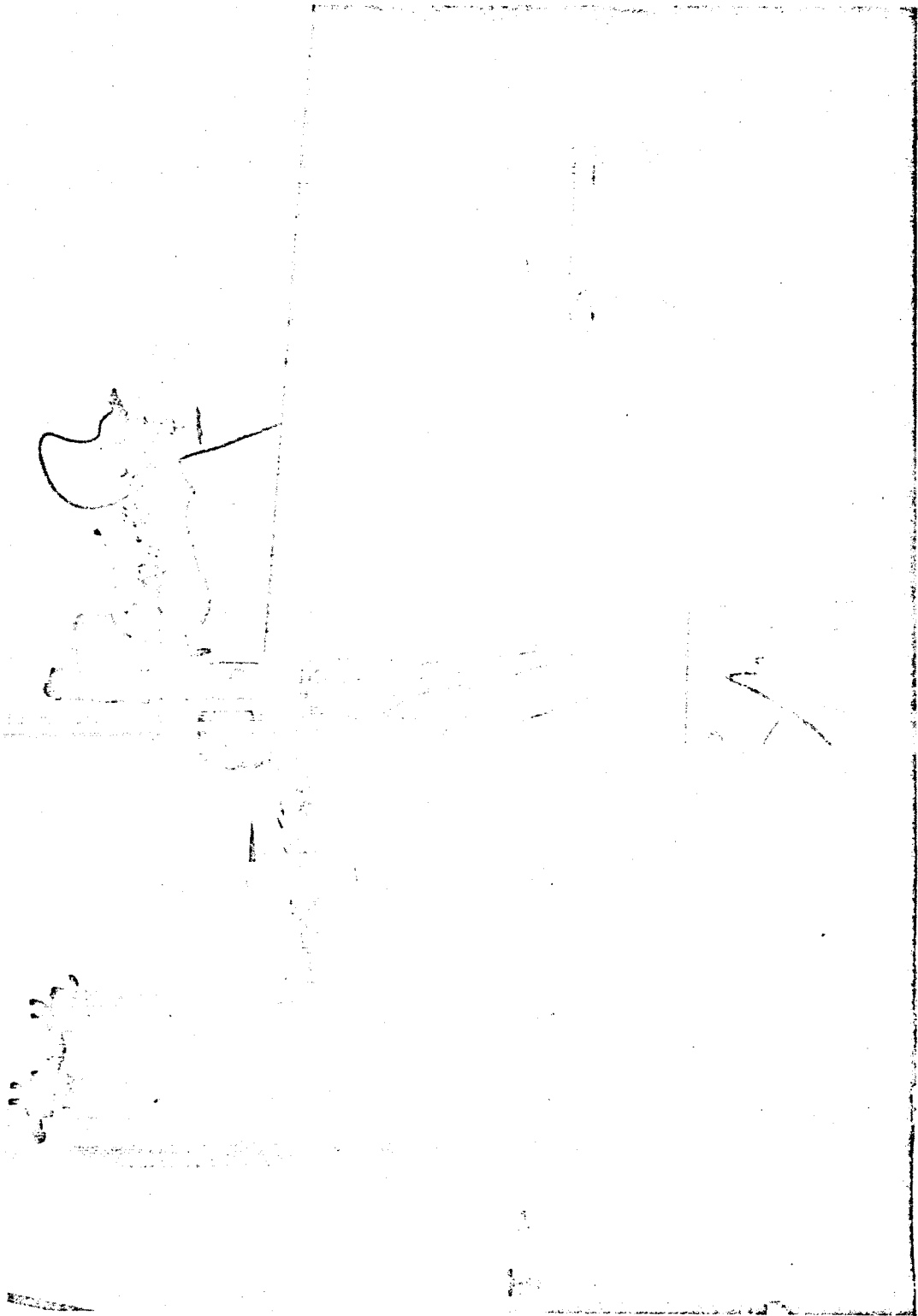
Figure 3. Bubble Chamber and Measurement Equipment

nitrogen bottle, and with the solenoid valve to chamber B closed, the
chamber A solenoid was opened. A third quick opening manual valve was
located above both chambers for safety against power failure in the
solenoid valves.

Instrumentation

Transient pressure in the inner chamber was measured by a Kistler,
model 606L, piezoelectric transducer with charge amplifier and oscillo-
scope. Drift in this system made it undesirable for static pressure
measurement. Static pressure above the liquid in the inner chamber
could be measured by the two manometers connected to chambers A and B.
For this measurement, it was necessary that at least one of the solenoid
valves to these chambers be open.

The copper-constantan thermocouples were used to measure the liquid
nitrogen temperature. The ice point was used for a reference junction
and a Digitec potentiometer, made by United Systems Corporation, was
used to measure the thermocouple emf. The complete calibration of this
experimental system is discussed in the next chapter.

The Wollensak Fastax camera shown in Figure 4 was used to record
the events occurring in the inner chamber. Experimental data were taken
for camera speeds up to 3500 pictures per second using one hundred foot
rolls of sixteen millimeter, Kodak Tri-x reversal film. Bright and dark
field photography were used at the start of data recording. However,
best results were obtained with bright field photography. For bright
field photography, two 625 watt sun guns were placed on the side of the
test chamber opposite the camera side and a sheet of paper was placed
between the lights and the plexiglas window to provide a diffusion
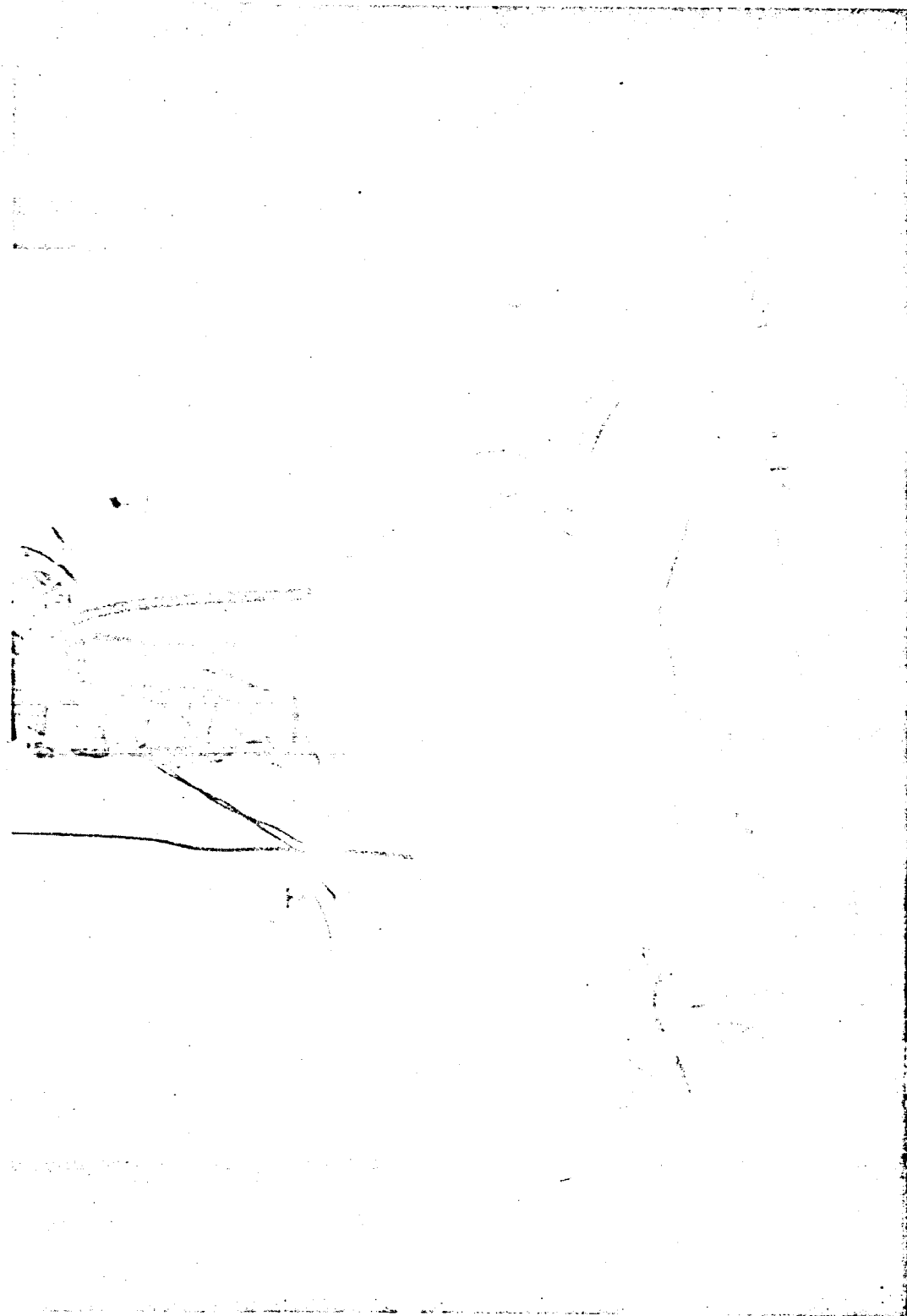
Figure 4. Bubble Chamber and Fastax Camera

screen. For dark field photography, the lights were placed on the camera side of the test chamber.

Operation of the Chamber

The procedure for filling the inner chamber with liquid nitrogen was to first turn on the Sargent duo-seal vacuum pump until the pressure in the vacuum space was 10^{-2} mm of mercury. Then, the oil diffusion pump was put into operation. When the vacuum reached 10^{-3} mm of mercury, no additional decrease in pressure could be obtained in this system. Liquid nitrogen from the container of Figure 5 was forced through the cooling coil placed around the connections to the inner chamber. This cooled the inner chamber very slowly and the cool-down was monitored using the thermocouples inside the inner chamber. After the inner chamber had cooled down to approximately 350°R, a nitrogen fill line located under the horizontal heater of Figure 1 (not visible in the figure) was used to allow nitrogen vapor to flow into the inner chamber. Chamber B was opened to the atmosphere and the solenoid valve between this chamber and the inner chamber was open. During the cool-down phase, the heat in the external lines was the source used to vaporize the liquid nitrogen and a low vapor flow rate insured relatively slow cool-down. The problem associated with very fast cool-down was the thermal stresses developed on the inside surfaces and at the interfaces between the different materials of the inner chamber.

Eventually, the system would fill with no change in the above conditions, but more rapid cool-down was accomplished by increasing the nitrogen flow at the time when a small amount of liquid nitrogen had accumulated in the bottom of the inner chamber. From the time when the
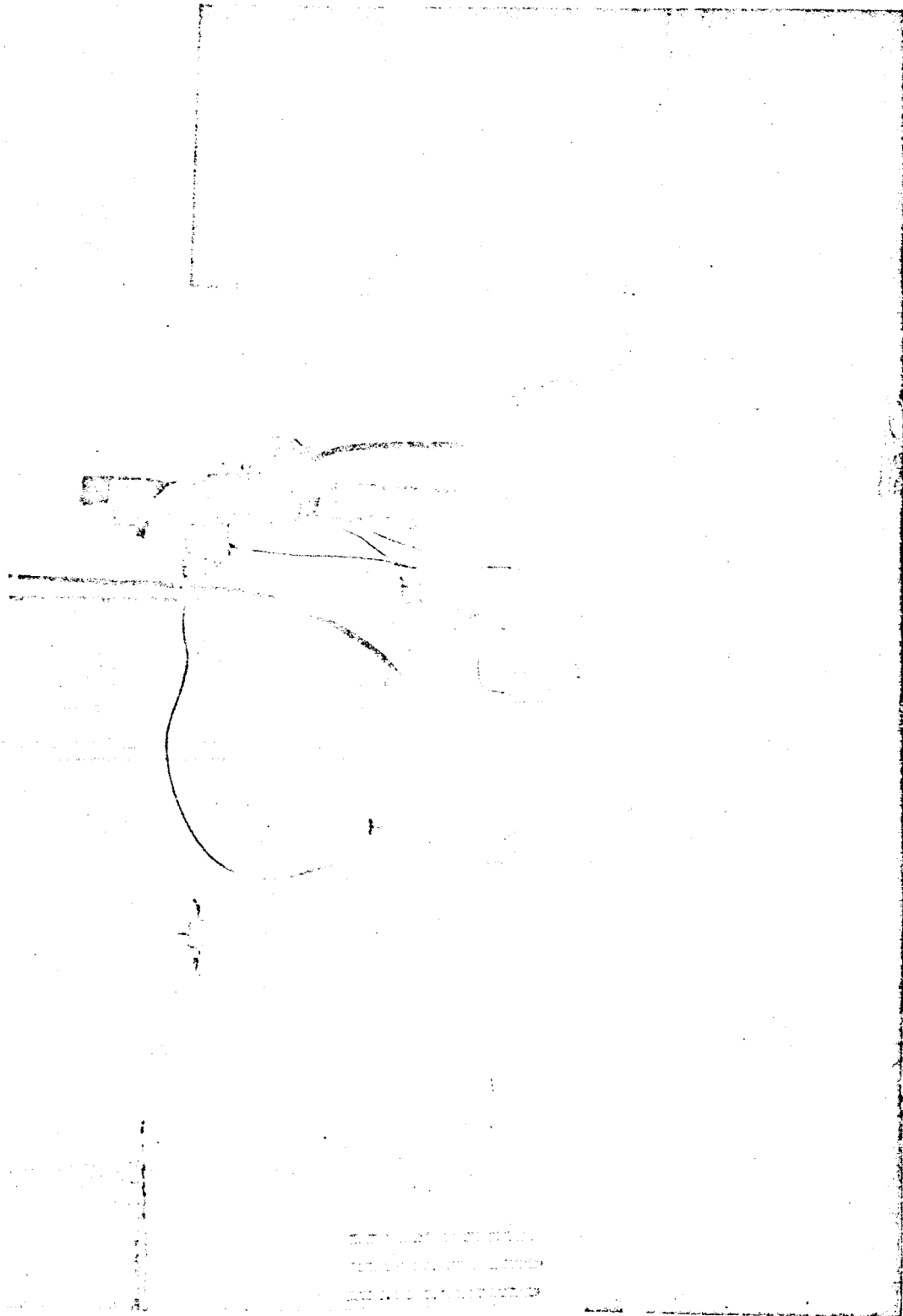
Figure 5. Bubble Chamber and Associated Equipment

liquid nitrogen was first used, approximately three hours were required to fill the inner chamber with liquid nitrogen. Once the inner chamber was filled, the fill line was closed and the liquid temperature was adjusted to the desired conditions. Lower temperatures were obtained by reducing the pressure and allowing the liquid to boil. The liquid temperature was increased by pressurizing the system and allowing the heat transfer to the inner chamber to result in higher temperature.

Approximately thirty minutes were available for experimental work before it was necessary to refill the inner chamber with liquid nitrogen. This elapsed time depended upon the liquid conditions desired in the inner chamber. The liquid nitrogen lines outside the test chamber warmed up when they were not in use, and the refill process took approximately thirty minutes.

Termination of the experiment was accomplished by opening to the atmosphere all lines and chambers containing liquid nitrogen. All valves were opened except the one to the liquid nitrogen source.

CHAPTER V

EXPERIMENTAL TECHNIQUES

One of the most important techniques in an experimental investigation is the calibration of all measuring equipment. The calibration procedure for this investigation is given in the following paragraphs. This procedure was completed before and after each day of experimentation.

Calibration of Measurements

The static pressures from either chamber A or chamber B of Figure 3 were measured using the mercury filled manometers shown. Barometric pressure was read on each day of experimental observation. The mercury manometer and known barometric pressure combination was considered to be a standard for pressure measurement. The combined error in static pressure measurement on these instruments was 0.12 inches of mercury or 0.06 psia. The pressure at the thermocouple level in the inner chamber was approximately 4.5 inches of liquid nitrogen or 0.011 psia higher than the pressure measured in chambers A and B. This correction was neglected in comparison to the error in the manometer reading.

Dynamic pressure was measured with a Kistler 606L piezoelectric transducer, charge amplifier, and oscilloscope. This dynamic pressure measuring system was calibrated statically under liquid nitrogen conditions using the manometers and high pressure nitrogen gas. The

calibration was conducted over the pressure range used in the experiments. The dynamic response of the Kistler transducer was rated at 150,000 cycles per second. The fastest transient pressure change in the liquid occurred in 0.2 seconds. Therefore, the dynamic response of this transducer was completely reliable in representing the pressure.

The temperature signal was sensed by copper-constantan thermocouples, referenced to the ice point using tap water, and measured with a Digitec potentiometer, made by United Systems Corporation. Reference (26, page 159) stated that the ice point is a reproducible standard. Figure 6, taken from page 206 of this reference, shows a plot of some calibration work on several thermocouples for the same arrangement as the one used in this investigation. The range of temperatures in the present investigation was from 140 to 150 degrees Rankine. For this small range Figure 6 indicates that the change in the microvolt error per change in temperature is very small. However, this information was not directly used in the calibration since a complete calibration of the temperature measuring system used here was made for each period of operation. The liquid nitrogen was allowed to boil at a pressure measured by a manometer connected to chamber A, and the saturation temperatures from Strobridge (27) were calibrated against the millivolt readings. The day-to-day variation in the calibration curve of a given thermocouple was negligible. The calibration data for each day of operation is given in Appendix D. Errors in the measurement of temperature were less than 0.2 degrees Rankine.

The Wollensak Fastax camera was equipped with a timing light to mark the film. This light was driven by a sixty cycles per second voltage. The driving voltage was checked on an oscilloscope, with time base
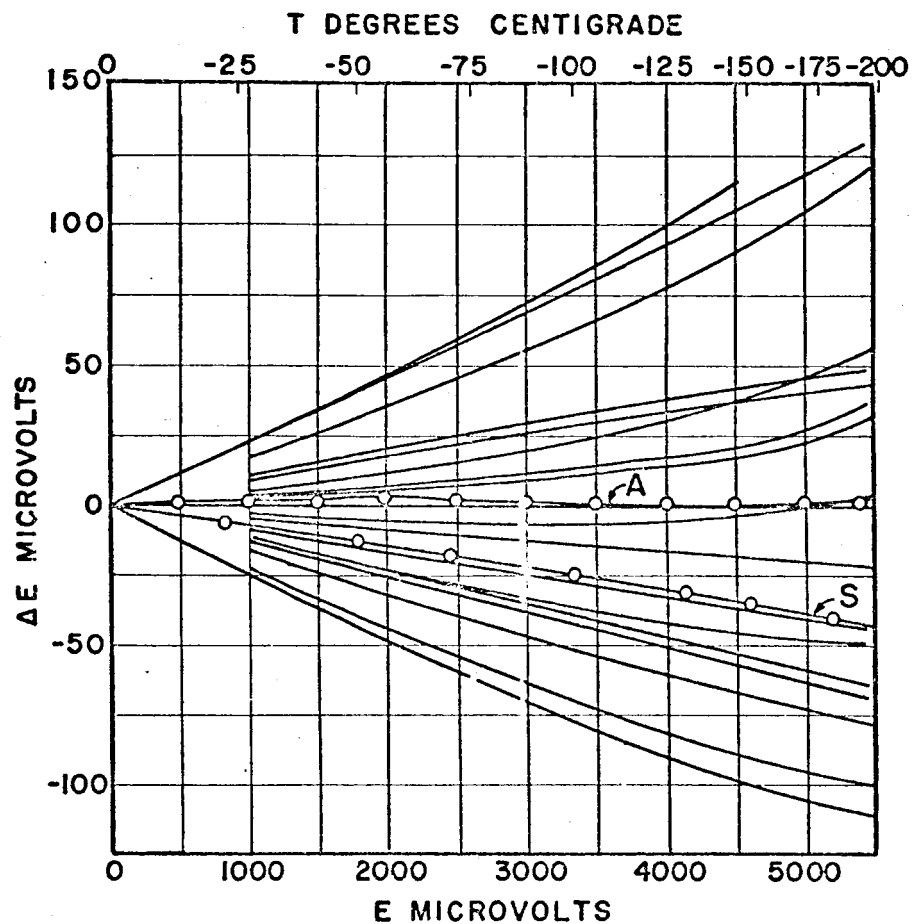
Figure 6. Differences Between the emfs of
Some Copper-Constantan Thermo-
couples and True Values (26)

calibrated from station WWV; variation from the expected sixty cycles per second frequency could not be detected. For exactly sixty cycles per second driving frequency, one hundred and twenty time marks were recorded on the film each second. An additional check on the sixty cycle driving voltage was obtained by counting the frames between two timing marks after the camera had reached constant velocity operation. Any change in the driving voltage frequency would have resulted in a noticeable difference in the picture count between successive timing marks. No difference was detected. From this double check, it was assumed that the film was marked one hundred and twenty times per second.

When transient pressure conditions were studied, it was necessary to synchronize the picture of the transient pressure taken from the oscilloscope with the pictures taken on the Fastax camera. This was accomplished by using one switch to trigger the oscilloscope sweep and to turn on a light simultaneously. The light was reflected to the Faxtax camera film and this mark on the film indicated the time of the start of the oscilloscope sweep. Thus, the oscilloscope picture gave pressure as a function of time such that the bubble pictures could be related to the same time.

Length measurement of the bubble diameters was accomplished using dividers and a steel scale marked in sixty-fourths of an inch. This measurement was checked by a cathetometer, made by the Gaertner Scientific Corporation. The pictures were projected onto a screen and one known dimension was included on each picture. The small vapor tube on Figure 2 was made of twenty-six gauge hypodermic needle. The diameter was 0.018 inches at room temperature. This dimension is the same as

that published in tables for hypodermic needles; it was also duplicated by micrometer measurement. At liquid nitrogen temperature, this dimension was calculated from the data of Scott (28) to be 0.0178 inches. The diameter of this tube was measured for each picture by dividers and scale and was used for the standard length. The projector remained in one position, and the measured diameter of the hypodermic needle was constant at $8/64$". The information gained from the above procedure was used to convert measured bubble diameter to actual bubble diameter. This step completes the calibration of every measurement made in the experimental investigation.

Techniques in Recording Data

Experimental data were taken for bubble growth and collapse with constant pressure above the liquid and for bubble growth with variable pressure above the liquid. For constant pressure, the Kistler transducer was not used. Approximately five minutes were allowed for the pressure above the liquid to reach a steady state condition, and vapor bubbles were generated either by forcing gaseous nitrogen through the steel tubes or by passing a current through the heater. The high pressure gaseous nitrogen bottle was equipped with a pressure regulator valve for adjusting the source pressure. Flow from the bottle was controlled by a microswitch valve. The flow branched to two pipes connected to the two vapor buble tubes shown in Figure 2. Each pipe had a gate valve to allow the selection of the tube to be used to generate vapor bubbles. The tube selected determined the size of the vapor bubble to be studied.

Since the bubbles produced by this method were superheated, they

were not measured until they had risen through approximately one inch of liquid nitrogen. Any superheat left in the bubble after this time was neglected. The bubble measurements were terminated when the bubble moved to within one inch of the liquid surface. Turbulence at the surface made study of the bubbles there useless since fluid conditions were unknown. The same procedure was followed for bubbles forming on the electrical heater. The thermocouple readings were not affected when current was passed through the electrical heater. No change in thermocouple output was observed to accompany the start of operation of the electrical heater.

When transient pressures were studied, it was necessary for the operator to perform four functions in approximately one second. The operations consisted of starting the camera, switching on the oscilloscope sweep, generating vapor bubbles with a microswitch, and switching one solenoid valve to either chamber A or B to the open position. An electronic delay circuit was not feasible because the bubble generation method was not reliable enough to assure the presence of a bubble by one microswitch operation. This procedure required several practice runs before a roll of film could be used. Although the experimental techniques could be improved, excellent results were obtained.

The measurements of bubble diameter were taken along the major and minor axis of the bubble, and the average diameter was used. The two-dimensional shape of nearly all bubbles was ellipsoidal. The experimental data of references (1), (2), (12), (13), (14), (19), and (20) were analyzed by this method. Florschuetz and Chao (1) used a drop chamber in their experimental work and still had non-spherical bubbles. The experimental work done in these references has compared favorably with

the theoretical work where the spherical shape was assumed. Apparently

the spherical assumption caused only small error in the analysis since

all experimental work has actually been done on the non-spherical

bubble.

CHAPTER VI

RESULTS AND DISCUSSION OF RESULTS

The experimental data recorded in this investigation were used to determine whether or not the theoretical solutions of Chapter III could be applied to liquid nitrogen. The experimental liquid nitrogen conditions, resulting in bubble growth with constant liquid pressure, were similar to the conditions in non-cryogens investigated by other authors. A summary of the experimental work in non-cryogens was presented in Table II.

Experimental data on vapor bubble collapse controlled by heat transfer was previously limited to the work of Florschuetz and Chao (1). Their study was made using a drop chamber to eliminate the effect of gravity. The present investigation considered heat transfer controlled collapse in the presence of a gravitational field. Both experimental investigations gave indication that the theoretical predictions for heat transfer controlled collapse need modification.

The present investigation also considered a limited amount of data on bubble growth with a transient liquid pressure and some information on the persistence time of vapor bubbles. The experimental results for bubble growth with constant liquid pressure, bubble collapse with constant liquid pressure, bubble growth with variable liquid pressure, and bubble persistence time are presented in the following pages.

39

Discussions of each of the above experimental results are also included.

Bubble Growth With Constant Liquid Pressure

Vapor bubble histories were recorded on four rolls of film for liquid nitrogen superheated above equilibrium conditions 3.8, 4.1, 6.8, and 8.0 degrees Rankine. The pressure above the liquid was constant for the time when the measurements of bubble diameter were made. The first measurement of bubble diameter for each set of experimental results was taken at an arbitrary but unknown time, t_o, corresponding to a particular frame of film where a timing mark was recorded. The time between the first measurement and all other measurements was determined by counting the timing marks and knowing that the distance between two timing marks represented 1/120 seconds.

The Plesset-Zwick solution for bubble growth was the theoretical solution selected for the correlation of experimental data. The solution used was Equation (III-7),

$$R = \sqrt{\frac{12}{\pi}} \ \frac{k_L \Delta T}{L \ \rho_V \sqrt{\alpha}} \ t^{\frac{1}{2}} .$$

(VI-1)

Several other references, (19), (20), and (21), used this same equation for correlation. The temperature and pressure of the liquid nitrogen were measured for each experimental observation. This information and information on the properties of nitrogen from Strobridge (27) and Johnson (29) were used to determine the coefficient of $t^{\frac{1}{2}}$ in Equation (VI-1). The theoretical curve for each set of fluid conditions was calculated and plotted along with the experimental results. A set of sample calculations for one theoretical curve is given in Appendix D.

Tables of all theoretical and experimental values plotted for each set
of fluid conditions are also given in Appendix D.

The problem of determining the initial time, t_o, when the bubble
was first measured has been encountered in all experimental investiga-
tions. According to Equation (VI-1), the bubble radius is zero when
time is zero, and bubble radius is an increasing function of time. In
some experimental work, (19), (20), and (21), one frame on a roll of
bubble data film was blank and the next frame had a measurable bubble
on it. The time when the bubble first started to grow could not be
determined more accurately than the time between frames of film.
Dergarabedian (19) experimentally determined the initial time to be less
than 0.001 seconds by this method. Since the exact determination of t_o
was impossible experimentally, a combination of analytical and experi-
mental techniques has been applied to the selection of the initial time.
A look at the coordinates of the first two experimental points, (R_o, t_o)
and $(R_1, t_o + \Delta t)$, shows that the selection of t_o physically represents
a shift of the time axis. In all experimental work, the time shift has
been selected by some combination of analytical and experimental tech-
niques. Two of these methods are discussed in the following paragraphs.

In the present investigation, the method of generating vapor
bubbles and the technique of measuring the vapor bubbles after they had
moved through one inch of liquid resulted in very large initial bubble
diameters. Therefore, the initial time, t_o, was large. The time axis
was shifted so that the first measured diameter was forced to lie on the
theoretical line.

It is obvious that a selection of initial time, t_o, by an averaging
method would result in a better fit between experiment and theory. One

averaging scheme would be:

$$R_n = A(t_{on} + n\Delta t)^{\frac{1}{2}} \qquad\qquad (VI\text{-}2)$$

and

$$t_o = \frac{1}{k} \sum_{n=1}^{n=k} t_{on}$$

where

R_n = measured radius

A = coefficient of $t^{\frac{1}{2}}$ in Equation (VI-1)

Δt = time between timing marks on the frame where the bubble was measured

n = index of timing marks

k = the number of measurements

and t_{on} = initial time calculation from Equation (VI-2).

However, one purpose of this investigation was to determine how accurately the theoretical work of Plesset and Zwick could predict bubble growth. For this purpose, the method of requiring the first data point to fit the theory exactly was more appropriate. The accuracy of prediciting all other points was a measure of the validity of the Plesset-Zwick theory. One disadvantage of the method of selecting the time shift, used in this investigation, was that an error in the measurement of the first bubble produced an error in the selected time shift.

Figures 7, 8, 9, and 10 show the comparison between the theoretical Equation (VI-1) and the experimental data of nine different vapor bubbles under four different liquid conditions. The initial data point for each experimental run was required to lie on the theoretical solution by a shift of the time axis.
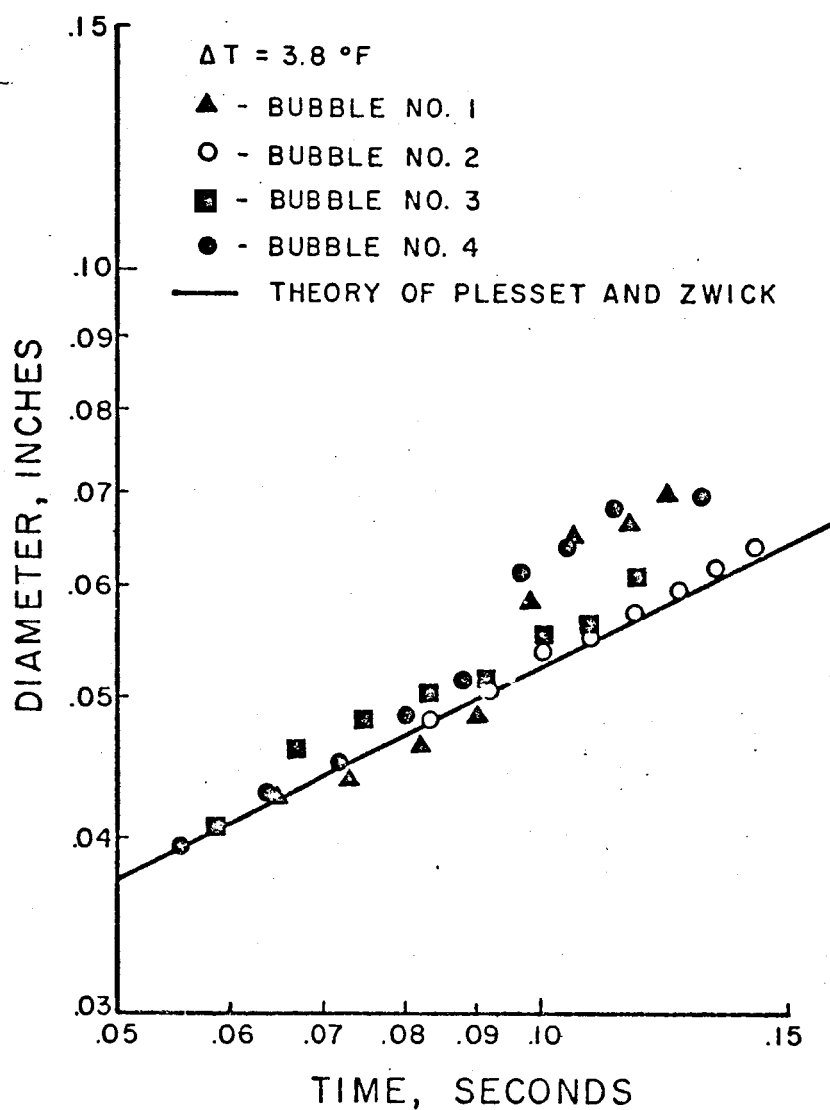
Figure 7. Bubble Growth in a Superheated Liquid –
Bubble Nos. 1-4
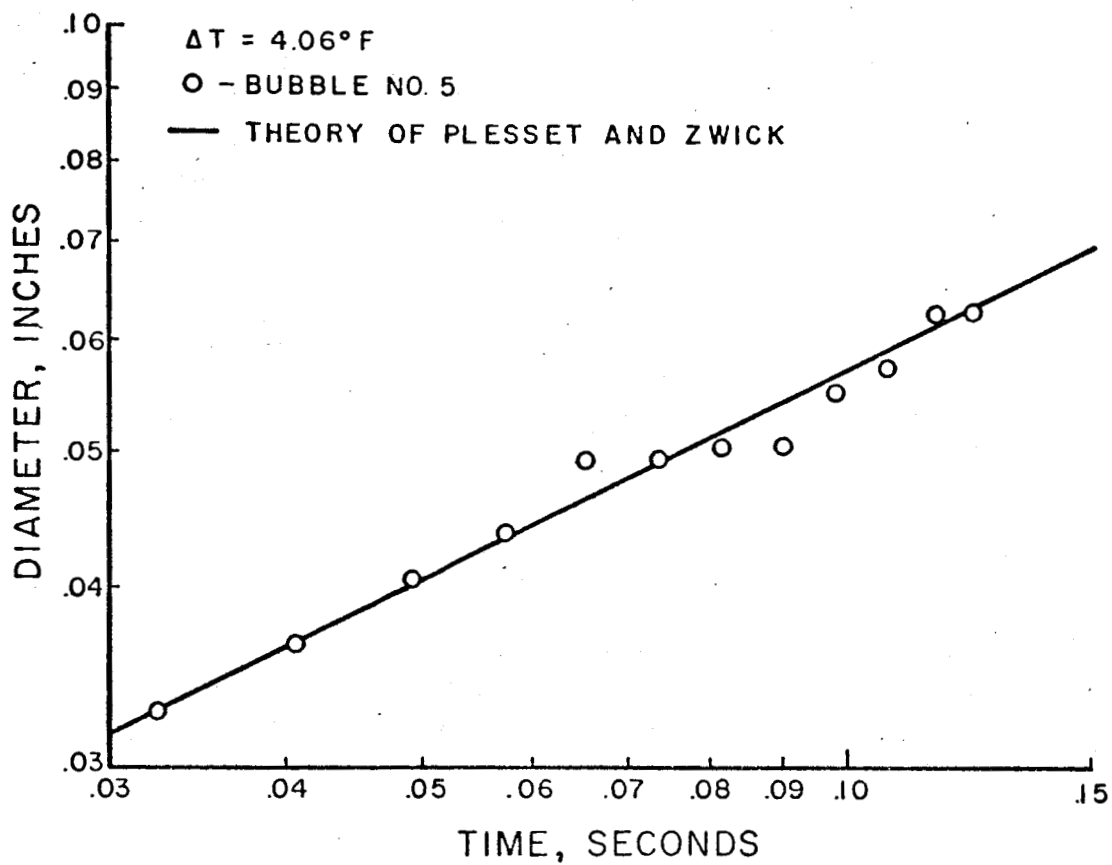
Figure 8. Bubble Growth in a Superheated Liquid – Bubble No. 5
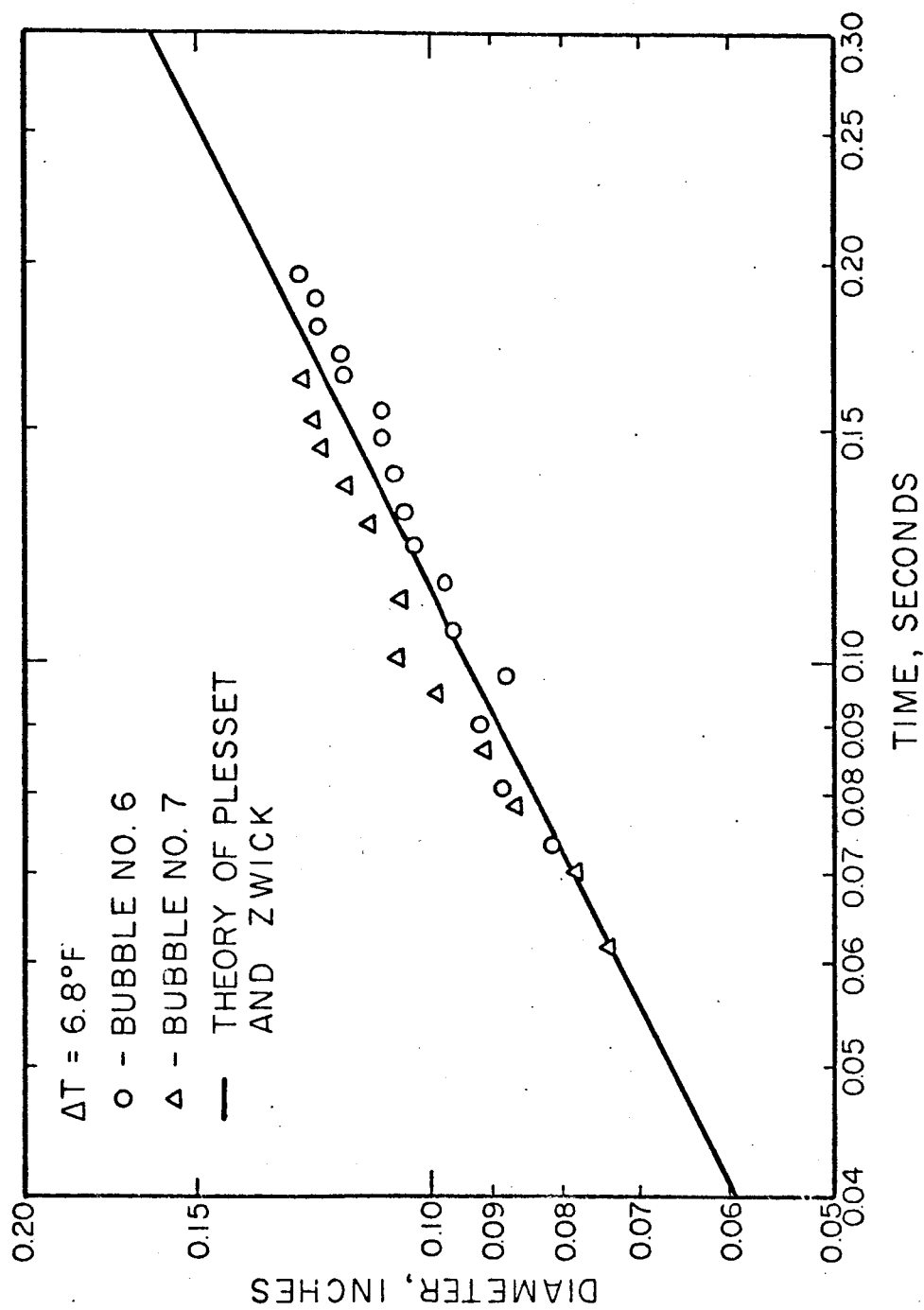
Figure 9. Bubble Growth in a Superheated Liquid — Bubble Nos. 6 and 7
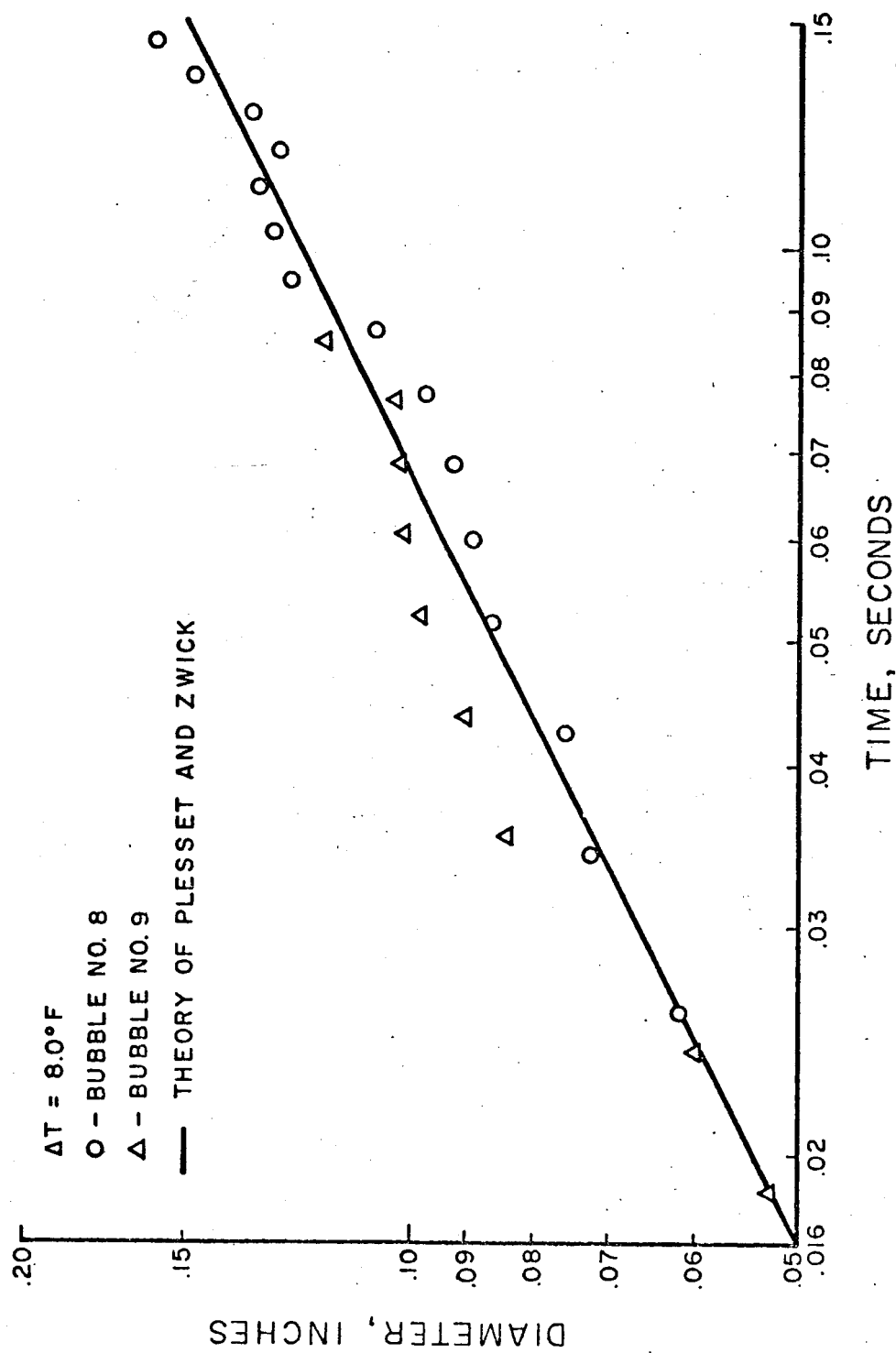
Figure 10. Bubble Growth in a Superheated Liquid — Bubble Nos. 8 and 9

ΔT = 8.0°F
O – BUBBLE NO. 8
△ – BUBBLE NO. 9
▬ THEORY OF PLESSET AND ZWICK

TIME, SECONDS

DIAMETER, INCHES

Dergarabedian (19) recorded the bubble history for a period of 0.015 seconds. This was the longest period of measured bubble history for all previous investigations. The present investigation measured bubble histories for periods of time ten times longer than this. All data points deviated from the theoretical curve by less than twenty-five percent. However, eighty-nine percent of all data points were in error from the theoretical curve by less than ten percent. The only bubbles deviating from the theoretical curve by more than fifteen percent are bubbles number 1 and 4 of Figure 7. Some of these points deviated by twenty-two percent. These two bubbles were replotted assuming that the initial bubble radius measurement was in error by ten percent. The time shift was calculated for a ten percent larger bubble and the deviation between these altered data points and theory was calculated. All of these data points deviated from the theoretical solution by less than fourteen percent. This points out the fact that any error in the measurement of the initial bubble radius could cause a relatively large deviation between the theoretical and experimental results.

Bubble Collapse With Constant Liquid Pressure

Photographic records of vapor bubbles were made for liquid nitrogen subcooled below equilibrium conditions 0.74, 0.90, 1.0, 1.2, 2.16, 2.23, 2.88, 3.60, and 3.71 degrees Rankine. Twelve bubble histories were measured and are recorded in Appendix D. A bubble was observed until the bubble wall velocity was approximately zero and this frame was arbitrarily selected to be at the initial time of zero. The reason for this selection was to satisfy the initial conditions imposed on the theoretical solution. They were:

at $t = 0$, $\qquad R = R_o$, and $\overset{\circ}{R} = 0$.

The bubble radius-time histories were taken from these films and plotted in Figures 11 through 20. The results of Florschuetz and Chao (1) indicated that the experimental results for small degrees of subcooling could be correlated by the theoretical solution, (Equation (C-24))

$$\frac{R}{R_o} = 1 - \sqrt{t_H} \qquad\qquad (VI\text{-}3)$$

where t_H and R_o are defined in the list of symbols. Therefore, this equation was plotted on each figure for comparison.

Two equations predicting the collapse of vapor bubbles controlled by heat transfer were developed in Appendix C. Equation (VI-3) was the equation that best predicted the Florschuetz and Chao data for a subcooling of 5.6 degrees Kelvin and less. The other solution, Equation (C-22), gave the best prediction for subcooling of 9 to 13 degrees Kelvin for water. These conclusions came from the data plotted by Florschuetz and Chao. Equation (C-22) was an upper limit in that no experimental data collapsed more slowly than the collapse predicted by this equation. Neither solution could handle the full range of subcooling. Figure 21a is a comparison of the two solutions, Equations (C-22) and (VI-3).

The scatter of data both in the present investigation and in the investigation of Florschuetz and Chao was so great that it was impossible to determine experimentally the errors in the theoretical solution. A plot of R/R_o versus t_H (not presented here) was made for the liquid nitrogen data. The dimensionless parameters included in t_H were

$T_L = 141°R$

3.71 °R SUBCOOLING

$R_0 = 0.04162$ INCHES

○ – EXPERIMENTAL DATA

$\frac{R}{R_0} = 1 - \sqrt{t_H}$

TIME, SECONDS

$\frac{R}{R_0}$, DIMENSIONLESS
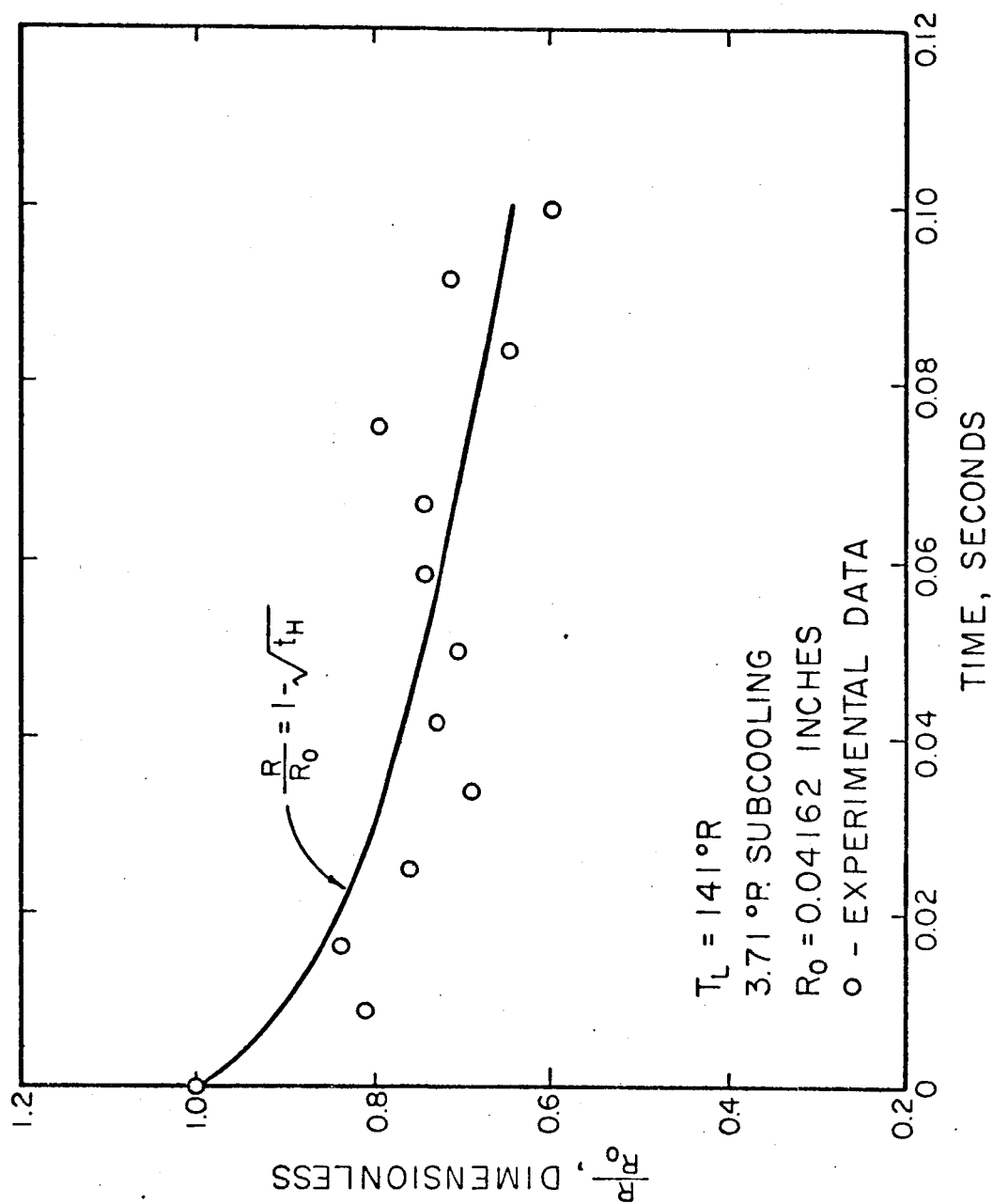
Figure 11. Bubble Collapse – Bubble No. 10

$$T_L = 143°R$$

3.6°R SUBCOOLING

$$R_0 = 0.0366 \text{ INCHES}$$

O – EXPERIMENTAL DATA

TIME, SECONDS

$$\frac{R}{R_0}, \text{ DIMENSIONLESS}$$

$$\frac{R}{R_0} = 1 - \sqrt{t_H}$$
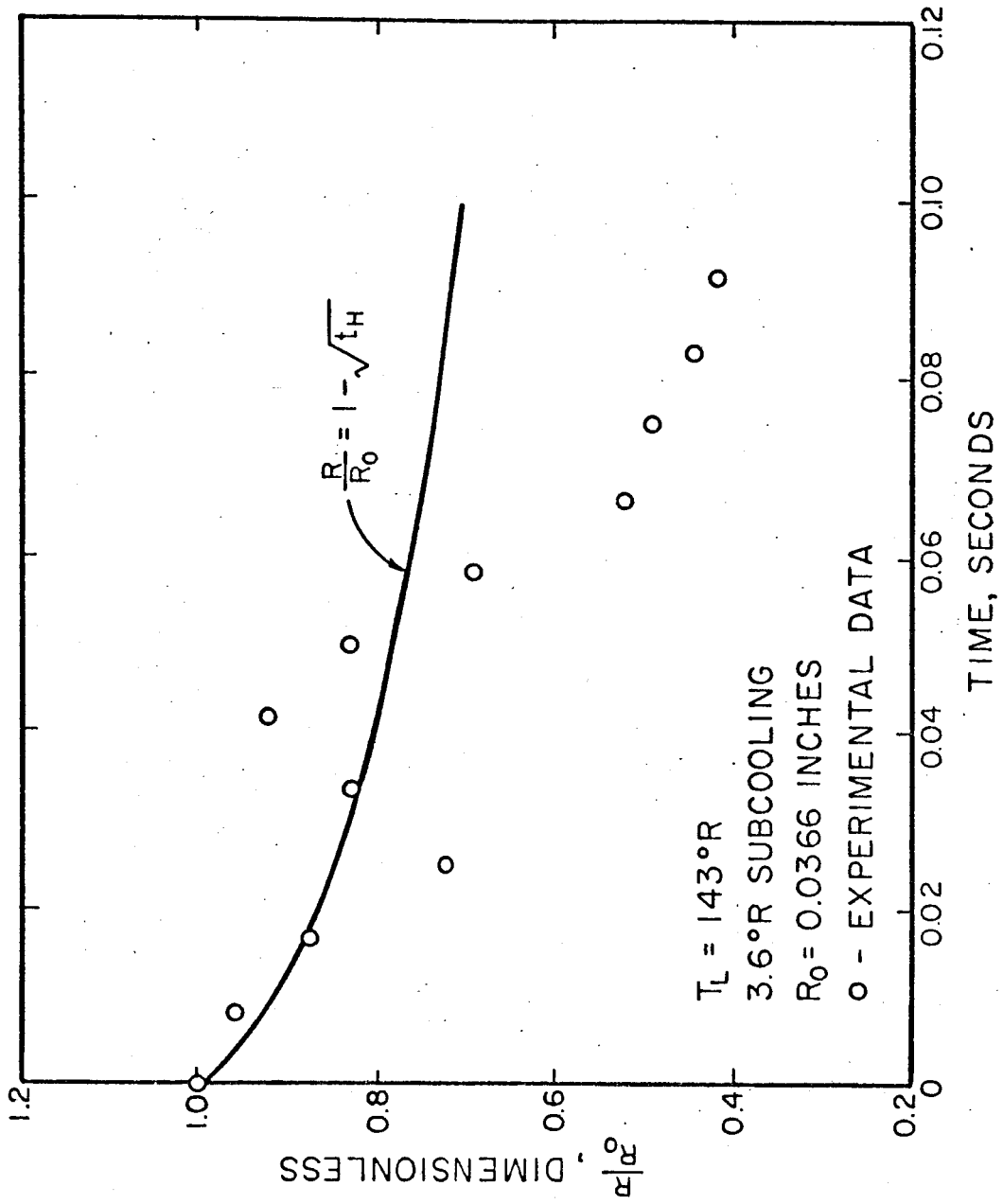
Figure 12. Bubble Collapse – Bubble No. 11

$$\frac{R}{R_0} = 1 - \sqrt{t_H}$$

$T_L = 143°R$

3.6°R SUBCOOLING

$R_0 = 0.03825$ INCHES

o – EXPERIMENTAL DATA

TIME, SECONDS

$\frac{R}{R_0}$, DIMENSIONLESS
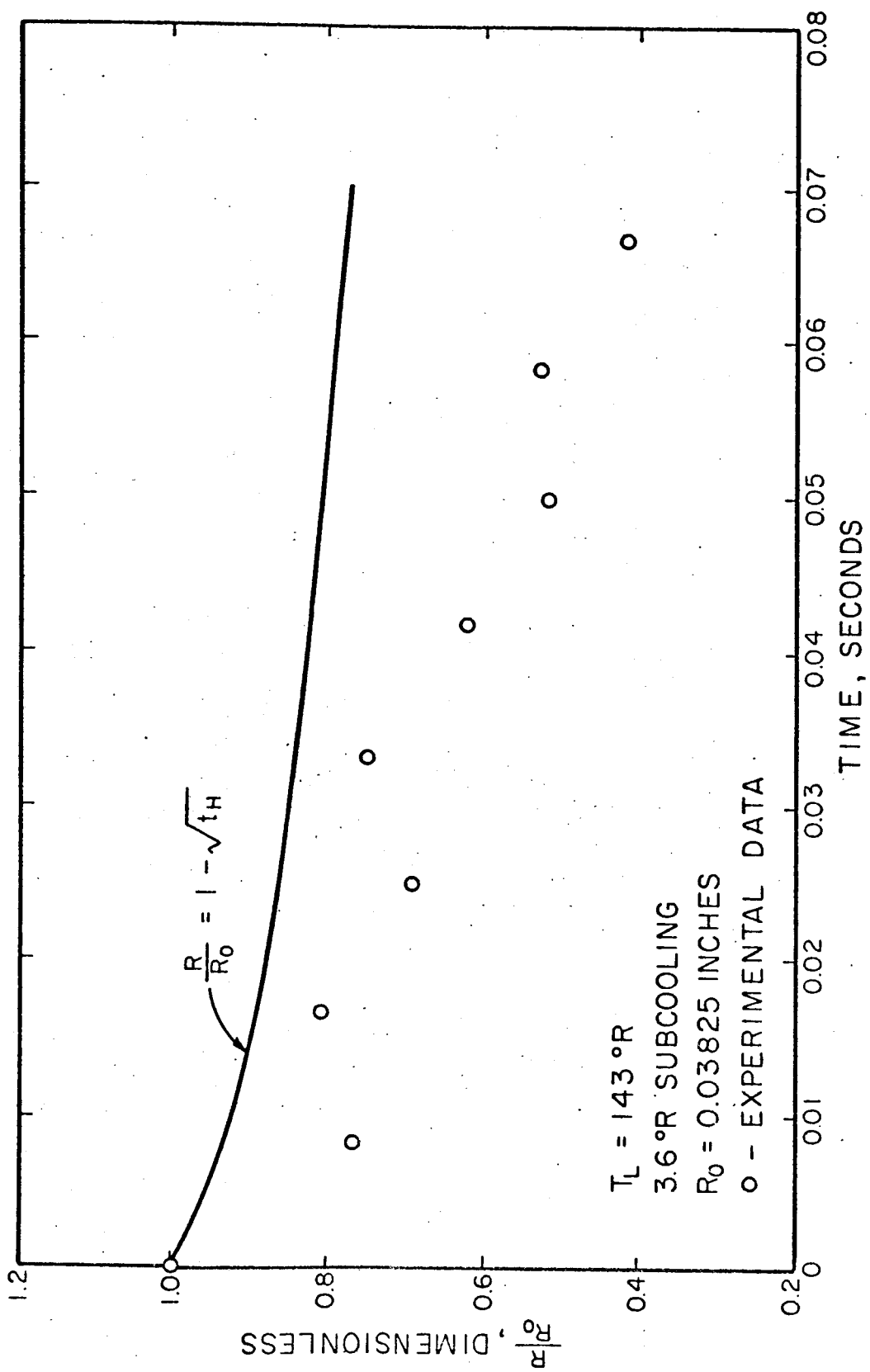
Figure 13. Bubble Collapse – Bubble No. 12

$$\frac{R}{R_0} = 1 - \sqrt{t_H}$$

T_L = 140.6 °R

2.88 °R SUBCOOLING

R_0 = 0.0686 INCHES

○ – EXPERIMENTAL DATA
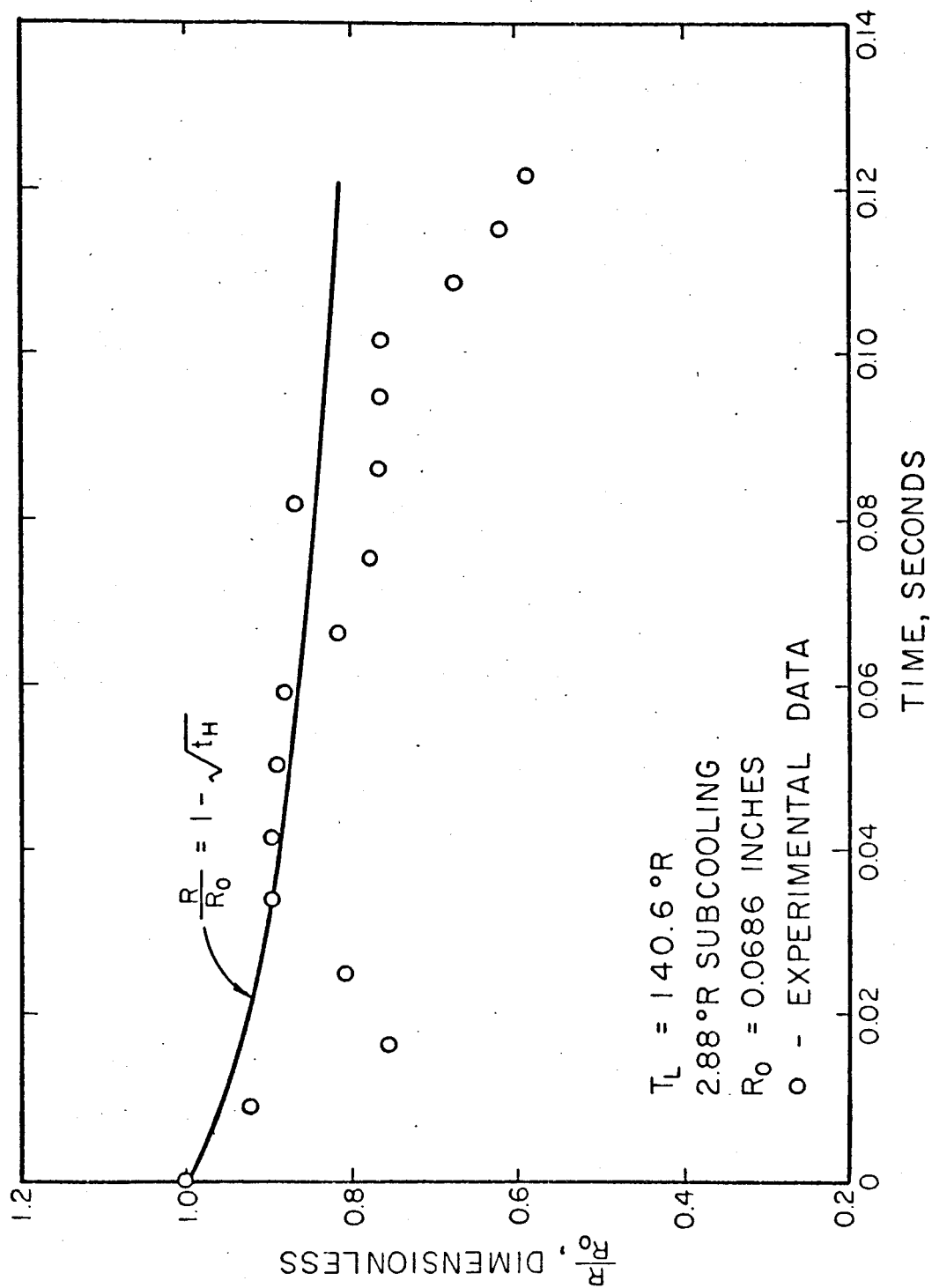
Figure 14. Bubble Collapse – Bubble No. 13
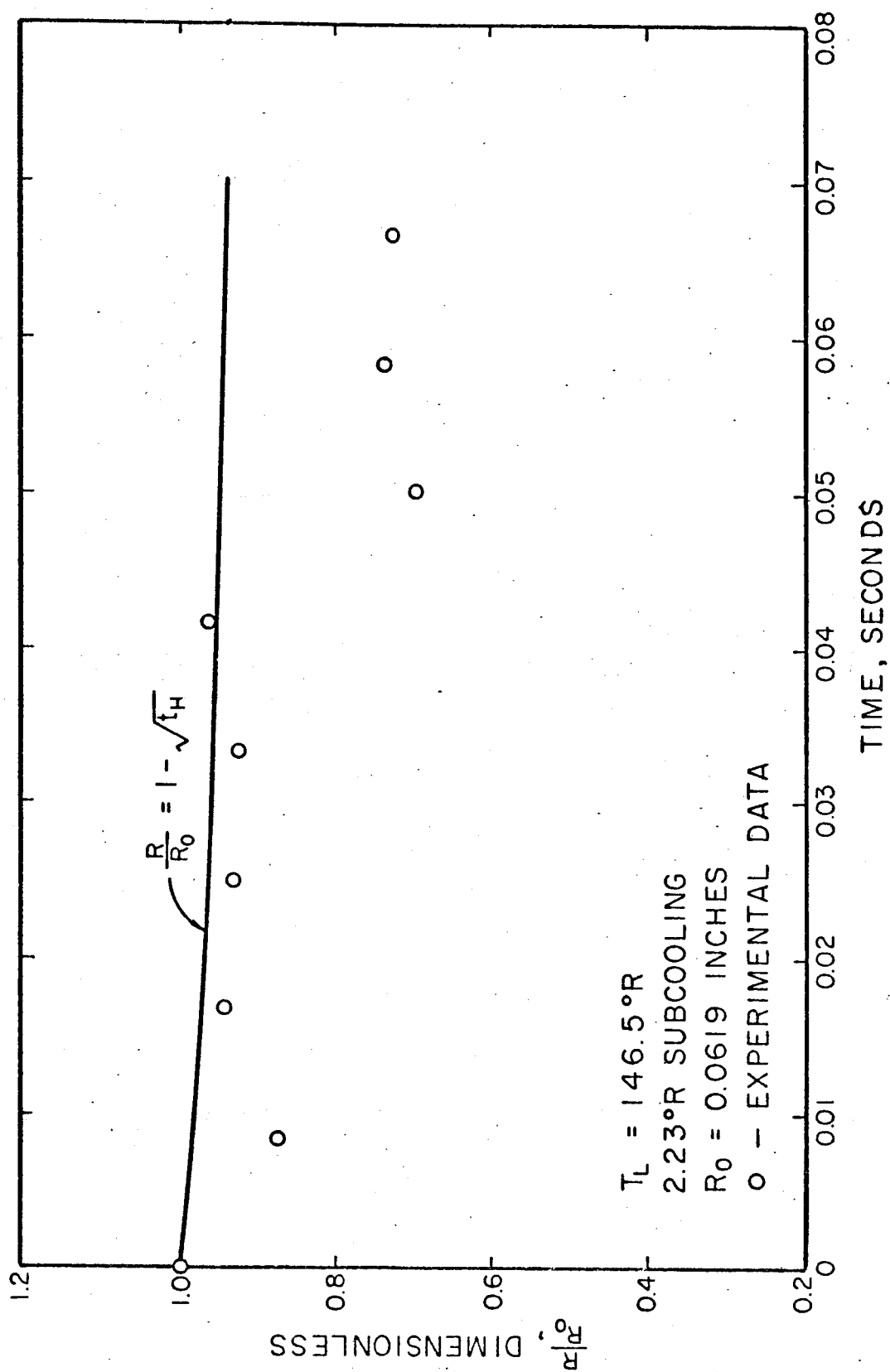
Figure 15. Bubble Collapse – Bubble No. 14

The plot shows $\frac{R}{R_0}$, DIMENSIONLESS (vertical axis, from 0.2 to 1.2) versus TIME, SECONDS (horizontal axis, from 0 to 0.08).

Curve label:
$$\frac{R}{R_0} = 1 - \sqrt{t_H}$$

$T_L = 146.5°R$

$2.23°R$ SUBCOOLING

$R_0 = 0.0619$ INCHES

O – EXPERIMENTAL DATA
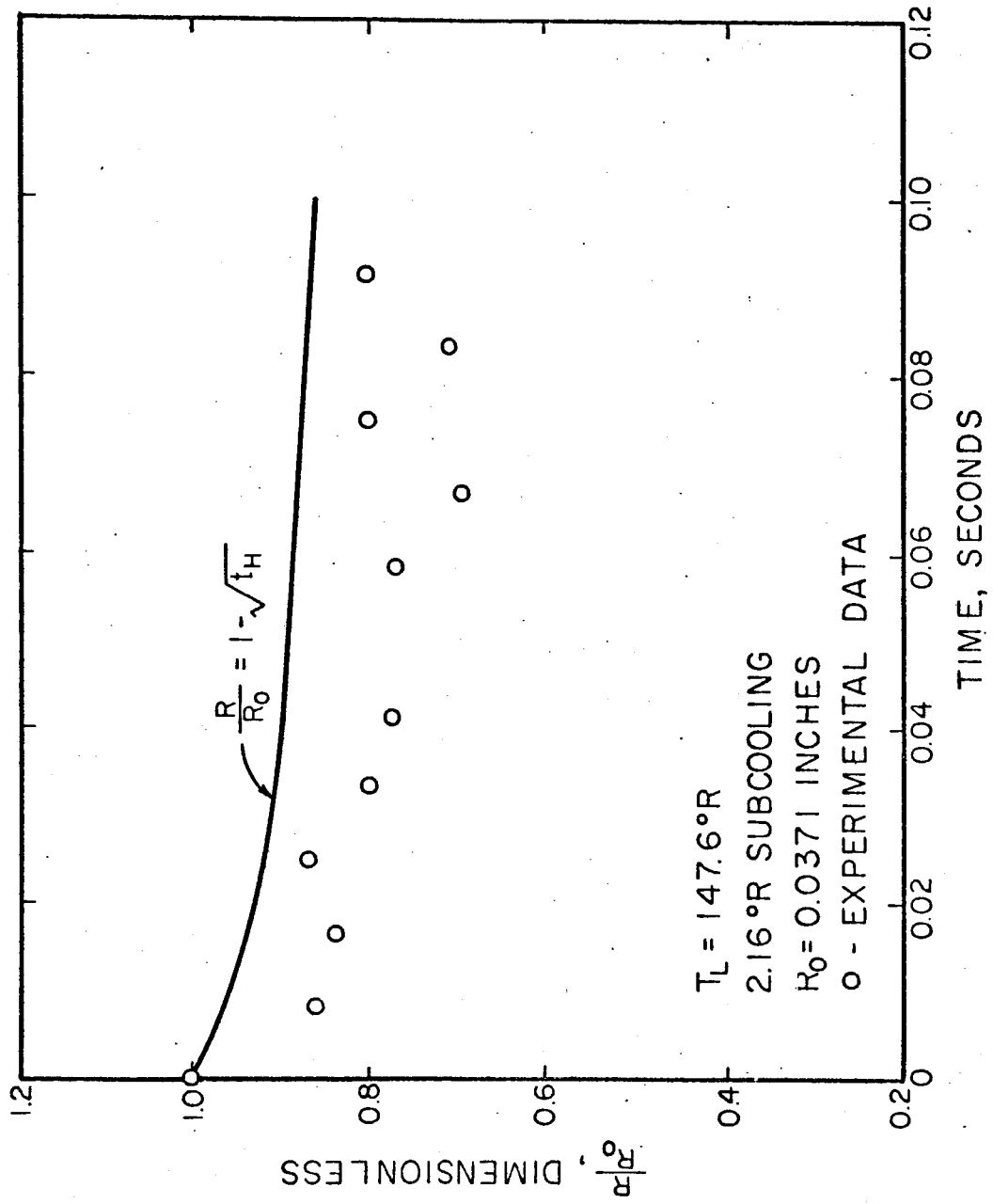
Figure 16. Bubble Collapse – Bubble No. 15

$$\frac{R}{R_0} = 1 - \sqrt{t_H}$$

$T_L = 143.8 \ °R$

$1.2 \ °R$ SUBCOOLING

$R_0 = 0.0332$ INCHES

$\circ$ - EXPERIMENTAL DATA

TIME, SECONDS

$\frac{R}{R_0}$, DIMENSIONLESS
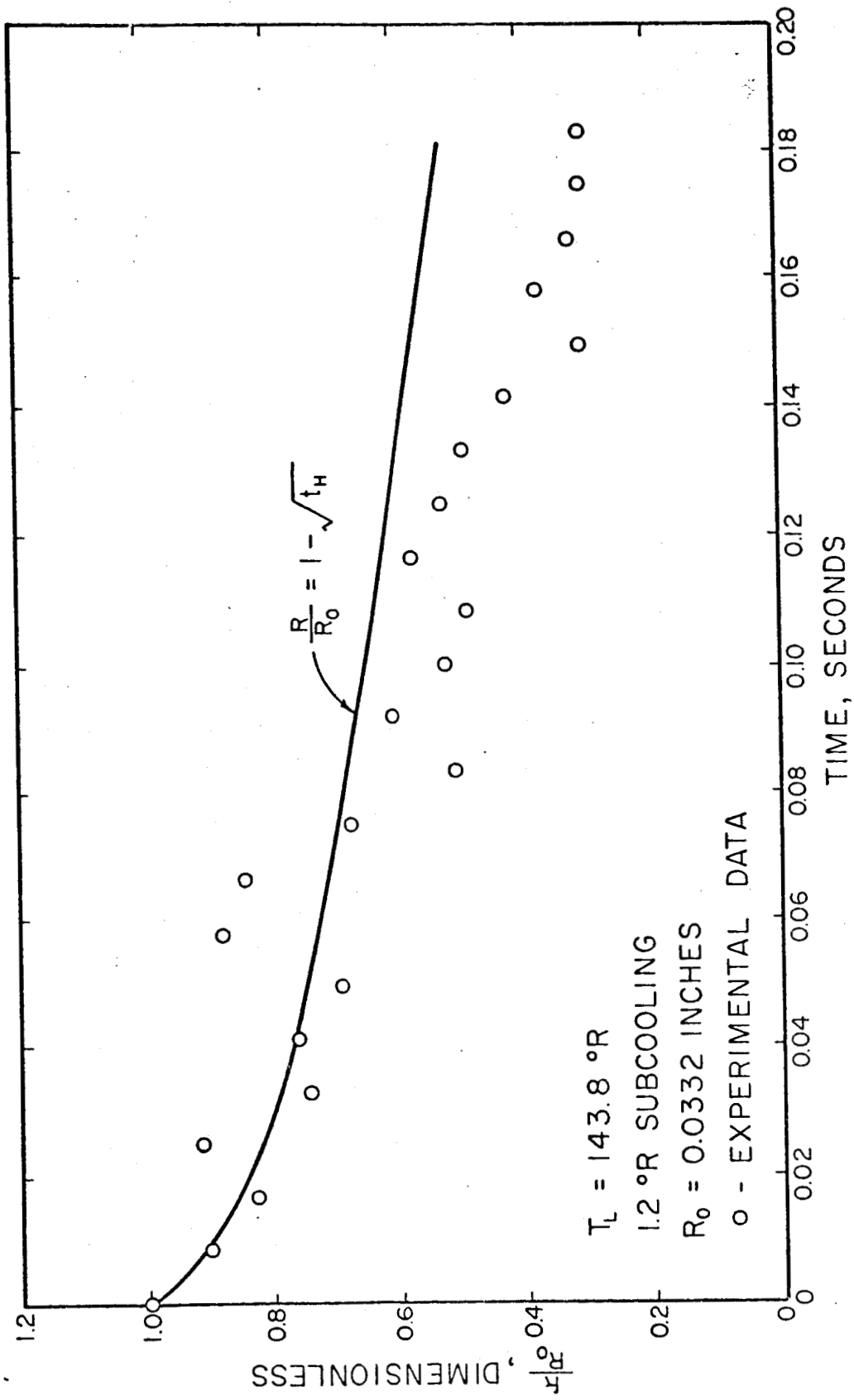
Figure 17. Bubble Collapse – Bubble No. 16
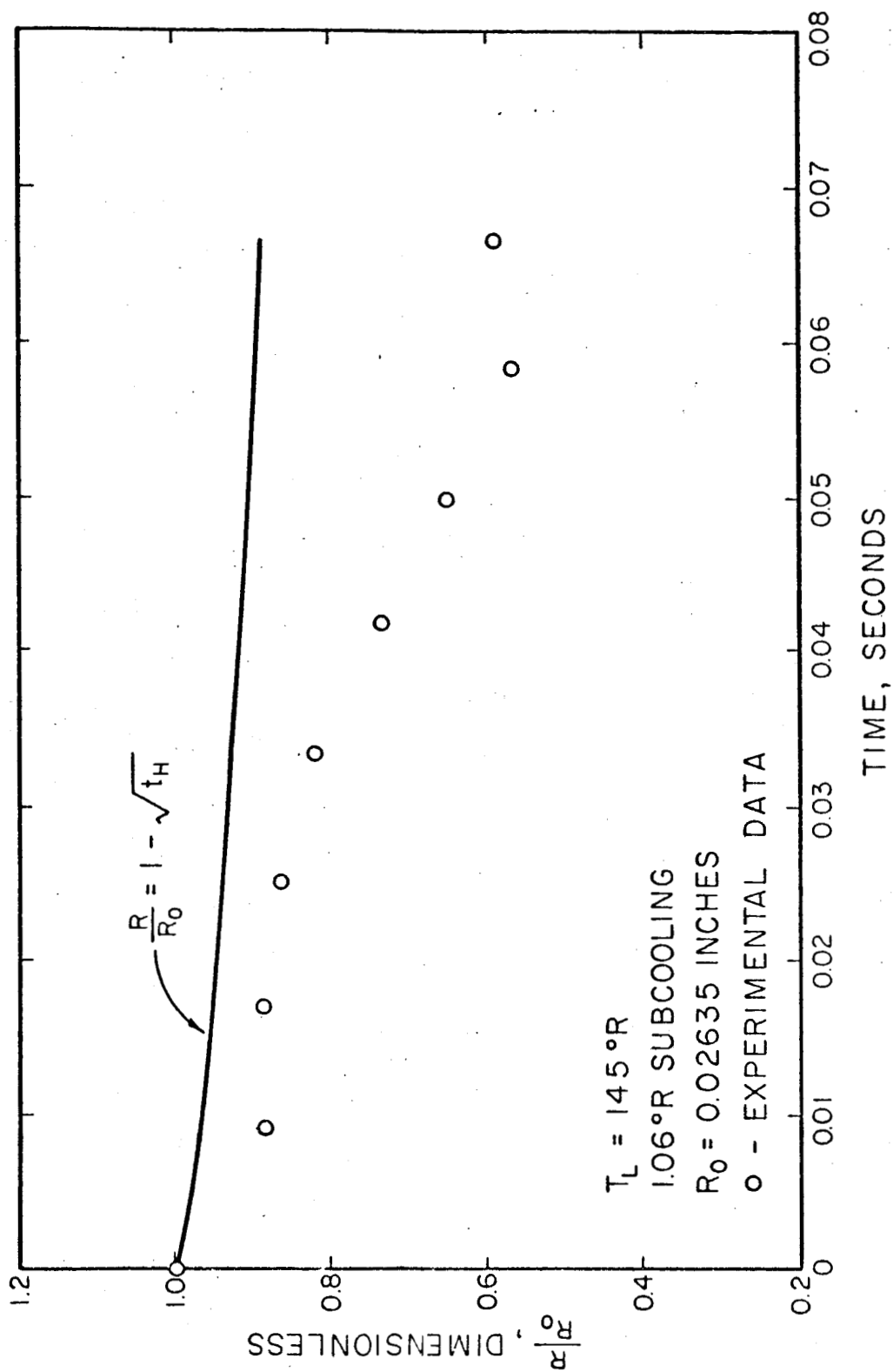
Figure 18. Bubble Collapse - Bubble No. 17
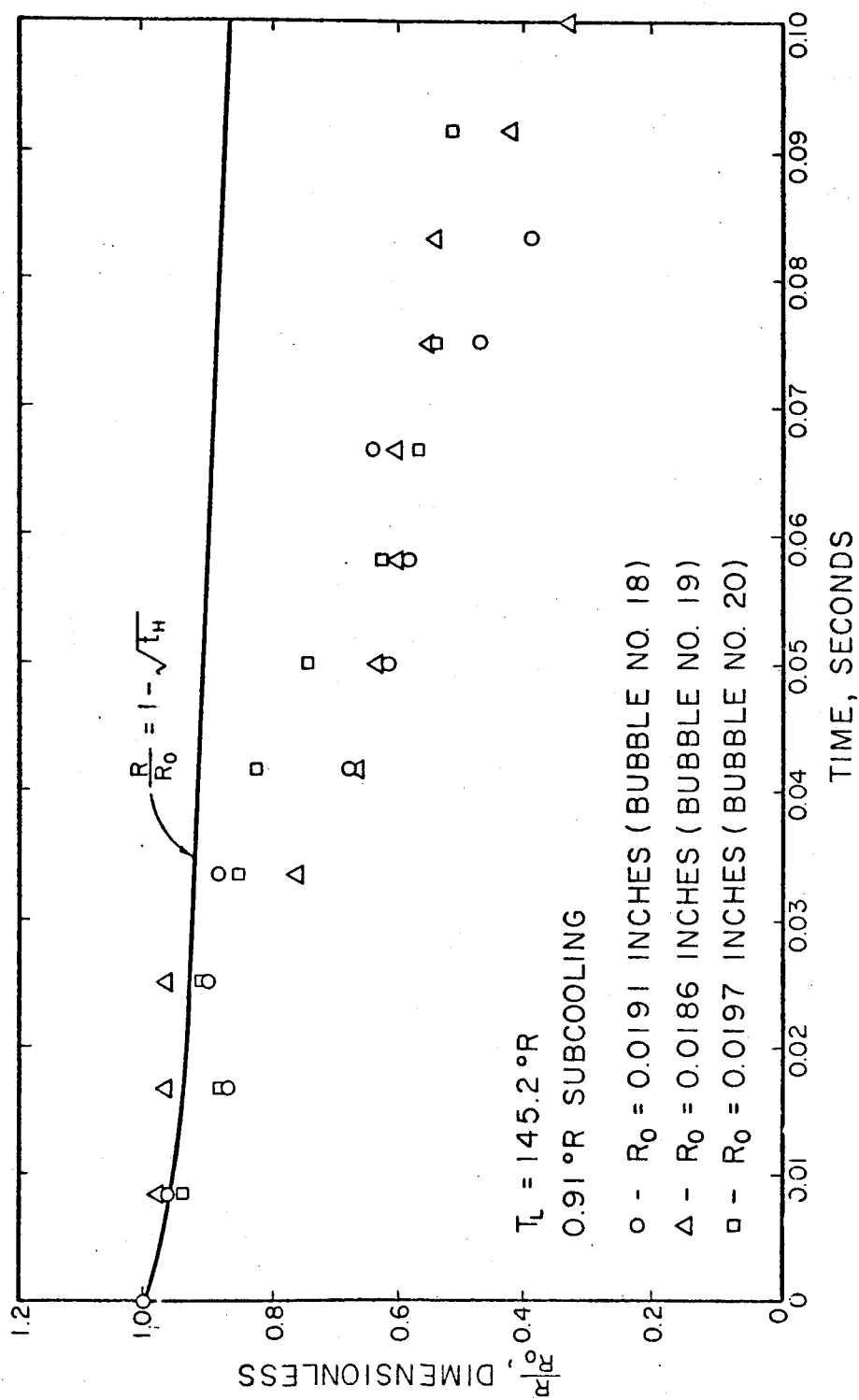
Figure 19. Bubble Collapse — Bubble Nos. 18-20

$$\frac{R}{R_0} = 1 - \sqrt{t_H}$$

$T_L = 142.6\,°R$

$0.74\,°R$ SUBCOOLING

$R_0 = 0.0461$ INCHES

o - EXPERIMENTAL DATA
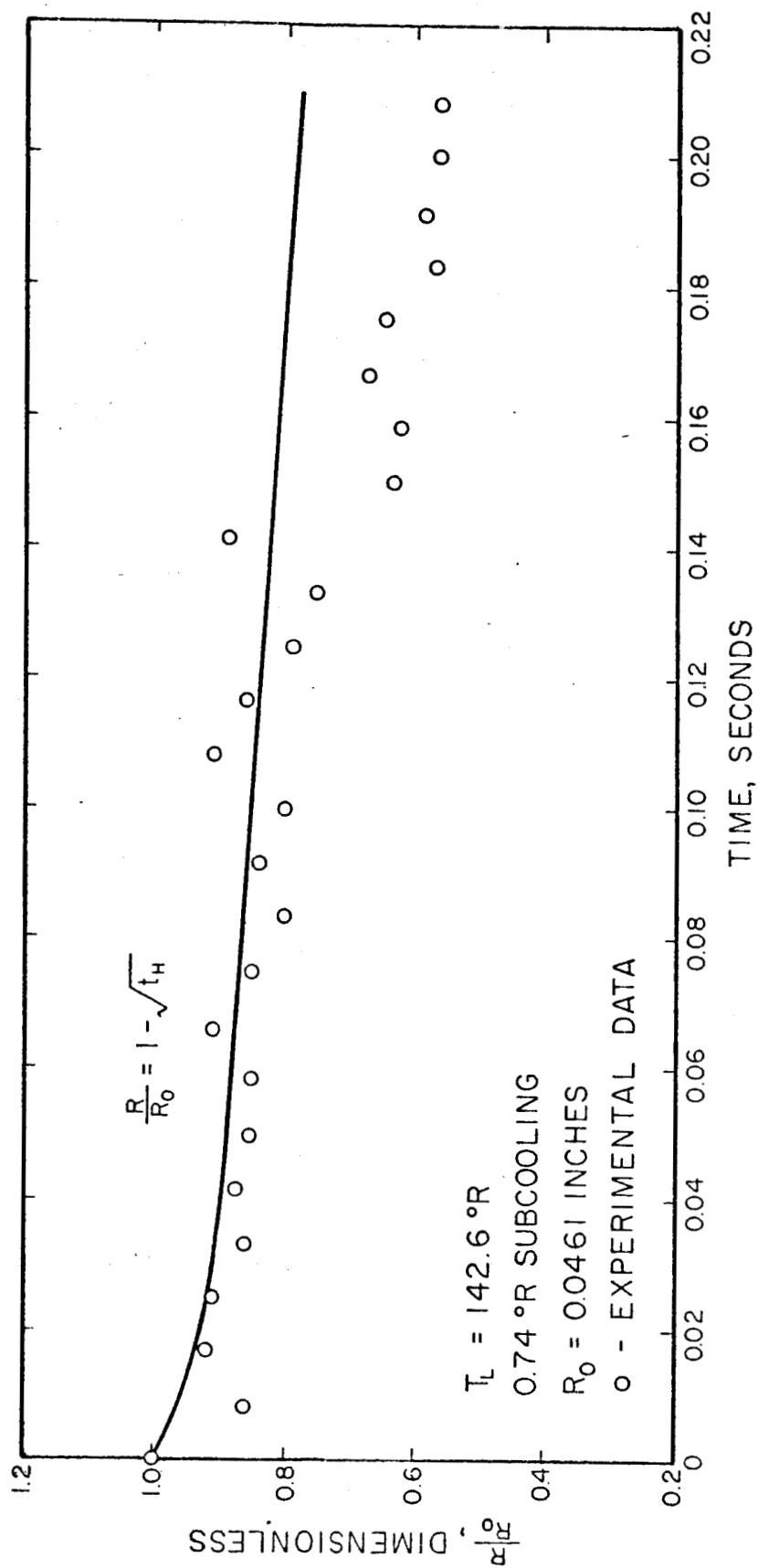
Figure 20. Bubble Collapse – Bubble No. 21
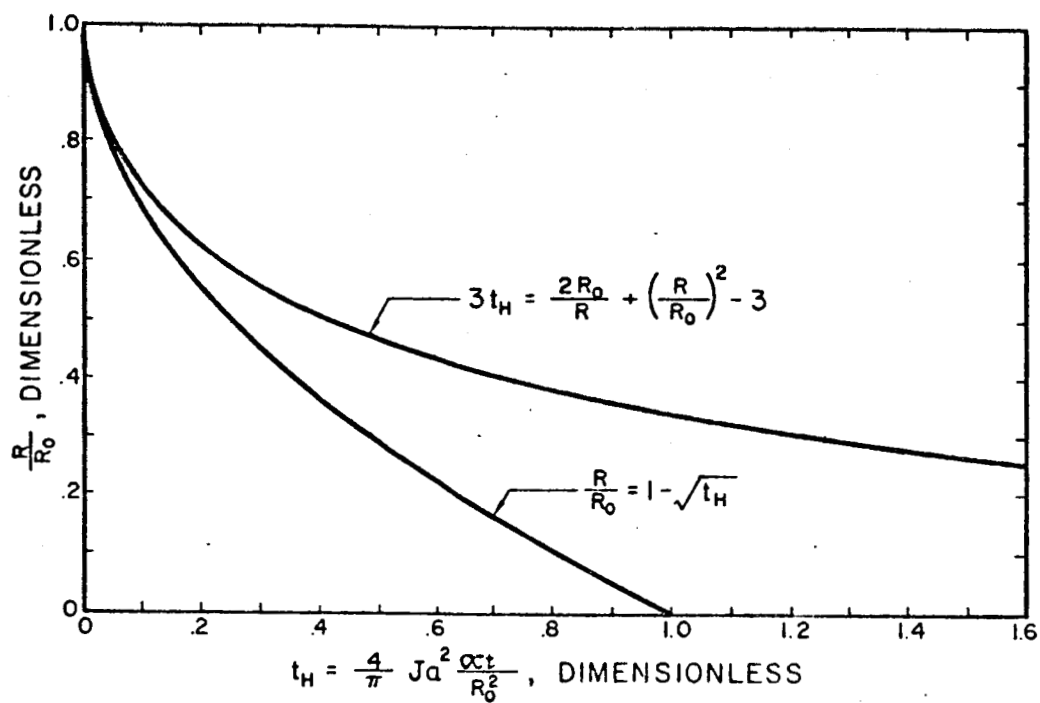
a. Comparison of Two Collapse Equations.

$$3t_H = \frac{2R_0}{R} + \left(\frac{R}{R_0}\right)^2 - 3$$

$$\frac{R}{R_0} = 1 - \sqrt{t_H}$$

$$t_H = \frac{4}{\pi} Ja^2 \frac{\alpha t}{R_0^2}, \text{ DIMENSIONLESS}$$
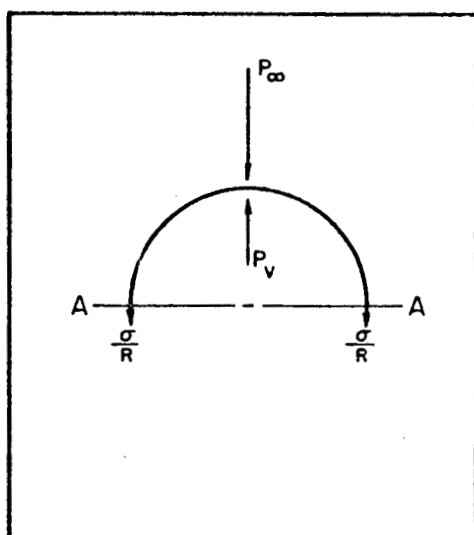
b. Static Pressures on Free Body Diagram of a Vapor Bubble. (Two Dimensional View)

$$F_D = C_P \frac{\rho_L V^2}{2g_c} (\pi R^2)$$

$$F_b = \frac{4}{3} \pi R^3 \frac{g}{g_v} (\rho_L - \rho_v)$$
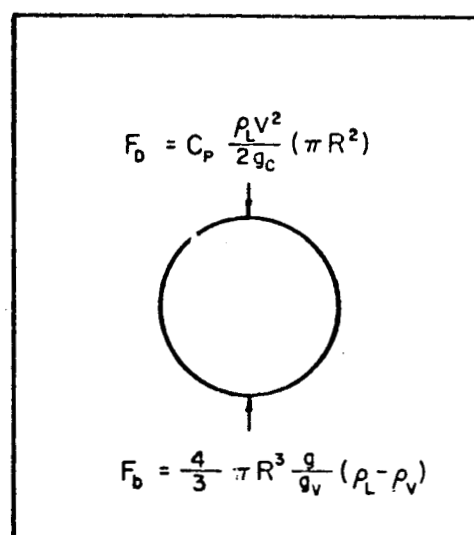
c. Forces on a Vapor Bubble in a Gravitational Field.

Figure 21.   Considerations in Bubble Collapse

found to be inadequate in the correlation of the experimental data. Using the theoretical Equation (VI-3) as a guide, a search was made to determine the additional parameters necessary to improve the correlation of data. This study eventually resulted in the correlation Equation (VI-10).

The results of Florschuetz and Chao indicated that the experimental results available were insufficient to resolve the basic dependency of the data upon subcooling. The present experiment with liquid nitrogen gave the same conclusion. However, the collapse rate for liquid nitrogen increased, beyond that predicted by theory, near the end of collapse. This result was noted in Figures 11 through 20. This phenomenon of higher collapse rate near the end of collapse was absent in the data of Florschuetz and Chao.

Three possible sources for the deviation between the two experimental works were found: (1) two different fluids, water and liquid nitrogen, were used, (2) the bubble diameters of Florschuetz and Chao were approximately ten times larger than those of the present study, and (3) Florschuetz and Chao used a drop-chamber to eliminate the gravity effect while the gravity effect existed in the present study. Since one object of this investigation was to demonstrate that no difference exists between non-cryogens and liquid nitrogen, the first possible source of deviation was reserved to be studied only if no other reason could be found for this conflict.

The bubble radii of the present study were an order of magnitude smaller than those of Florschuetz and Chao. Therefore, the surface tension pressure, $2\sigma/R$, was an order of magnitude higher for the present study. The static pressures acting on the vapor bubble, given in

Figure 21b, are

$$P_R = P_v(T_w) - P_\infty(t) - 2\sigma/R. \tag{VI-4}$$

The surface tension was neglected in the theoretical work. The effect of including this term in the theoretical solution would be the prediction of higher collapse rate which could explain the observed results. The order of magnitude of the terms of Equation (VI-4) was considered for the case where the surface tension effect would be greatest. The smallest radius was measured in the data of Figure 12. For this result, the liquid pressure, $P_\infty(t)$, was 23.148 psia. Using Figure 12, Equation (C-18), and the thermodynamic properties for nitrogen, $P_v(T_w)$ was approximately 19.8 psia (by a curve fitting approximation). For the smallest value of R, 0.0157 inches, the surface tension term was 0.006 psia. The static force neglecting surface tension was 0.18 percent less than the force when the surface tension term was included. This error could not account for the large deviation between experiment and theory.

A vapor bubble in a liquid must have a velocity with respect to the bulk liquid when the system is in a gravitational field. Figure 21c shows an ideal case of a vapor bubble with the buoyancy forces and drag forces acting on it. The photographic records of vapor bubbles were used to measure the velocity of various sizes of vapor bubbles with respect to the bulk liquid. The value of C_D of Figure 21c was determined to be approximately 0.4 from the drag coefficient data of Binder (30) and the range of velocities measured. Newton's second law was applied to the vapor bubble to give the equation of motion of the bubble with respect to the bulk liquid,

$$\frac{dV_b}{dt} = \frac{g\,\rho_L}{\rho_V} - \frac{0.15\,\rho_L}{R\,\rho_V}\,V_b^2$$

where $\quad V_b$ = bubble velocity with respect to the bulk liquid

and $\quad\quad$ g = local acceleration of gravity.

One integration of this equation together with the boundary condition,

when t = 0, $\quad V_b = 0$,

gives

$$V_b = \sqrt{\frac{gR}{0.15}}\left[\frac{e^{Dt} - 1}{e^{Dt} + 1}\right] \tag{VI-5}$$

where

$$D = 2\sqrt{\frac{gR}{0.15}}\,.$$

The asymptotic solution of Equation (VI-5) for large t is

$$V_b = 50.76\,\frac{(\text{inch})^{\frac{1}{2}}}{\text{second}}\,\sqrt{R} \tag{VI-6}$$

where $\quad$ R is in inches.

This equation compared favorably with the experimental measurements. Eckert and Drake (31, page 250) discussed the heat transfer to a sphere, of constant diameter, moving through a fluid. The equation for the Nusselt number for this type sphere was

$$Nu_d = 0.37\,(Re_d)^{0.6}(Pr)^{1/3}\,. \tag{VI-7}$$

Assuming that a vapor bubble has a fixed diameter instantaneously, the heat transfer rate from the bubble wall, using the above value for Nu_d,

is given by:

$$\dot{q} = \frac{Nu_d\, k_L}{2R}\, (4\,\pi\, R^2)(\Delta T). \qquad\qquad (VI\text{-}8)$$

The heat transfer rate used in Equation (B-2), a boundary condition for the energy equation, was

$$\dot{q} = \frac{4\,\pi\, L}{3}\, \frac{d}{dt}\, [R^3(t)\, \rho_V]. \qquad\qquad (VI\text{-}9)$$

An order of magnitude comparison of the heat transfer predicted by Equations (VI-8) and (VI-9) was made for Figure 12 from the theoretical curve at time equal 0.08 seconds. This point on the theoretical curve was marked. Equation (VI-9) gave $\dot{q} = 8.68 \times 10^{-6}$ Btu/sec. and Equation (VI-8) gave $\dot{q} = 4.8 \times 10^{-5}$ Btu/sec. This analysis indicated that the motion of the bubble relative to the bulk liquid caused more heat to be transferred away from the bubble wall than that assumed in the theoretical solution. This was only an order of magnitude estimate and gave only a trend of what was occurring.

In heat transfer controlled collapse, the collapse rate increases with increase in heat transfer rate. Therefore, a proper correlation of experimental data should include a parameter functionally related to the heat transfer due to bubble motion. The parameter, t_H, initially used in the correlation, contained all the parameters of Equation (VI-8) except bubble velocity, bubble radius, Prandtl number, and viscosity. The Prandtl number and viscosity were approximately constant for the temperature range of this study. Equation (VI-5) gave the bubble velocity with respect to the liquid to be a function of bubble radius alone. The new parameter for correlation resulted from a modification of the original parameter and was:

$$t'_H = t_H(R_o/R)^2.$$

This modified parameter, t'_H, was used to correlate the experimental data.

A plot of R/R_o versus t'_H was made for all the data on bubble collapse. The application of correlating techniques to this plot resulted in the correlation,

$$R/R_o = 1 - \sqrt{t_R} \qquad\qquad \text{(VI-10)}$$

where
$$t_R = t'_H(2.6°R/T)^{1.5}.$$

All data was compared to this correlation in Figure 22. Two 20% error bands are drawn around the correlation Equation (VI-10).

This type of correlation leaves much to be desired in terms of completeness of solution. The correlation was shown to be valid only for heat transfer controlled collapse in liquid nitrogen subcooled less than four degrees Rankine in the earth's gravitational field. To gain more insight to a complete solution, the mechanisms of heat transfer from the bubble wall must be more clearly understood. Equation (VI-8) resulted from the experimental correlation of data. Therefore, advances in the theoretical area must be proceeded by a basic study of the heat transfer process at the bubble wall. The experimental method of producing a more complete solution requires the study of collapsing vapor bubbles in a wide variety of fluids, fluid conditions, and gravitational fields. The present experimental knowledge is limited to this investigation and the work of Florschuetz and Chao. Because the amount of effort involved in obtaining a complete solution exceeded the time

$$t_s = \sqrt{\frac{\pi}{12}} \; Ja^2 \; \frac{\alpha t}{R_0^2} \; \left(\frac{R_0}{R}\right)^2 \left(\frac{2.6 \cdot R}{\Delta T}\right)^{1.6}, \text{DIMENSIONLESS}$$
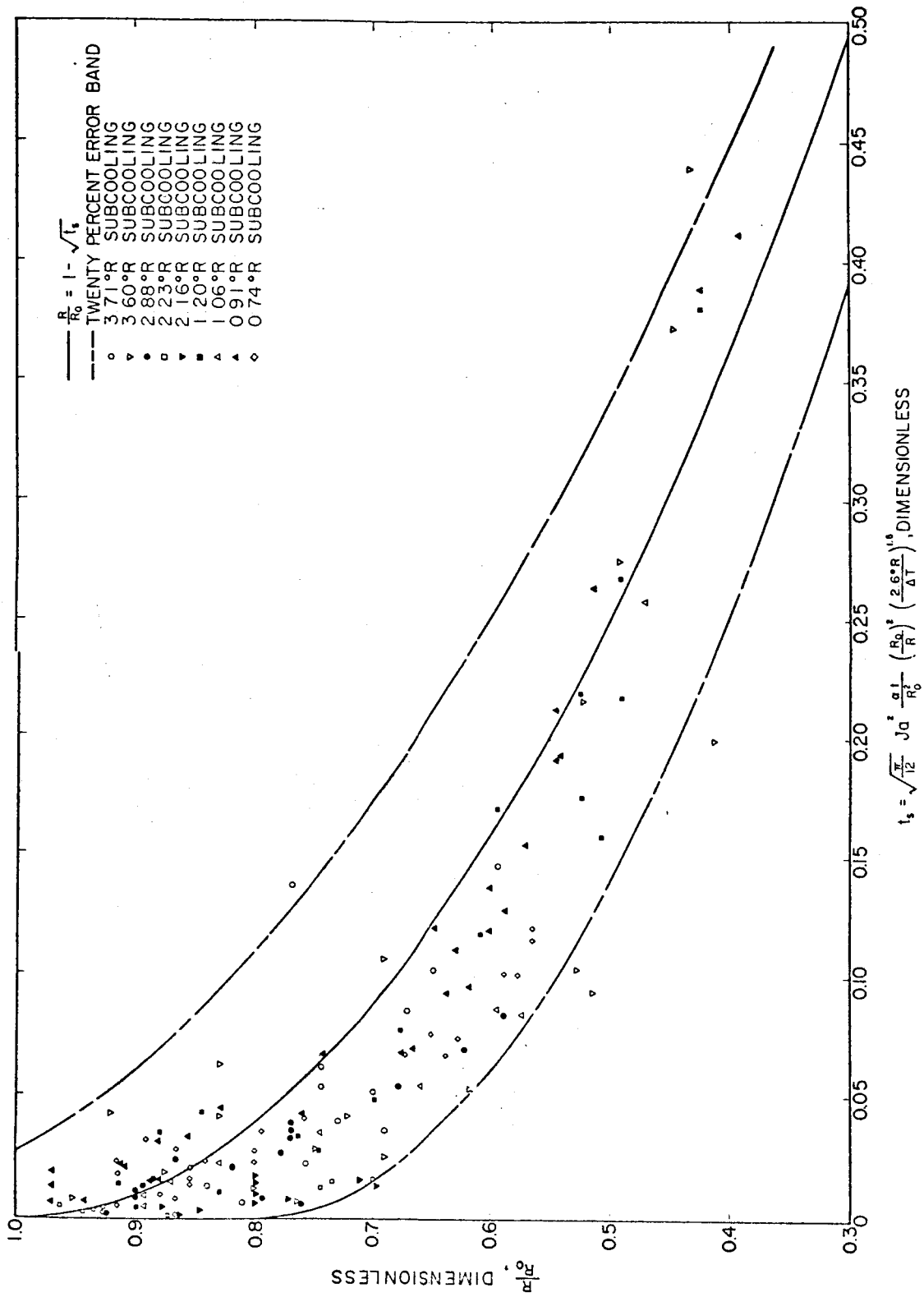
Figure 22. Bubble Collapse Correlation

capabilities of this investigation, the present study terminated with the correlation Equation (VI-10).

Bubble Growth With a Variable Liquid Pressure

Bubble histories were measured for three bubbles initially collapsing in a subcooled liquid then subjected to a decrease in liquid pressure. The pressure decreased from 22.5 psia to 16.5 psia in 0.13 seconds. The diameter-time measurements are presented in Appendix D along with the pressure-time measurements. Figures 23, 24, and 25 were plotted from this data. In Figure 23, the initial time was selected to show a portion of the bubble collapse before the pressure decrease occurred.

The computer program of Figure 26 was written to calculate the bubble growth for this transient pressure (shown in Figure 27 of Appendix D) for an inertia controlled process. Inertia controlled growth or collapse was defined to be growth or collapse predicted by Equation (C-1) neglecting the effect of change in bubble wall temperature. The computer was used in solving Equation (C-1) by a Runge-Kutta numerical integration method. The results of this solution are also shown in Figure 23.

A comparison of the experimental results with the inertia controlled solution demonstrates that the bubble growth was not inertia controlled. A theoretical solution, which would predict the experimental results, could be obtained only by the simultaneous solution of Equations (C-1) and (C-3). To solve these equations by numerical methods, Equation (C-3) must be rearranged to avoid the appearance of a zero in the denominator. The technique required was an integration by parts
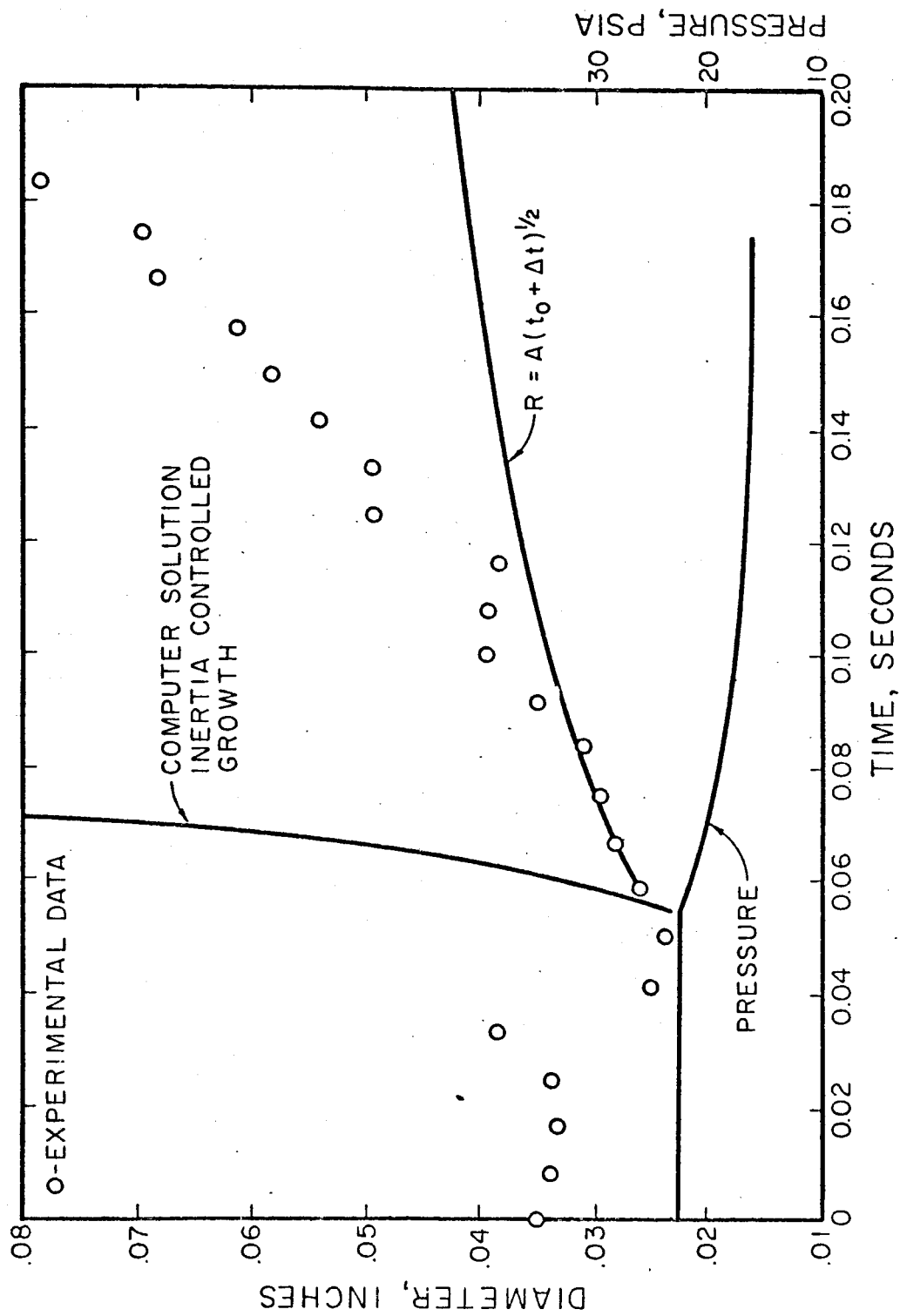
Figure 23. Bubble Growth With Variable Pressure - Bubble No. 22
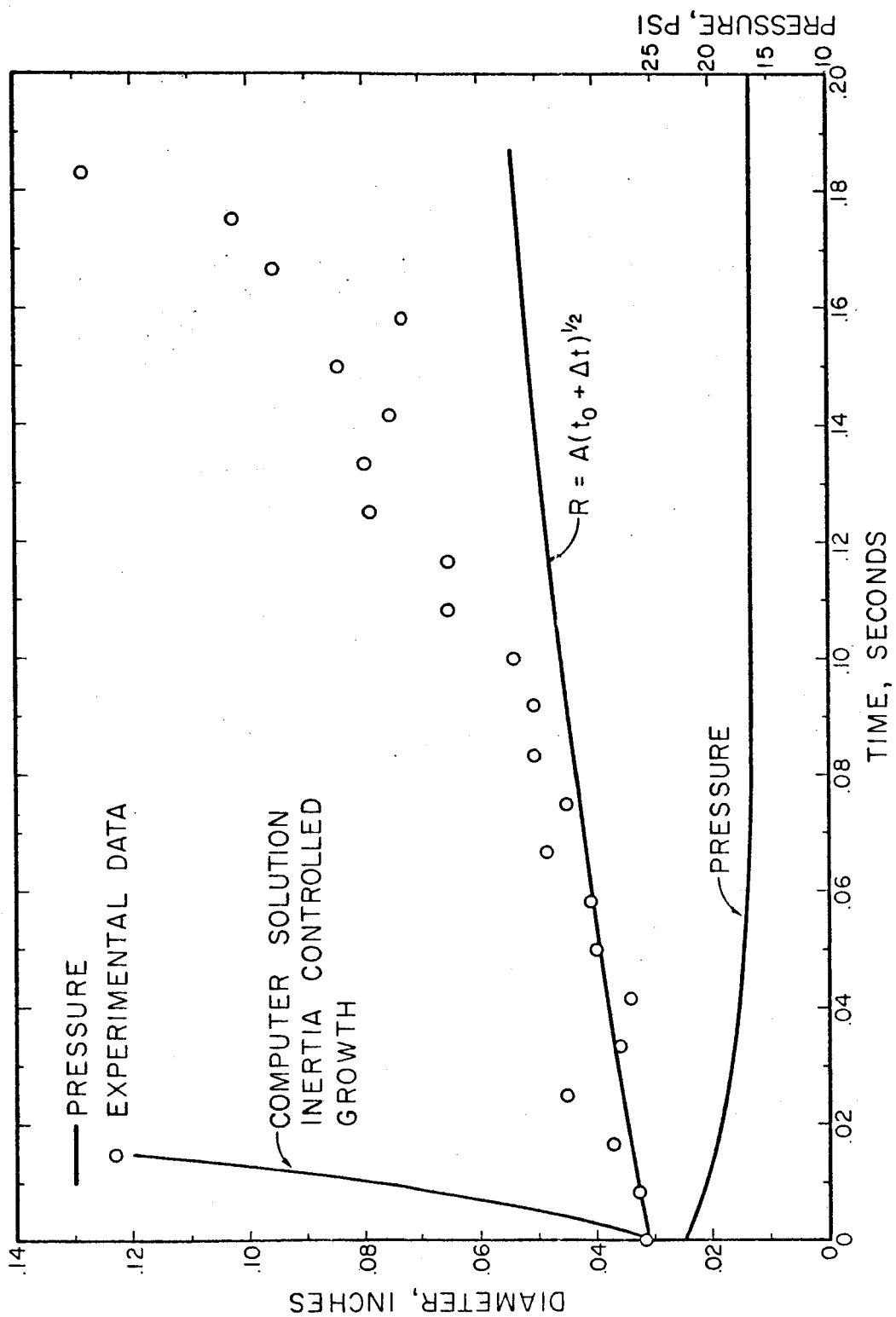
Figure 24. Bubble Growth With Variable Pressure – Bubble No. 23

performed on the integrand. Upon integration by parts and assuming ρ_v constant, Equation (C-3) becomes

$$T_w(t) - T_o = - \sqrt{\frac{\alpha}{\pi}} \frac{2}{3} \frac{L}{k_L} \int_0^t \left\{ \int_x^t R^4(y)dy \right\}^{\frac{1}{2}} \left\{ \frac{3\rho_v}{R^2} \overset{\infty}{R} - \frac{6\rho_v \dot{R}^2}{R^3} \right\} dx \; .$$

(VI-11)

Equation (C-1) was solved numerically for the case where the liquid pressure and the vapor pressure were assumed to be constant. This solution is the Rayleigh solution and sources of its solution are available (6) (7). The numerical solution written in this thesis was shown to converge with less than one percent error when the step size in time was less than 10^{-6} seconds. Since Equation (C-1) must be solved simultaneously with Equation (VI-11), the time step for both problems must be less than one microsecond. The numerical solution of Equation (VI-11) involves the storage of each of the variables R, $\dot{R}$, and $\ddot{R}$ for each value assigned in time. This would require 600,000 storage spaces to integrate to time equal 0.2 seconds for step sizes of one microsecond. The variable limit of integration inside the integral sign of Equation (VI-11) requires that the integral be calculated from time equal zero for each increment of the time variable. Storing R, $\dot{R}$, and $\ddot{R}$ in blocks on tape is the only method of obtaining the storage capacity required. When time in the problem is 0.1 seconds, one increment on time requires approximately one hundred exchanges of information between core and tape. One hundred thousand iterations remain to be made at this time. The time requirement on the computer is so large that the simultaneous solution of Equations (C-1) and (VI-11) was not completed.

The experimental data was bounded by fitting an equation for bubble

growth through the first two data points occurring after the decrease in pressure started. These two data points furnished the information for determining the values of t_o and A from the two equations below:

$$R_o = A(t_o)^{\frac{1}{2}}$$

and

$$R_1 = A(t_o + 1/120)^{\frac{1}{2}} .$$

The A and t_o from the above equations determined the equation:

$$R = A(t_o + \Delta t)^{\frac{1}{2}}. \qquad (VI-12)$$

This equation was also plotted in Figure 23.

One reason for showing Equation (VI-12) in Figure 23 was to demonstrate that the parameter A was not constant for variable pressure conditions. From Equation (VI-1), A was shown to depend on ΔT which depends on $P_V(T_W) - P_\infty(t)$. Since this collapse was not inertia controlled, the effect of $P_V(T_W)$ decreasing was large enough to be considered. $P_\infty(t)$ was measured to be decreasing. The plot in Figure 23 demonstrated that $P_V(T_W)$ must be decreasing more slowly than $P_\infty(t)$ because A must increase to fit the experimental data. In order for A to increase, ΔT must increase. The pressure difference must increase if ΔT is to increase.

This data on bubble growth with relatively slow transient liquid pressure was presented because no other data of this type has been found in the literature. Data of this type must be made available to obtain a knowledge of bubble dynamics on a low velocity fluid flowing through valves and piping.

Persistence Time of Vapor Bubbles

When a vapor bubble collapses to a point where it is no longer visible, the heat of condensation remains stored in the liquid in the area where the bubble was located. Under some conditions of inertia controlled collapse, the energy stored in this liquid has been large enough to cause the bubble to reappear or rebound (2). In other cases the bubble rebound may result from a combination of this energy and a liquid pressure decrease created by a valve or pipe fitting in a flowing stream. A bubble containing an inert gas would always be susceptible to these conditions because the inert gas would never completely collapse. Complete collapse is defined in this thesis to mean collapse to the point where no nucleation site remains. An inert gas that is not soluble in the fluid would always be a nucleation site. Since vapor bubbles create problems in the pumping of liquids and in cavitation damage, a criterion for determining the time required for a vapor bubble to collapse completely should be established.

Knapp and Hollander (2) established one set of liquid conditions where rebound did occur. These conditions prevailed for inertia controlled collapse with no reduction in liquid pressure. In the present investigation of heat transfer controlled collapse, several bubbles were observed to collapse and disappear before a liquid pressure reduction occurred. Any tendency to rebound should have been realized. The last bubble to disappear before the pressure drop occurred had the best chance to rebound. This bubble had a diameter of 0.0225 inches 4/120 seconds before the pressure drop of Figure 23 started. At 3/120 seconds before the pressure drop, the diameter was 0.0202 inches. The

diameter was 0.0157 inches at 2/120 seconds, and the bubble was visible but not distinct at 1/120 seconds before the pressure drop. The bubble disappeared completely in the next 1/120 seconds; the pressure drop occurring at that time did not cause the bubble to rebound.

From this limited amount of data, bubbles collapsing by a heat transfer controlled process with less than four degrees Rankine subcooling have no tendency to rebound once they are no longer visible. The heat transfer process removes enough energy to cause complete collapse.

Knowledge of fluid conditions where bubble rebound did occur and where rebound did not occur is available. Additional studies of bubbles collapsing with higher degrees of subcooling must be made to determine the exact fluid conditions necessary to insure that a bubble will not rebound.

CHAPTER VII

CONCLUSIONS AND RECOMMENDATIONS

Conclusions

Much of the knowledge on the dynamic behavior of vapor bubbles in non-cryogens can be applied to the dynamic behavior of vapor bubbles in liquid nitrogen. It is most likely that it is safe to extend this knowledge to include most cryogens with the most probable exception being liquid helium II. Liquid helium II has exhibited so many unexpected phenomena that only experimental evidence can determine the reliability of applying theories to its behavior.

Solutions of the bubble dynamics problem for asymptotic bubble growth in a superheated liquid can be used with confidence. Excellent results were obtained using the Plesset-Zwick solution,

$$R = \sqrt{\frac{12}{\pi}} \; \frac{k_L \, \Delta T}{L \, \rho_V \sqrt{\alpha}} \, t^{\frac{1}{2}} \; .$$

The present technique for correlating data in nucleate pool boiling heat transfer is to base the Reynold's number on bubble diameter and bubble wall velocity,

$$Re = \frac{2 \rho_L \, R \, \dot{R}}{\mu_L} \; .$$

Zuber and Fried (32) showed that their correlation, using this Reynold's

74

number was valid for both subcooled and superheated nucleate pool boiling data. A correct calculation of bubble radius and bubble wall velocity can be used by the engineer as an important aid in the correlation of nucleate pool boiling data.

Theoretical solutions for heat transfer controlled bubble collapse in a subcooled liquid must be used with caution. Existing solutions depend on the degree of subcooling, external body forces, and bubble size. The dependency on these variables is not well established and the solutions can be applied only in physical situations where all of the boundary conditions are met. Florschuetz and Chao (1) suggested two theoretical solutions:

$$3 \, t_H = \frac{2 \, R_o}{R} + \left(\frac{R}{R_o}\right)^2 - 3 \qquad\qquad (VII-1)$$

and

$$R/R_o = 1 - \sqrt{t_H}. \qquad\qquad (VII-2)$$

They plotted these two solutions (see Figure 21a) on one plot and compared all of their data to these solutions. For subcooling between 8 and 13 degrees Kelvin the data were approximated by Equation (VII-1), but for subcooling between 5 and 6 degrees Kelvin the data were approximated by Equation (VII-2). This experimental data deviated from the respective theoretical curves by less than sixty-five percent. All of the experimental data of the present investigation deviated from Equation (VII-2) by less than sixty percent. An equation derived from the data of this experiment,

$$R/R_o = 1 - \sqrt{t_R}, \qquad\qquad (VII-3)$$

fits ninety-two percent of all the data points with a deviation less than twenty percent. None of these correlations can be strongly recommended for the prediction of heat transfer controlled collapse. Equations (VII-1) and (VII-2) can be expected to predict results with sixty percent error, and Equation (VII-3) has been verified only for liquid nitrogen subcooled less than four degrees Rankine in the earth's gravitational field.

Bubble dynamics with variable liquid pressure was studied experimentally. Bubble growth with decreasing liquid pressure is experimentally shown to lie between growth predicted by an inertia controlled process and that predicted by bubble growth in a superheated liquid with constant liquid pressure. The equation of motion and the energy equation

$$R \, \ddot{R} + 1.5\dot{R}^2 = \frac{P_v(T_w) - P_\infty(t)}{\rho_L} \qquad \text{(VII-4)}$$

and

$$T_w(t) - T_o = - \sqrt{\frac{\alpha}{\pi}} \, \frac{L}{3k} \int_0^t \frac{\frac{d}{dx}[R^3(x) \, \rho_V]}{\left\{\int_x^t R^4(y)dy\right\}^{\frac{1}{2}}} \, dx \qquad \text{(VII-5)}$$

must be solved simultaneously to determine whether a theoretical solution can be used to predict bubble dynamics with variable liquid pressure. The computer storage requirement for the simultaneous solution of these equations was too large to be handled in the present investigation.

Persistence time in this investigation is defined to be the time during which a bubble has the potential to rebound after it has apparently collapsed. The persistence time for a vapor bubble collapsing in

liquid nitrogen subcooled less than four degrees Rankine was found to be less than 1/120 seconds. Rebound was not observed. No numerical value was measured for the persistence time of completely inertia controlled collapse in water, but the persistence time is large (2). Rebound did occur in the experimental work of Knapp and Hollander. From the above definition of persistence time, a vapor bubble containing an inert gas has an infinite persistence time if solubility of the inert gas may be neglected.

Recommendations

A reliable and accurate computer method for simultaneously solving Equations (VII-4) and (VII-5) is a necessity for additional work in bubble dynamics. This solution would be a step toward resolving the problem of temperature controlled collapse. The solution is also necessary in the study of bubble dynamics with variable liquid pressure.

A careful revision of the theoretical equations governing temperature controlled collapse is suggested. The error in the present theory results either from neglecting the effect of some of the terms of Equations (VII-4) and (VII-5) or from an incomplete analysis of the heat transfer process at the bubble wall. The error of neglecting some terms of the equations could be determined by the computer solution suggested above; however, a combination of both errors should be considered.

An experimental study of heat transfer controlled collapse for a wide range of different liquids, different degrees of subcooling, and different gravitational fields would aid the theoretical analysis suggested. Since experimental verification must be available for the proof of any theory, the experimental investigation could precede the

theoretical investigation. This experimental study should concurrently provide data on persistence time by having a pressure drop occur near the end of each experimental observation. Knowledge of the magnitude of subcooling, at which bubble rebound occurs, would allow the investigator to know the conditions for complete bubble collapse.

A SELECTED BIBLIOGRAPHY

(1) Florschuetz, L. W., and B. T. Chao. "On the Mechanics of Vapor Bubble Collapse," Trans. ASME. Paper No. 64-HT-23.

(2) Knapp, R. T., and A. Hollander. "Laboratory Investigations of the Mechanism of Cavitation," Trans. ASME. Vol. 70 (1948) 419-35.

(3) Besant. Hydrostatics and Hydrodynamics. Cambridge, 1859.

(4) Rayleigh, Lord. Phil. Mag. Vol. 34 (1917) 94-98.

(5) Zwick, S. A. "The Growth and Collapse of Vapor Bubbles." Jet Propulsion Laboratory Report 21-19. December, 1954, AD No. 54059.

(6) Fritz, C. G. "Study of Gas Bubble Dynamics (Part 1)." George Marshall Space Flight Center, IN-P and VE-P-64-5.

(7) McNieto, J., and W. Smith. "An Exact Solution of the Rayleigh-Besant Equation." Heat Transfer and Fluid Mechanics Laboratory, University of Michigan, October (1962) Internal Report No. 18.

(8) Plesset, M. S., and S. A. Zwick. "A Nonsteady Heat Diffusion Problem With Spherical Symmetry." Journal of Applied Physics. Vol. 23 (1952) 95-98.

(9) Zwick, S. A., and M. S. Plesset. "On the Dynamics of Small Vapor Bubbles in Liquids." Journal of Mathematics and Physics. Vol. 33 (1955) 308-30.

(10) Hsieh, D. "Some Analytical Aspects of Bubble Dynamics." Trans. ASME. (1965) Paper No. 65-FL-19.

(11) Plesset, M. S. "The Dynamics of Cavitation Bubbles." Journal of Applied Mechanics. Vol. 71 (1949) 277-82.

(12) Ellion, M. E. "A Study of the Mechanism of Boiling Heat Transfer." Jet Propulsion Laboratory Report Memo. 20-88, Calif. Inst. Tech., 1954.

(13) Gunther, F. C. "Photographic Study of Surface-Boiling Heat Transfer to Water With Forced Convection." Trans. ASME. Vol. 73 (1951) 115-23.

(14) Levenspiel, O. "Collapse of Steam Bubbles in Water," _Ind. and Eng. Chem._ Vol. 51, No. 6 (1959) 787-90.

(15) Forster, H. K. "Diffusion in a Moving Medium With Time-Dependent Boundaries," _A. I. Ch. E. Journal._ Vol. 4 (1957) 535-38.

(16) Forster, H. K., and N. Zuber. "Growth of a Vapor Bubble in a Superheated Liquid," _Journal of Applied Physics._ Vol. 25 (1957) 474-78.

(17) Scriven, L. E. "On the Dynamics of Phase Growth," _Chem. Engr. Journal._ Vol. 10 (1959) 1-13.

(18) Birkhoff, G., R. S. Margulies, and W. A. Horning. "Spherical Bubble Growth," _The Physics of Fluids._ Vol. 1, No. 3, (1958) 201-04.

(19) Dergarabedian, P. "Observations on Bubble Growth in Various Superheated Liquids," _Journal of Fluid Mechanics._ Vol. 9, Pt. 1 (1960) 39-48.

(20) Dergarabedian, P. "The Rate of Growth of Vapor Bubbles in Superheated Water," _Journal of Applied Mechanics._ Vol. 75 (1953) 537-45.

(21) Fareuff, C. E., E. A. McLean, and V. E. Scheffer. "Some Aspects of Vapor Bubbles," _Journal of Applied Physics._ Vol. 29, No. 1 (1958) 80-84.

(22) Semeria, R. L. "An Experimental Study of the Characteristics of Vapor Bubbles," _Proc. Instr. Mech. Engrs._ Symposium of Two-Phase Flow (1962) 57-65.

(23) Staniszewski, B. M. "Nucleate Boiling Bubble Growth and Departure." August, 1959, AD-227262.

(24) Zuber, N. "The Dynamics of Vapor Bubbles in Nonuniform Temperature Fields," _International Journal of Heat and Mass Transfer._ Vol. 2 (1961) 83-98.

(25) Chelton, D. B., and D. B. Mann. "Cryogenic Data Book." March, 1959, AD-208155.

(26) _Temperature: Its Measurement and Control in Science and Industry._ Vol. I, Amer. Inst. of Physics, N. B. S. National Research Council.

(27) Strobridge, T. A. "The Thermodynamic Properties of Nitrogen From 114 to 540 R Between 1.0 and 3000 psia." N. B. S. Technical Note 129 A, February, 1963.

(28) Scott, R. B. _Cryogenic Engineering_. Princeton, New Jersey:
        D. van Nostrand, 1959.

(29) Johnson, U. J. "A Compendium of the Properties of Materials at
        Low Temperatures (Phase I), Part 1. Properties of Fluids."
        WADD Technical Report 65-56. Part 1. October, 1962.

(30) Binder, R. C. _Fluid Mechanics_. 2nd ed. New York, N. Y.:
        Prentice-Hall, 1954.

(31) Eckert, E. R. G., and R. M. Drake, Jr. _Heat and Mass Transfer_.
        2nd ed. New York, N. Y.: McGraw-Hill, 1959.

(32) Zuber, N., and E. Fried. "Two-Phase Flow and Boiling Heat Trans-
        fer to Cryogenic Liquids." _ARS Journal_. Vol. 32 (1962)
        1332-40.

LIST OF SYMBOLS

A = Constant

A(t) = Variable of integration

$a = \sqrt{(2\sigma/\rho_L R^3_o)}$

B(t) = Variable of integration

c = Specific heat

C(t) = Variable of integration

D = Bubble diameter

E = Internal energy of an
element of mass

g = local acceleration of
gravity

$h = \int_o^t R^4(t)dt$

Ja = Jacob number, $\rho_L c_L \Delta T / \rho_v l$

K = thermal conductivity

l = heat of vaporization

L = Laplace operator

$m = \frac{1}{3}[r^3 - R^3(t)]$

Nu = Nusselt number

P = Pressure

$\Delta P = P_v(T_w) - P_\infty(t)$

Pr = Prandtl number

$\dot{q}$ = Heat generation rate per
unit volume

r = Spatial coordinant

R = Bubble radius

$\dot{R}$ = Bubble velocity

$\ddot{R}$ = Bubble acceleration

R(t) = Bubble radius dependent
on t

R(x) = Bubble radius dependent
on x

R(y) = Bubble radius dependent
on y

Re = Reynold's number

s = Laplace variable

t = Time

T = Temperature

T_o = Initial temperature of the
liquid

T(t) = Bubble wall temperature

$\Delta T = T_\infty - T_{sat}$

T_{sat} = Saturation temperature at
$P_{\infty L}$

82

$T(R,t)$ = Bubble wall temperature

$t_H = \frac{4}{\pi} Ja^2 \tau$

$t'_H = t_H (R_o/R)^2$

$t_R = t'_H (2.6^\circ R/T)^{1.5}$

$U = \int_0^m \theta dm$

$\bar{V}$ = Vector liquid velocity

V_b = Linear bubble velocity

$V(R)$ = Radial bubble wall velocity

x = Dummy integration variable

y = Dummy integration variable

$z = (R/R_o)^3$

Greek Letters

α = Thermal diffusivity

$\gamma = R/R_o$

$\eta(t)$ = Heat source per unit volume

$\theta = T - T_o$

μ = Dynamic viscosity

ρ = Density

σ = Surface tension

$\tau = \alpha t/R_o^2$

φ = Velocity potential

Subscripts

d = Diameter

L = Liquid

o = Initial

s = Saturation

v = Vapor

V = Volume

w = Bubble wall

∞_L = Liquid away from the bubble

APPENDIX A

DEVELOPMENT OF THE GOVERNING EQUATIONS

An understanding of the equations governing bubble dynamics can be obtained by following the development of these equations from the continuity equation, the equation of motion, and the energy equation. The development given by Zwick (5) is followed in this appendix. A discussion of the assumptions made in developing these equations for application to liquid nitrogen is given.

Continuity Equation

The Eulerian continuity equation for a liquid or vapor is

$$\frac{d\rho}{dt} + \nabla \cdot \rho \vec{V} = 0 \tag{A-1}$$

where

$\frac{d}{dt}$ = the total derivative with respect to time

ρ = density

and

$\vec{V}$ = vector velocity, $u\vec{i} + v\vec{j} + w\vec{k}$ for rectangular coordinates.

Equation of Motion

The equation of motion, neglecting external body forces, becomes

$$\rho \frac{d\vec{V}}{dt} = \nabla \cdot \vec{P} \tag{A-2}$$

where

$$\vec{P} = -p\vec{I} - \frac{2}{3}\mu(\nabla \cdot \vec{V})\vec{I} + \mu(\nabla;\vec{V} + \vec{V};\nabla)$$

p = normal pressure

μ = viscosity

$\vec{I} = \vec{i};\vec{i} + \vec{j};\vec{j} + \vec{k};\vec{k}$, for rectangular coordinates and $\vec{I} \cdot \vec{A} = \vec{A}$

$\nabla;\vec{V}$ = dyadic product

and

$\vec{V};\nabla$ = dyadic product conjugate to $\nabla;\vec{V}$.

That is, for rectangular coordinates:

$$\nabla;\vec{V} = (\vec{i}\,\frac{\partial}{\partial x} + \vec{j}\,\frac{\partial}{\partial y} + \vec{k}\,\frac{\partial}{\partial z});\ (u\,\vec{i} + v\,\vec{j} + w\,\vec{k})$$

$$= \vec{i};\vec{i}\,\frac{\partial u}{\partial x} + \vec{i};\vec{j}\,\frac{\partial v}{\partial x} + \vec{i};\vec{k}\,\frac{\partial w}{\partial x}$$

$$\vec{j};\vec{i}\,\frac{\partial u}{\partial y} + \vec{j};\vec{j}\,\frac{\partial u}{\partial y} + \vec{j};\vec{k}\,\frac{\partial w}{\partial y}$$

$$\vec{k};\vec{i}\,\frac{\partial u}{\partial z} + \vec{k};\vec{j}\,\frac{\partial v}{\partial z} + \vec{k};\vec{k}\,\frac{\partial w}{\partial z}$$

and

$$\vec{V};\nabla = \vec{i};\vec{i}\,\frac{\partial u}{\partial x} + \vec{j};\vec{i}\,\frac{\partial u}{\partial y} + \vec{k};\vec{i}\,\frac{\partial u}{\partial z}$$

$$\vec{i};\vec{j}\,\frac{\partial v}{\partial x} + \vec{j};\vec{j}\,\frac{\partial v}{\partial y} + \vec{j};\vec{k}\,\frac{\partial v}{\partial z}$$

$$\vec{i};\vec{k}\,\frac{\partial w}{\partial x} + \vec{j};\vec{k}\,\frac{\partial w}{\partial y} + \vec{k};\vec{k}\,\frac{\partial w}{\partial z}\ .$$

Then

$$\nabla \cdot \vec{P} = -\nabla p - \frac{2}{3}\nabla[\mu(\nabla \cdot \vec{V})] + 2\nabla[\mu(\nabla \cdot \vec{V})] - \nabla \times \mu(\nabla \times \vec{V}).$$

And for constant viscosity

$$\nabla \cdot \vec{P} = -\nabla p + \frac{4}{3}\mu\nabla(\nabla \cdot \vec{V}) - \mu\nabla \times(\nabla \times \vec{V}).$$

If the flow is irrotational, then $\nabla \times \vec{V} = 0$, and

$$\nabla \cdot \vec{P} = -\nabla p + \frac{4}{3}\mu\nabla(\nabla \cdot \vec{V}) \qquad\qquad (A-3)$$

For an incompressible fluid, $\nabla \cdot \vec{V} = 0$, and

$$\nabla \cdot \vec{P} = -\nabla p . \qquad (A-4)$$

The equation of motion for irrotational flow and constant viscosity is

$$\rho \frac{d\vec{V}}{dt} = -\nabla p + \frac{4}{3} \mu \nabla (\nabla \cdot \vec{V}) \qquad (A-5)$$

and if the additional requirement of incompressibility is considered, Equation (A-5) becomes

$$\rho \frac{d\vec{V}}{dt} = -\nabla p. \qquad (A-6)$$

Energy Equation

The energy equation in a moving fluid is

$$\rho \frac{dE}{dt} = \vec{P} : \nabla ; \vec{V} + \nabla k \nabla T + \dot{q} \qquad (A-7)$$

where

E = the internal energy of an element of mass

k = thermal conductivity

$\dot{q}$ = heat generation rate per unit volume

and

$\vec{P} : \nabla ; \vec{V}$ = trace of the product of the stress and rate of

strain tensors.

For the $\vec{P}$ and $\nabla ; \vec{V}$ given above for constant viscosity

$$\vec{P} : \nabla ; \vec{V} = -p(\nabla \cdot \vec{V}) + \frac{4}{3} \mu (\nabla \cdot \vec{V})^2 + \mu (\nabla \times \vec{V})^2$$

$$+ 2\mu \nabla \cdot \frac{1}{2}(\nabla ; \vec{V})^2 - \vec{V} \times (\nabla \times \vec{V}) - v(\nabla \cdot \vec{V})].$$

Again, for irrotational flow

$$\vec{P}:\nabla;\vec{V} = -p(\nabla \cdot \vec{V}) + \mu \left[\nabla^2 V^2 - \frac{2}{3}(\nabla \cdot \vec{V})^2 - 2\vec{V} \cdot \nabla(\nabla \cdot \vec{V})\right]. \tag{A-8}$$

When the fluid may be assumed to be incompressible,

$$\vec{P}:\nabla;\vec{V} = \mu \nabla^2 V^2. \tag{A-9}$$

Equations Applied to the Liquid

From the assumption that the liquid motion is irrotational, it follows that there is a velocity potential, φ, throughout the liquid such that

$$\vec{V} = -\nabla\varphi. \tag{A-10}$$

Since the liquid is assumed incompressible (or $\nabla \cdot \vec{V} = 0$), the velocity potential is a solution of Laplace's equation

$$\nabla^2\varphi = 0. \tag{A-11}$$

The spherically symmetric solution to Equation (A-11) is of the form:

$$\varphi = \frac{A(t)}{r} + B(t) \tag{A-12}$$

where

r = radial coordinate

and

$A(t)$ and $B(t)$ = functions to be determined from the boundary

conditions.

Then,

$$V = A(t)/r^2. \tag{A-13}$$

The velocity evaluated at the interface between a spherical vapor bubble and the liquid surrounding it is given by $V(R)$ where $r = R$ at the

bubble wall. A(t) can be evaluated for this boundary condition:

$$A(t) = V(R) \ R^2(t).$$

Equation (A-13) becomes

$$V(r,t) = V(R) \ R^2(t)/r^2. \qquad \text{(A-14)}$$

B(t) is zero if the velocity potential is zero at $r = \infty$, and

$$\varphi = V(R) \ R^2(t)/r.$$

The equation of motion from Equations (A-2) and (A-4) is

$$\rho\left[\frac{\partial \vec{V}}{\partial t} + \vec{V}\nabla\vec{V}\right] = -\nabla p. \qquad \text{(A-15)}$$

By the identity

$$\vec{V}\times(\nabla\times\vec{V}) = \tfrac{1}{2}\nabla V^2 - \vec{V} \cdot \nabla\vec{V}$$

where

$$\nabla \times \vec{V} = 0, \text{ for irrotational flow,}$$

the identity, $\vec{V} \cdot \nabla\vec{V} = \tfrac{1}{2}\nabla V^2$, results.

With Equation (A-15) this gives

$$\rho\nabla(-\frac{\partial\varphi}{\partial t} + \tfrac{1}{2}V^2) = -\nabla p. \qquad \text{(A-16)}$$

For constant density, integration of Equation (A-16) gives

$$-\frac{\partial\varphi}{\partial t} + \tfrac{1}{2}V^2 = -\frac{P(r,t)}{\rho} + C(t) \qquad \text{(A-17)}$$

where C(t) from the boundary condition, when $r = \infty$ then $P = P_{\infty}$, becomes P_{∞}/ρ.

For a limited temperature range, the assumption of constant density

allows the internal energy to be written

$$E = c_V T$$

where

c_V = the specific heat of the liquid at constant volume.

Equations (A-7), (A-9), and the above can be combined to give

$$\rho c_V \left[\frac{dT}{dt} + \vec{V} \cdot \nabla T \right] = k\nabla^2 T + \mu \nabla^2 V^2 + \dot{q}. \tag{A-18}$$

Some insight on the size of the term, $\mu \nabla^2 V^2$, can be gained using $V(r,t)$ from Equation (A-15):

$$\nabla \cdot [\nabla(\vec{V} \cdot \vec{V})] = \frac{\partial}{\partial_r^2} \left[\frac{R^4(t)}{r^4} V^2(R) \right] + \frac{\partial}{\partial r} \left[\frac{R^4(t)}{r^4} V^2(R) \right]$$

$$= \frac{12 \, R^4(t)}{r^6} V^2(R).$$

Evaluating this at the bubble wall and multiplying by viscosity,

$$\mu \nabla^2 V^2 = 12\mu \, \frac{V^2(R,t)}{R^2}. \tag{A-19}$$

This is the viscous heat generated per unit volume of liquid per unit time and is a maximum at the bubble wall where velocity is a maximum and r is a minimum.

An order of magnitude approximation for this term can be made. Zwick (5) demonstrated that

$$\vec{V}_L = \dot{R}\left[1 - \frac{\rho_v}{\rho_L} \left(1 - \frac{V_v}{\dot{R}} \right) \right] \tag{A-20}$$

where

L = subscript for liquid conditions

v = subscript for vapor conditions

$$\dot{R} = \text{bubble wall velocity}$$

and

$$V = \text{velocity.}$$

In the present investigation for liquid nitrogen near atmospheric pressure

$$\vec{V}_L = \dot{R}\left[1 - 0.006\left(1 - \frac{V_v}{\dot{R}}\right)\right] \approx 0.994\,\dot{R}$$

or $\vec{V}_L = \dot{R}$ is a good approximation of the fluid velocity at the bubble wall. The maximum value for viscosity in the range of this investigation was less than 10^{-9} lb_f-sec./in.^{2}. The maximum velocity measured experimentally was less than 40 inches/second when the radius of the bubble was 0.02 inches. Therefore,

$$\mu\nabla^2 V^2 \approx 12\mu\left(\frac{\dot{R}}{R}\right)^2 \approx 7 \times 10^{-4} \text{ Btu/sec. in.}^3.$$

The total temperature drop at the bubble wall, according to Zwick, is approximately $10^4\,°F$/sec. and the change in internal energy for this condition is

$$\rho\,c_V\,\frac{dT}{dt} \approx 100 \text{ Btu/sec. in.}^3.$$

This comparison shows that the viscous heating may be neglected in comparison to the heating or cooling at the bubble wall resulting from the condensation or evaporation that occurs there.

The energy equation for the liquid is:

$$\rho\,c_V\left[\frac{\partial T}{\partial t} + \vec{V}\cdot\nabla T\right] = k\nabla^2 T + \dot{q} \tag{A-21}$$

for the assumption of an incompressible liquid, neglecting the viscous

heating, and constant density. These assumptions for bubble growth in a superheated liquid are good approximations and for the relatively slow heat transfer controlled collapse the bubble wall velocity is much less than sonic velocity and compressibility may also be neglected for this case. Near the point of total collapse, high fluid velocities, variable fluid properties, and non-spherical shape all make the above assumptions invalid. However, experimental observations are not available for these conditions because the bubbles were too small to photograph properly.

Equations Applied to the Vapor

The vapor must be considered compressible and the equation of motion for a compressible, irrotational fluid with constant viscosity is Equation (A-5).

$$\rho\left[\frac{\partial \vec{V}}{\partial t} + \vec{V} \cdot \nabla \vec{V}\right] = -\nabla p + \frac{4}{3}\mu\nabla(\nabla \cdot \vec{V}).$$

The principal result of this analysis is to indicate that the vapor inertia is negligible when compared to the liquid inertia effects. The vapor density is approximately 1/10 of the liquid density, the coefficient of viscosity in the vapor is approximately 1/2 of the coefficient of viscosity in the liquid, and the velocity and velocity changes in the vapor are at least as small as those in the liquid. The pressure gradient in the vapor is, therefore, less than 1/2 of that in the liquid. Zwick gave a value for pressure gradient in water superheated three degrees Kelvin to be 1.5 atm./inch. The pressure gradient in liquid nitrogen is similar in magnitude for bubble growth. For a bubble radius of 10^{-2} inches, the pressure variation in the vapor is 0.75×10^{-2}

atmospheres. However, the vapor pressure is of the same order of magnitude as the external pressure of one atmosphere. The pressure variation in the vapor is two orders of magnitude smaller than the pressure level. The vapor pressure is essentially uniform throughout the interior of the bubble and can be written:

$$P_v = f(t).$$

Zwick (5) obtained approximate relationships from the energy equation indicating that the vapor temperature and density were also functions of time alone. These approximations resulted by considering the vapor to be thermally and calorically perfect and from order of magnitude arguments. The experimental results of this investigation were insufficient to verify that the approximations of Zwick were also valid for liquid nitrogen, however, a very rough order of magnitude check for liquid nitrogen points to this conclusion.

Equations at the Bubble Wall

The solutions in the liquid and in the vapor must be matched at the bubble wall with respect to temperature. Otherwise, there would be infinite heat transfer by conduction at the wall. Therefore, temperature at the bubble wall equals the temperature in the liquid at the wall and the temperature of the vapor at the wall.

The velocity in the liquid has been shown to be approximately equal to the bubble wall velocity and the heat transfer relation at the wall is

$$k \left. \frac{\partial T}{\partial r} \right|_{r=R} = L \, \rho_v (\dot{R} - \vec{V}_v) \qquad \text{(A-22)}$$

This equation may be written in the form:

$$R^2 \left(k \frac{\partial T}{\partial r} \right)_{r=R} = \frac{L}{3} \frac{d}{dt} (R^3 \rho_v) \qquad (A\text{-}23)$$

where the vapor velocity is neglected in comparison to the bubble wall velocity.

Finally, neglecting viscous and kinematic corrections, the force balance across the bubble boundary can be written:

$$P_v = P_L + (2\sigma)/R. \qquad (A\text{-}24)$$

Equations (A-10), (A-17), (A-20), and (A-24) can be combined to give at the bubble wall

$$P_L(t) - P_\infty(t) = \rho_L \left[R \ddot{R} + 2\dot{R}^2 - \tfrac{1}{2} \dot{R}^2 \right]$$

or

$$R \ddot{R} + \frac{3}{2} \dot{R}^2 = \frac{P_v(t) - P_\infty(t)}{\rho_L} - \frac{2\sigma}{\rho_L R} \qquad (A\text{-}25)$$

where

$P_v(t)$ = equilibrium vapor pressure of the liquid at the temperature of the bubble wall.

The energy equation for the liquid is Equation (A-21),

$$\rho_L c_v \left[\frac{\partial T}{\partial t} + \vec{V} \cdot \nabla T \right] = k \nabla^2 T + \dot{q} . \qquad (A\text{-}26)$$

The boundary conditions for Equation (A-26) at the bubble wall are:

$$R^2 k \left. \frac{\partial T}{\partial r} \right|_{r=R} = \frac{L}{3} \frac{d}{dt} (R^3 \rho_v) \qquad (A\text{-}27)$$

and

$$T(r, t = 0) = T_o. \qquad (A\text{-}28)$$

Equations (A-25), (A-26), (A-27), and (A-28) define the problem being
considered and for given boundary conditions on Equation (A-25) the
simultaneous solution of the coupled equations results in the theoreti-
cal bubble behavior.

APPENDIX B

APPROXIMATE SOLUTION OF THE ENERGY EQUATION

The solution of the energy equation presented here is essentially that of Plesset and Zwick (8). The energy equation and boundary conditions for a vapor bubble are Equations (A-26), (A-27), and (A-28). For no heat generation by radiation or chemical reactions, $\dot{q} = 0$, and the energy equations become

$$\nabla^2 T = \frac{1}{\alpha}\left[\frac{\partial T}{\partial t} + \vec{V} \cdot \nabla T\right] \tag{B-1}$$

$$\left.\frac{\partial T}{\partial r}\right|_{r=R} = \frac{L}{3k\,R^2}\,\frac{d}{dt}\,(R^3\rho_v) \tag{B-2}$$

and

$$T(r,\,0) = T_o. \tag{B-3}$$

The temperature in the liquid at an infinite distance from the bubble is T_o. And, with the substitution of $\theta = T - T_o$, the equations become

$$\nabla^2\theta = \frac{1}{\alpha}\left[\frac{\partial\theta}{\partial t} + \vec{V}\cdot\nabla\theta\right] \tag{B-4}$$

$$\left.\frac{\partial\theta}{\partial r}\right|_{r=R} = \frac{L}{3k\,R^2}\,\frac{d}{dt}\,(R^3\rho_v) \tag{B-5}$$

and

$$\theta(r,\,0) = \theta(\infty,\,t) = 0. \tag{B-6}$$

95

Using the change of variables:

$$m = (r^3 - R^3(t))/3$$

$$t = t$$

and neglecting $\vec{V} \cdot \nabla T$ gives

$$\frac{\partial}{\partial m}\left(r^4 \frac{\partial\theta}{\partial m}\right) = \frac{1}{\alpha}\frac{\partial\theta}{\partial t} \qquad (B-7)$$

$$\left.\frac{\partial\theta}{\partial m}\right|_{m=0} = \frac{L}{3k\,R^4(t)}\frac{d}{dt}\left(R^3(t)\,\rho_V\right) \qquad (B-8)$$

and

$$\theta(m, 0) = \theta(\infty, t) = 0. \qquad (B-9)$$

A form of these equations more suitable for solution results by assuming a temperature potential, U, defined by

$$\theta = \frac{\partial U}{\partial m}. \qquad (B-10)$$

Equations (B-7) and (B-10) can be combined to give

$$\frac{\partial}{\partial m}\left(r^4 \frac{\partial^2 U}{\partial m^2} - \frac{1}{\alpha}\frac{\partial U}{\partial t}\right) = 0.$$

Then, partial integration with respect to m gives

$$r^4 \frac{\partial^2 U}{\partial m^2} - \frac{1}{\alpha}\frac{\partial U}{\partial t} = A(t) \qquad (B-11)$$

where A(t) is an arbitrary function of time. But from Equation (B-10)

$$U = \int_0^m \theta\, dm + K(t) \qquad (B-12)$$

and K(t) can be chosen so that A(t) = 0 and K(0) = 0. Therefore, U(m, 0) = 0 since $\theta(m, 0) = 0$.

The system of equations to be solved is:

$$r^4 \frac{\partial^2 U}{\partial m^2} - \frac{1}{\alpha} \frac{\partial U}{\partial t} = 0 \tag{B-13}$$

$$\frac{\partial^2 U}{\partial m^2}\bigg|_{m=0} = \frac{L}{3K} \frac{1}{R^4(t)} \frac{d}{dt} \left(R^3(t)\rho_v \right) \tag{B-14}$$

and

$$U(m,0) = \frac{\partial U}{\partial m}\bigg|_{m=\infty} = 0. \tag{B-15}$$

For the assumption that a very thin thermal boundary exists where the significant heat transfer takes place, the transposing and adding of terms in Equation (B-13) give:

$$R^4(t) \frac{\partial^2 U}{\partial m^2} - \frac{1}{\alpha} \frac{\partial U}{\partial t} = \left(R^4(t) - r^4 \right) \frac{\partial^2 U}{\partial m^2}. \tag{B-16}$$

The term, $\left(R^4(t) - r^4 \right) \frac{\partial^2 U}{\partial m^2}$, has the properties of a perturbing heat source. The magnitude of this term is small under the assumption of a thin thermal boundary layer.

Another change of variables,

$$h = \int_0^t R^4(t) \, dt,$$

in Equation (B-16) results in the differential equation:

$$\frac{\partial^2 U}{\partial m^2} - \frac{1}{\alpha} \frac{\partial U}{\partial h} = \left(1 - \frac{r^4}{R^4(t)} \right) \frac{\partial^2 U}{\partial m^2}. \tag{B-17}$$

The unperturbed case, or the zeroth order approximation, of this equation results when $r^4 = R^4(t)$. Equation (B-17) becomes

$$\frac{\partial^2 U}{\partial m^2} - \frac{1}{\alpha} \frac{\partial U}{\partial h} = 0 \tag{B-18}$$

The solution of Equations (B-18), (B-14), and (B-15) gives the zeroth order solution of the heat problem where the thickness of the thermal boundary layer is zero. Arguments by Zwick (5) indicate that the error in using this zeroth order approximation was less than 0.5 degrees Kelvin for water. The temperature difference between the zeroth order solution and the first order solution for bubble growth in a superheated liquid was:

$$\Delta T < 3 \sqrt{\frac{\alpha (t - t_o)}{R}}.$$

For identical degrees of superheat, a bubble growing from an initial radius, R_o, in liquid nitrogen and one growing from the same R_o in water have approximately the same radius for a given time change. The thermal diffusivity in liquid nitrogen is less than that of water. Therefore, the temperature difference in liquid nitrogen is less than that in water. Zwick (5) shows that this error does not affect the dynamic problem for growth in water, and it causes the same magnitude error in liquid nitrogen.

The solution of Equation (B-18) is obtained by taking the Laplace transformation with respect to h.

$$u(m,s) = \int_0^\infty \rho^{-sh} \, U(m,h) \, dh \equiv \mathcal{L}[U] \qquad (B-19)$$

$$F(h) = \frac{L}{3k} \frac{d}{dh} (R \, \rho_v)$$

and

$$f(s) = \mathcal{L}(F(h)). \qquad (B-20)$$

The equations to be solved after transformation are:

$$\frac{d^2u}{dm^2} - \frac{s}{\alpha}u = 0 \tag{B-21}$$

$$\left.\frac{d^2u}{dm^2}\right|_{m=0} = f(s) \tag{B-22}$$

$$\left.\frac{du}{dm}\right|_{m=\infty} = 0, \tag{B-23}$$

and the solution has the form:

$$u(m,s) = A \exp\left(-m\sqrt{\frac{s}{\alpha}}\right) + B \exp\left(m\sqrt{\frac{s}{\alpha}}\right).$$

Substituting in the boundary conditions results in

$$u(m,s) = \frac{\alpha}{s} f(s) \exp\left(-m\sqrt{\frac{s}{\alpha}}\right). \tag{B-24}$$

Then,

$$\theta = \mathcal{L}^{-1}\left[\frac{du}{dm}\right] = \mathcal{L}^{-1}\left[-\sqrt{\frac{\alpha}{s}} f(s) e^{-m\sqrt{\frac{s}{\alpha}}}\right]$$

$$= -\sqrt{\frac{\alpha}{\pi}} \int_0^h \frac{F(\beta)d\beta}{\sqrt{h-\beta}} \rho^{\frac{m^2}{4\alpha(h-\beta)}}. \tag{B-25}$$

Equation (B-25), written in terms of the original r and t variables, becomes

$$T(r,t) - T_o = -\sqrt{\frac{\alpha}{\pi}} \int_0^t \left[\frac{R^2(x) \left.\frac{\partial T}{\partial r}\right|_{r=R(x)} dx}{\left\{\int_x^t R^4(y)dy\right\}^{\frac{1}{2}}}\right] \times$$

$$\left[\exp\left\{\frac{(r^3 - R^3(x))^2}{36\alpha\int_x^t R^4(y)dy}\right\}\right] \tag{B-26}$$

The temperature at the bubble wall, where $r = R(t)$, is

$$T(R,t) - T_o = -\sqrt{\frac{\alpha}{\pi}} \int_o^t \frac{R^2(x) \left.\frac{\partial T}{\partial r}\right|_{r=R(x)} dx}{\left\{\int_o^t R^4(y)dy\right\}^{\frac{1}{2}}}. \qquad (B\text{-}27)$$

And using the boundary condition of Equation (B-2), the solution is

$$T(R,t) - T_o = \frac{-L}{3k}\sqrt{\frac{\alpha}{\pi}} \int_o^t \frac{\frac{d}{dx}(R^3(x)\rho_v)dx}{\left\{\int_x^t R^4(y)dy\right\}^{\frac{1}{2}}}. \qquad (B\text{-}28)$$

This solution for the temperature at the bubble wall is based on the assumptions that there is no radiation heat transfer or chemical reactions, that there is no heat transferred from the bubble wall by convection, and that the thickness of the thermal boundary is zero. However, this is the best solution presently available, and it has been demonstrated experimentally that good prediction of bubble dynamic behavior results with the above assumptions.

APPENDIX C

SOLUTIONS OF THE BUBBLE DYNAMICS PROBLEM FOR SPECIAL CASES

Bubble Growth in a Superheated Liquid

The equations to be solved in this section are:

$$R\ddot{R} + \frac{3}{2}\dot{R}^2 = \frac{P_v(T_w) - P_\infty(t)}{\rho_L} - \frac{2\sigma}{R\rho_L} , \qquad (C-1)$$

$$R(0) = R_0, \quad \dot{R}(0) = \dot{R}_0, \qquad (C-2)$$

and

$$T(R,t) - T_0 = -\frac{L}{3k}\sqrt{\frac{\alpha}{\pi}} \int_0^t \frac{\frac{d}{dx}(R^3(x)\rho_v)\,dx}{\left\{\int_x^t R^4(y)\,dy\right\}^{\frac{1}{2}}}. \qquad (C-3)$$

For asymptotic growth it was stated in Chapter III that the solution of Equation (C-3) approaches

$$T(R,t) - T_0 = T_{s\infty} - T_0.$$

The following variables and constants, suggested by Plesset and Zwick (8), are defined to simplify the writing of the above equations:

$$z = \left(\frac{R}{R_0}\right)^3 \quad , \quad a = \sqrt{\frac{2\sigma}{\rho_L R_0^3}} ,$$

$$E' = \frac{L\rho_v R_0}{3k}\sqrt{\frac{a\alpha}{\pi}} \quad , \quad \varphi = \frac{R_0}{2\sigma}\left[P_\infty(t) - P_v(T_w)\right] ,$$

101

and

$$u = \frac{a}{R^4_o} \int_0^t R^4(y)dy.$$

The equations become:

$$\frac{1}{6} \frac{d}{dZ} \left[z^{7/3} \left(\frac{dZ}{du} \right)^2 \right] + \frac{1}{z^{1/3}} + \varphi = 0 \qquad \text{(C-5)}$$

$$T - T_o = -E' \int_0^u \frac{\frac{dZ}{dV} \, dV}{\sqrt{u - V}} \qquad \text{(C-6)}$$

and

$$\text{at } u = 0, \; z = 1 \text{ and } \frac{dz}{du} = 0. \qquad \text{(C-7)}$$

Initially, the static condition, $P_v(T_o) - P_\infty(t) = \frac{2\sigma}{R_o}$, holds and

$$\varphi(T_o) = -1. \qquad \text{(C-8)}$$

A liquid can support only a few degrees of superheat, and for a small temperature range the approximate relationship between pressure and temperature,

$$\frac{P_v(T_w) - P_\infty(t)}{\rho_L} = A'(T - T_s), \qquad \text{(C-9)}$$

is valid.

Combining Equations (C-6), (C-8), and (C-9) gives

$$-\varphi = 1 - \frac{A'E'}{R_o^2 a^2} \int_0^u \frac{\frac{dZ}{dV} \, dV}{\sqrt{u - V}} . \qquad \text{(C-10)}$$

The integro-differential equation to be solved is

$$\frac{1}{6}\frac{d}{dZ}\left[Z^{7/3}\left(\frac{dZ}{du}\right)^2\right] + \frac{1}{Z^{1/3}} = 1 - \frac{A'E'}{R_o^2 a^2}\int_o^u \frac{\frac{dZ}{dV}\, dV}{\sqrt{u-v}} \; . \qquad (C-11)$$

The asymptotic case, for $u \to \infty$, has $z \to \infty$ and $\frac{dz}{du} \to 0$. The inertia term, $\frac{1}{6}\frac{d}{dZ}\left[Z^{7/3}\left(\frac{dZ}{du}\right)^2\right]$, and the surface tension term, $z^{-1/3}$, become negligible in the asymptotic behavior of the bubble. Then,

$$\frac{A'E'}{R_o^2 a^2}\int_o^u \frac{\frac{dZ}{dV}\, dV}{\sqrt{u-V}} = 1 \qquad (C-12)$$

is a good approximation of the bubble dynamics solution. Equation (C-12) has the solution

$$Z(u) = \frac{2R_o^2 a^2}{\pi A'E'}\sqrt{u} \; . \qquad (C-13)$$

The boundary condition, $z(u_1) = z_1$ when $u = u_1$, results from the solution of Equation (C-11) from time zero to time when asymptotic growth occurs. This time occurs when the bubble radius and velocity attain the values where the neglect of inertia and surface tension terms is permissible.

Plesset and Zwick matched the solution, Equation (C-13), to the required initial solution and transformed the solution back into the original variables of the problem. The result of this manipulation gives

$$R = \sqrt{\frac{12}{\pi}}\, \frac{k\Delta T}{L\rho_V \sqrt{\alpha}}\; t^{\frac{1}{2}} \qquad (C-14)$$

and

$$\Delta T = T_o - T_{s\infty} .$$

Bubble Collapse in a Subcooled Liquid

Inertia controlled collapse was given in Chapter III. The present section concerns temperature or heat transfer controlled collapse. Florschuetz and Chao (1) non-dimensionalized Equations (C-1) and (C-3) using the definitions:

$$\gamma = \frac{R}{R_o} , \qquad\qquad \pi_V = \frac{P_v(T_w) - P_{v,o}}{P^*_\infty - P_{v,o}} ,$$

$$\pi_\infty = \frac{P_\infty(t) - P_{v,o}}{P^*_\infty - P_{v,o}} , \qquad \tau = \frac{\alpha t}{R_o^2} ,$$

and $\qquad \theta_w = \dfrac{T_w - T_o}{T_{s\infty} - T_o}$

where

P^*_∞ = final system pressure

$P_{v,o}$ = vapor pressure corresponding to T_o.

Applying these notations in Equations (C-1) and (C-3) gives

$$\gamma \ddot\gamma + \frac{3}{2}\dot\gamma^2 = \frac{R_o^2}{\rho_V \alpha^2} (P^*_\infty - P_{v,o})[\pi_v(\theta_w) - \pi_\infty(\tau)] \qquad (C\text{-}15)$$

and

$$\theta_w(\tau) = \frac{-\rho_V L}{(T_{s\infty} - T_o)\, \rho_L C_p \sqrt{\pi}} \int_o^\tau \frac{\gamma^2(x)\, \dot\gamma(x)\, dx}{\left\{\int_x^\tau \gamma^4(y) dy\right\}^{\frac{1}{2}}} . \qquad (C\text{-}16)$$

Now, defining

$$C = R_o \left(P^*_\infty - P_{v,o}\right)/\rho_V \alpha^2$$

and

$$Ja = \rho_L C_p (T_{s\infty} - T_o)/\rho_V L$$

the equations can be written

$$\frac{1}{C}[\gamma \ddot{\gamma} + \frac{3}{2} \dot{\gamma}^2] = \pi_r(\theta_w) - \pi_\infty(\tau) \tag{C-17}$$

and

$$\theta_w(\tau) = \frac{-1}{\sqrt{\pi} Ja} \int_o^t \frac{\gamma^2(x) \dot{\gamma}(x) \, dx}{\left\{\int_x^\tau \gamma^4(y) dy\right\}^{\frac{1}{2}}}. \tag{C-18}$$

When C is large enough that the left side of Equation (C-17) is approximately zero, $\pi_V(\theta_w) = \pi_\infty(\tau)$ and $\theta_w(\tau) = 1$. When this physical situation occurs, bubble collapse is said to be controlled by heat transfer. For the experimental data taken in the present investigation, the range of values of C was from 2.73×10^8 to 5.59×10^8. The solution of Equation (C-18) is obtained in terms of new variables:

$$t_H = \frac{4}{\pi} Ja \ \tau \quad , \quad V = \int_o^x \gamma^4(x) dx,$$

and

$$u = \int_o^{t_H} \gamma^4(x) dx.$$

Applying these variables to Equation (C-18) gives

$$-\frac{3}{2} \pi = \int_o^u \frac{\frac{dZ}{dV} \, dV}{\sqrt{u - V}}. \tag{C-19}$$

For the boundary condition z = 1 at u = 0, the solution of Equation

(C-19) is

$$\gamma^3 = 1 - 3u^{\frac{1}{2}}.$$ (C-20)

The solution in terms of the original variables is

$$t_H = \int_0^u \frac{dV}{z^{4/3}(v)}.$$ (C-21)

Integration of the right hand side of Equation (C-21) gives

$$t_H = \frac{1}{3}\left(\frac{2}{\gamma} + \gamma^2 - 3\right).$$ (C-22)

Equation (C-22) is the solution of the bubble dynamics equations for fluid conditions such that the bubble collapse is heat transfer controlled.

A disadvantage in the form of Equation (C-22) is the necessity of solving a cubic equation to obtain an explicit expression for γ as a function of t_H. Another approximate solution, using simplified boundary conditions on the energy Equation (B-1), results in an explicit expression for γ in terms of t_H.

The boundary conditions of Florschuetz and Chao (1) assume heat transferred to a semi-infinite region with uniform initial temperature and time dependent surface flux, $\left.\frac{\partial \theta}{\partial r}\right|_{r=R} = \frac{\rho_V L \dot{R}}{k}$. The solution of the heat equation for these boundary conditions is

$$\theta_w(\tau) = \frac{-1}{\sqrt{\pi}\, Ja} \int_0^\tau \frac{\dot{\gamma}(x)\, dx}{\sqrt{\tau - x}}.$$ (C-23)

For heat transfer controlled collapse (for $\theta_w(\tau) = 1$) the solution of

Equation (C-23) is

$$\Upsilon = 1 - \sqrt{t_H}. \qquad\qquad (C\text{-}24)$$

Florschuetz and Chao (1) concluded that a bubble would collapse more rapidly than the collapse predicted by Equation (C-22). All terms neglected in that solution tended to make the collapse rate higher than the predicted rate. The collapse rate predicted by Equation (C-24) was higher than that predicted by Equation (C-22). Both solutions neglected radial convection and free convection due to bubble motion with respect to the bulk liquid. Therefore, a vapor bubble in a gravitational field would collapse more rapidly than an identical vapor bubble subjected to the same fluid conditions but having no gravitational field.

Bubble Dynamics With a Fast Transient Liquid Pressure

A fast transient liquid pressure is defined to be a transient pressure occurring so rapidly that the change in vapor pressure inside a bubble can be neglected. More simply, when bubble behavior can be predicted from Equation (C-1) where $P_V(T_W)$ is assumed to be constant, the transient liquid pressure is called a fast transient liquid pressure. No closed form solution exists for this problem. However, the problem is well adapted to numerical solution on a digital computer.

A Runge-Kutta integration technique gave very good approximate solutions to Equation (C-1). An accuracy check on the integration program used here was made with the right hand side of Equation (C-1) constant and with the increment size in time equal to 10^{-6} seconds. The results from the numerical integration were compared to the exact solution, or Rayleigh solution, and the maximum error was less than one

percent. Introduction of pressure variation into this program does not affect the convergence of the problem. Therefore, this integration technique was assumed to adequately predict bubble dynamic behavior under fast transient liquid pressures.

The computer program written for a particular pressure variation is given in Figure 26. This is the same program that was used to compare solutions of the Rayleigh solution except for the introduction of the variable pressure, PI. The particular pressure variation is given in Figure 27.

```
 1      51 FORMAT(11H R NEGATIVE)
 2       8 FORMAT(4E15.6)
 3      20 FORMAT(1X,E15.6,6X,E15.6,6X,E15.6)
 4      50 FORMAT(6X,1HT,16X,1HR,16X,1HZ)
 5      53 FORMAT(I3)
 6         L=1
 7         READ(5,53) N
11      45 READ(5,8) DEN, PV, PI, R
12         WRITE(6,8) DEN, PV, PI, R
13         WRITE(6,50)
14         K=1
15         M = 1001
16         T=0.0
17         Z=0.0
20         AH=0.000001
21       6 K = K + 1
22         AK1 = AH*Z
23         IF(R)11,11,2
24       2 AL1=AH*((PV-PI)/(DEN)-(1.5*(Z**2)))/R
25         T=T+AH/2.
26         R=R+AK1/2.
27         Z=Z+AL1/2.
30         AK2=AH*Z
31         W=38.7*T
32         PI=16.5+(6./(EXP(W)))
33         IF(R)11,11,3
34       3 AL2=AH*((PV-PI)/(DEN)-(1.5*(Z**2)))/R
35         R=R+AK2/2.
36         Z=Z+AL2/2.
37         AK3=AH*Z
40         IF(R)11,11,4
41       4 AL3=AH*((PV-PI)/(DEN)-(1.5*(Z**2)))/R
42         R=R+AK3-(AK2/2.)
43         Z=Z+AL3-(AL2/2.)
44         T=T+AH/2.
45         W=38.7*T
46         PI=16.5+(6./(EXP(W)))
47         IF(R)11,11,5
50       5 AK4=AH*Z
51         AL4=AH*((PV-PI)/(DEN)-(1.5*(Z**2)))/R
52         AK5=(AK1+2.*AK2+2.*AK3+AK4)/6.
53         AL5=(AL1+2.*AL2+2.*AL3+AL4)/6.
54         R=R+AK5-AK3
55         Z=Z+AL5-AL3
56         IF(K-M) 6,9,9
57       9 WRITE(6,20) T, R, Z
60         IF(K-200001) 22,23,23
61      22 M = M+ 1000
62         GO TO 6
63      11 WRITE(6,51)
64      23 L = L+ 1
65         IF(L - N) 45,10,10
66      10 STOP
67         END
```

Figure 26. Computer Solution for One Variable Pressure

PRESSURE IN THE LIQUID MEASURED
BY KISTLER TRANSDUCER. DRAWN
FROM OSCILLOSCOPE PHOTOGRAPH.
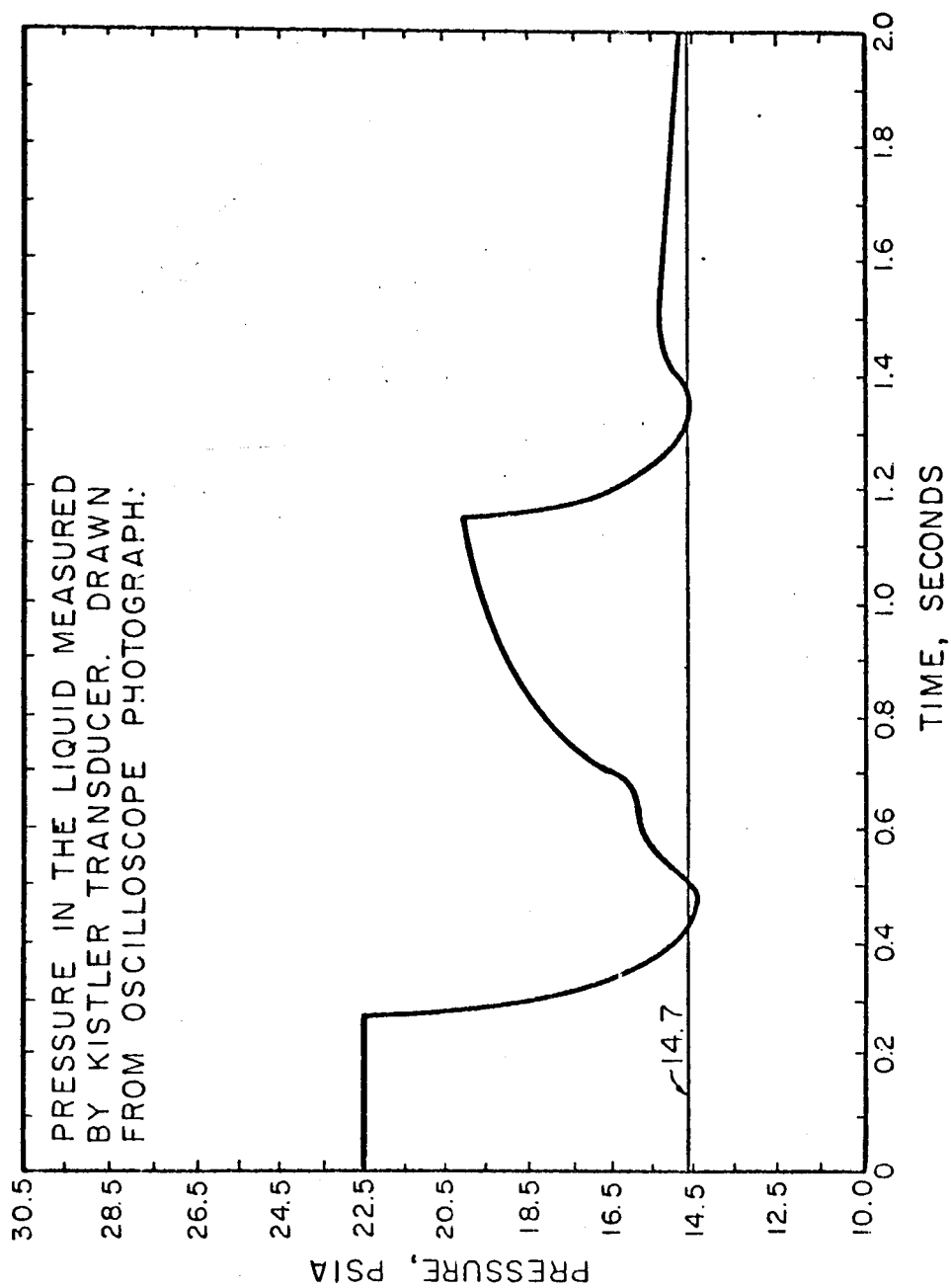
Figure 27. Pressure-Time Curve Photographed for One Transient Pressure
Study

APPENDIX D

CALIBRATION AND EXPERIMENTAL DATA

Thermocouple Calibration

The thermocouple output measurements were taken for each thermocouple simultaneously with the static pressure above boiling liquid nitrogen. Table III gives the measurements made for each day of operation. Thermocouples 1-1, 1-2, 1-3, and 2-1 were located in the liquid nitrogen while 2-2 was located in the electrical heater.

TABLE III

THERMOCOUPLE DATA

Date	Number	Barometric Pressure inches of mercury	Liquid Pressure inches of mercury	Thermocouple Output MV
12-13-65		29.23		
	1-1		0.0	5.494
	1-1		3.56	5.476
	1-1		5.18	5.471
	1-1		16.62	5.433
	1-2		0.0	5.487
	1-2		3.56	5.474
	1-2		5.36	5.468
	1-2		14.60	5.439
	1-2		19.23	5.420
	1-2		23.71	5.401
	1-2		24.75	5.397
	1-3		0.0	5.488

TABLE III (Continued)

Date	Number	Barometric Pressure inches of mercury	Liquid Pressure inches of mercury	Thermocouple Output MV
	1-3		3.21	5.476
	1-3		5.56	5.467
	1-3		13.26	5.444
	1-3		18.41	5.425
	1-3		20.35	5.414
	2-1		0.0	5.482
	2-1		2.12	5.472
	2-1		5.76	5.456
	2-1		11.10	5.439
	2-1		12.11	5.434
	2-1		21.74	5.403
	2-2		0.0	5.488
	2-2		2.80	5.481
	2-2		5.66	5.467
	2-2		10.50	5.452
	2-2		22.72	5.411
12-17-66		29.37		
	2-1		23.40	5.394
	2-1		17.58	5.412
	2-1		12.80	5.432
	2-1		9.59	5.444
	2-1		9.02	5.444
	2-1		0.0	5.478
	2-2		23.89	5.402
	2-2		16.99	5.420
	2-2		11.87	5.442
	2-2		10.65	5.452
	2-2		7.20	5.464
	2-2		0.0	5.492
12-20-65		29.06		
	1-1		11.68	5.452
	1-1		15.75	5.442
	1-1		18.33	5.432
	1-2		11.68	5.445
	1-2		16.55	5.438
	1-2		18.02	5.425
	1-2		18.33	5.427
	1-3		16.55	5.452
	1-3		17.18	5.442
	1-3		18.02	5.434
	2-1		11.68	5.439

TABLE III (Continued)

Date	Number	Barometric Pressure inches of mercury	Liquid Pressure inches of mercury	Thermocouple Output MV
	2-1		17.78	5.424
	2-1		17.78	5.419
	2-2		11.68	5.452
	2-2		18.40	5.438

Experimental Data

The measurements of liquid temperature and pressure were used to determine the constants in the theoretical solution of Plesset and Zwick. A sample calculation for determining the coefficient of $t^{\frac{1}{2}}$ in the equation,

$$R = \sqrt{\frac{12}{\pi}} \; \frac{k_L \Delta T}{L \, \rho_V \sqrt{\alpha}} \; t^{\frac{1}{2}}, \tag{D-1}$$

is given for bubbles No. 1-4. The measurements for these bubbles were taken from film roll number 10. For this run, liquid pressure = 29.23 inches of mercury, the thermocouple output was 5.462 mv. Table IV gives the information used in this calculation.

TABLE IV

THEORETICAL BUBBLE GROWTH DATA

Reference	Measurement Used	Variable Determined
(27)	$P_{\infty L}$ = 29.23 inches mercury	T_{sat} = 138.891°R
Table III	Thermocouple No. 1-3 = 5.462 mv	T_L = 142.7°R
(29)	T_L = 142.7°R	K_L = 0.0792 $^{Btu}/ft.hr.°R$
(29)	T_L = 142.7°R	ρ_L = 50.2 $^{lb_m}/ft$
(29)	T_L = 142.7°R	C_L = 0.492 $^{Btu}/lb_m°R$
(29)	T_L = 142.7°R	L = 85.0 $^{Btu}/lb_m$
(29)	T_{sat} = 138.891°R	ρ_V = 0.29 $^{lb_m}/ft$
	T_{sat} and T_L	T = 3.8°R

Using the values from Table IV, Equation (D-1) gives

$$R = 0.08354 \ \frac{\text{inches}}{(\sec)^{\frac{1}{2}}} \ (t)^{\frac{1}{2}}. \qquad (D-2)$$

Then, using D_o = 0.0427 from the measurement of the film, t_o = 0.06547 second. The theoretical curve is determined by substituting one other coordinant in Equation (D-2) when a log-log plot is used.

Tables V-VIII give the measured diameters and times plus the theoretical solution for bubbles No. 1-9.

115

TABLE V

DATA FOR FIGURE 7

Bubble Number	Diameter Inch	Time Second	Bubble Number	Diameter Inch	Time Second
1	0.0427	0.06547	3	0.0551	0.1004
	0.0439	0.0738		0.0563	0.1088
	0.0461	0.0821		0.0608	0.1171
	0.0484	0.0905			
	0.0585	0.0988	4	0.0394	0.0555
	0.0652	0.1071		0.0428	0.0639
	0.0664	0.1155		0.0450	0.0722
	0.0698	0.1238		0.0484	0.0805
				0.0518	0.0889
2	0.0434	0.0839		0.0619	0.0972
	0.0506	0.0922		0.0641	0.1055
	0.054	0.1005		0.0686	0.1139
	0.0551	0.1088		0.0697	0.1305
	0.0574	0.1172			
	0.0596	0.1255	Theoretical		
	0.0619	0.1339		0.01671	0.01
	0.0641	0.1422		0.03342	0.04
				0.05013	0.09
3	0.0405	0.0588		0.06684	0.16
	0.0461	0.0671			
	0.0484	0.0754			
	0.0506	0.0838			
	0.0568	0.0921			

TABLE VI

DATA FOR FIGURE 8

Bubble Number	Diameter Inch	Time Second	Bubble Number	Diameter Inch	Time Second
5	0.0326	0.0325	Theoreical		
	0.0360	0.0408		0.0362	0.04
	0.0405	0.0491		0.0543	0.09
	0.0439	0.0575		0.0724	0.16
	0.0495	0.0658			
	0.0495	0.0741			
	0.0506	0.0825			
	0.0506	0.0908			
	0.0551	0.0991			
	0.0574	0.1075			
	0.0630	0.1158			
	0.0630	0.1241			

TABLE VII

DATA FOR FIGURE 9

$P_{\infty L}$ = 29.37 inches mercury			Thermocouple 2-1 = 5.422 mv		
Bubble Number	Diameter Inch	Time Second	Bubble Number	Diameter Inch	Time Second
6	0.0743	0.0618	7	0.0810	0.0735
	0.0788	0.0701		0.0889	0.0819
	0.0866	0.0785		0.0923	0.0902
	0.0911	0.0868		0.0881	0.0985
	0.0990	0.0951		0.0967	0.1069
	0.1058	0.1005		0.0979	0.1152
	0.1058	0.1118		0.1035	0.1235
	0.1058	0.1201		0.1046	0.1319
	0.1125	0.1285		0.1069	0.1402
	0.1159	0.1368		0.1091	0.1485
	0.1215	0.1451		0.1091	0.1569
	0.1226	0.1529		0.1159	0.1652
	0.1237	0.1618		0.1170	0.1735
				0.1215	0.1319
Theoretical				0.1226	0.1302
	0.02988	0.04		0.1249	0.1985
	0.04482	0.09			
	0.05976	0.16			

TABLE VIII

DATA FOR FIGURE 10

$P_{\infty L}$ = 29.23 inches mercury			Thermocouple 1-3 = 5.434 mv		
Bubble Number	Diameter Inch	Time Second	Bubble Number	Diameter Inch	Time Second
8	0.0525	0.0188	9	0.0615	0.0258
	0.0600	0.0271		0.0720	0.0341
	0.0840	0.0354		0.0750	0.0425
	0.0900	0.0439		0.0855	0.0518
	0.0975	0.0522		0.0885	0.0601
	0.1005	0.0605		0.0915	0.0685
	0.1020	0.0690		0.0960	0.0778
	0.1035	0.0773		0.1065	0.0861
	0.1170	0.0856		0.1245	0.0945
				0.1275	0.1028
Theoretical				0.1305	0.1111
	0.03836	0.01		0.1260	0.1195
	0.07672	0.04		0.1335	0.1278
	0.10508	0.09		0.1470	0.1361
	0.14344	0.16		0.1560	0.1445

Tables IX-XVIII give the measured diameter ratios and time and the calculated variables, t_H and t_R, for bubbles No. 10-21.

TABLE IX

DATA FOR FIGURES 11 AND 22

$P_{\infty L}$ = 20.72 psia			Thermocouple 1-1 = 5.475 mv	
Bubble Number	D/D_o	Time Second	t_H	t_R
10	1.000	0.0000	0.000	0.0000
	0.811	0.0083	0.0074	0.0066
	0.840	0.0167	0.0149	0.0124
	0.757	0.0250	0.0223	0.0228
	0.694	0.0333	0.0297	0.0366
	0.735	0.0417	0.0371	0.0409
	0.703	0.0500	0.0446	0.0529
	0.744	0.0583	0.0520	0.0551
	0.744	0.0667	0.0594	0.0630
	0.673	0.0750	0.0669	0.0866
	0.648	0.0833	0.0773	0.1038
	0.770	0.0917	0.0817	0.1395
	0.595	0.1000	0.0892	0.1477

TABLE X

DATA FOR FIGURES 12, 13, AND 22

Bubble Number	$P_{\infty L}$ = 23.148 psia D/D_o	Time Second	t_H	Thermocouple 2-2 = 5.460 mv t_R
11	1.000	0.0000	0.0000	0.0000
	0.954	0.0083	0.0074	0.0050
	0.877	0.0167	0.0148	0.0118
	0.723	0.0250	0.0222	0.0261
	0.831	0.0333	0.0296	0.0263
	0.923	0.0417	0.0370	0.0267
	0.831	0.0500	0.0444	0.0395
	0.692	0.0583	0.0518	0.0664
	0.523	0.0667	0.0592	0.1329
	0.492	0.0750	0.0666	0.1689
	0.446	0.0833	0.0740	0.2285
	0.431	0.0917	0.0814	0.2691
12	1.000	0.0000	0.0000	0.0000
	0.765	0.0083	0.0068	0.0071
	0.809	0.0167	0.0135	0.0126
	0.691	0.0250	0.0203	0.0260
	0.750	0.0333	0.0270	0.0295
	0.618	0.0417	0.0338	0.0543
	0.515	0.0500	0.0405	0.0937
	0.529	0.0583	0.0473	0.1036
	0.412	0.0667	0.0540	0.1952

TABLE XI

DATA FOR FIGURES 14 AND 22

$P_{\infty L}$ = 19.22 psia			Thermocouple 1-1 = 5.478 mv	
Bubble Number	D/D_o	Time Second	t_H	t_R
13	1.000	0.0000	0.0000	0.0000
	0.925	0.0083	0.0021	0.0021
	0.762	0.0167	0.0043	0.0063
	0.795	0.0250	0.0064	0.0087
	0.902	0.0333	0.0086	0.0090
	0.902	0.0417	0.0107	0.0113
	0.895	0.0500	0.0129	0.0138
	0.886	0.0583	0.0150	0.0164
	0.820	0.0667	0.0171	0.0218
	0.778	0.0750	0.0193	0.0273
	0.868	0.0833	0.0214	0.0243
	0.770	0.0917	0.0236	0.0341
	0.770	0.1000	0.0257	0.0372
	0.770	0.1083	0.0278	0.0403
	0.680	0.1167	0.0300	0.0556
	0.623	0.1250	0.0321	0.0709
	0.590	0.1333	0.0343	0.0844

TABLE XII

DATA FOR FIGURES 15 AND 22

$P_{\infty L}$ = 25.16 psia			Thermocouple 2-1 = 5.422 mv	
Bubble Number	D/D_o	Time Second	t_H	t_R
14	1.000	0.0000	0.0000	0.0000
	0.873	0.0083	0.0008	0.0014
	0.945	0.0167	0.0016	0.0023
	0.936	0.0250	0.0025	0.0035
	0.928	0.0333	0.0033	0.0048
	0.964	0.0417	0.0041	0.0055
	0.700	0.0500	0.0049	0.0126
	0.745	0.0583	0.0057	0.0130
	0.736	0.0667	0.0066	0.0152

TABLE XIII

DATA FOR FIGURES 16 AND 22

$P_{\infty L}$ = 27.76 psia			Thermocouple 1-1 = 5.425 mv	
Bubble Number	D/D_o	Time Second	t_H	t_R
15	1.000	0.0000	0.0000	0.0000
	0.864	0.0083	0.0016	0.0029
	0.848	0.0167	0.0033	0.0060
	0.879	0.0250	0.0049	0.0084
	0.803	0.0333	0.0066	0.0135
	0.773	0.0417	0.0082	0.0182
	0.773	0.0583	0.0115	0.0255
	0.697	0.0667	0.0132	0.0358
	0.803	0.0750	0.0148	0.0303
	0.712	0.0833	0.0164	0.0429
	0.803	0.0917	0.0181	0.0371

TABLE XIV

DATA FOR FIGURES 17 AND 22

	$P_{\infty L}$ = 21.32 psia		Thermocouple 2-1 = 5.442 mv	
Bubble Number	D/D_o	Time Second	t_H	t_R
16	1.000	0.0000	0.0000	0.0000
	0.900	0.0083	0.0013	0.0050
	0.830	0.0167	0.0025	0.0117
	0.915	0.0250	0.0038	0.0144
	0.746	0.0333	0.0051	0.0290
	0.763	0.0417	0.0063	0.0346
	0.695	0.0500	0.0076	0.0500
	0.881	0.0583	0.0088	0.0363
	0.847	0.0666	0.0101	0.0449
	0.678	0.0750	0.0114	0.0789
	0.508	0.0833	0.0126	0.1590
	0.610	0.0917	0.0139	0.1191
	0.525	0.1000	0.0152	0.1754
	0.491	0.1083	0.0164	0.2172
	0.576	0.1167	0.0177	0.1700
	0.525	0.1250	0.0189	0.2193
	0.491	0.1333	0.0202	0.2674
	0.424	0.1416	0.0215	0.3310
	0.305	0.1500	0.0227	0.7795
	0.373	0.1583	0.0240	0.5502
	0.322	0.1667	0.0253	0.7772
	0.305	0.1750	0.0262	0.8975
	0.305	0.1833	0.0278	0.9529

TABLE XV

DATA FOR FIGURES 18 AND 22

$P_{\infty L}$ = 22.46 psia			Thermocouple 2-1 = 5.429 mv	
Bubble Number	D/D_o	Time Second	t_H	t_R
17	1.000	0.0000	0.0000	0.0000
	0.893	0.0083	0.0010	0.0050
	0.893	0.0167	0.0021	0.0100
	0.872	0.0250	0.0031	0.0158
	0.830	0.0333	0.0042	0.0232
	0.745	0.0417	0.0052	0.0360
	0.660	0.0500	0.0062	0.0551
	0.575	0.0583	0.0073	0.0847
	0.596	0.0667	0.0082	0.0877

TABLE XVI

DATA FOR FIGURES 19 AND 22

$P_{\infty L}$ = 22.48 psia			Thermocouple 2-1 = 5.428 mv	
Bubble Number	D/D_o	Time Second	t_H	t_R
18	1.000	0.0000	0.0000	0.0000
	0.943	0.0083	0.0016	0.0071
	0.886	0.0167	0.0036	0.0161
	0.914	0.0250	0.0050	0.0227
	0.857	0.0333	0.0076	0.0346
	0.829	0.0417	0.0102	0.0461
	0.743	0.0500	0.0152	0.0689
	0.629	0.0583	0.0248	0.1122
	0.571	0.0667	0.0344	0.1555
	0.543	0.0750	0.0428	0.1935
	0.514	0.0917	0.0584	0.2642
19	1.000	0.0000	0.0000	0.0000
	0.971	0.0083	0.0015	0.0071
	0.882	0.0167	0.0036	0.0163
	0.912	0.0250	0.0051	0.0229
	0.882	0.0333	0.0072	0.0326
	0.677	0.0417	0.0153	0.0692
	0.618	0.0500	0.0215	0.0971
	0.588	0.0583	0.0284	0.1284
	0.647	0.0667	0.0268	0.1212
	0.470	0.0750	0.0571	0.2582
	0.391	0.0833	0.0916	0.4145
20	1.000	0.0000	0.0000	0.0000
	0.970	0.0083	0.0015	0.0067
	0.970	0.0167	0.0030	0.0135
	0.970	0.0250	0.0045	0.0202
	0.760	0.0333	0.0097	0.0439
	0.667	0.0417	0.0158	0.0713
	0.636	0.0500	0.0208	0.0941
	0.606	0.0583	0.0267	0.1209
	0.606	0.0667	0.0305	0.1381
	0.546	0.0750	0.0423	0.1914
	0.546	0.0833	0.0470	0.2126
	0.424	0.0917	0.0858	0.3882
	0.333	0.1000	0.1517	0.6863

TABLE XVII

DATA FOR FIGURES 20 AND 22

$P_{\infty L}$ = 19.06 psia			Thermocouple 2-1 = 5.449 mv	
Bubble Number	D/D_o	Time Second	t_H	t_R
21	1.000	0.0000	0.0000	0.0000
	0.867	0.0083	0.0002	0.0021
	0.928	0.0167	0.0005	0.0036
	0.916	0.0250	0.0007	0.0056
	0.867	0.0333	0.0009	0.0083
	0.880	0.0417	0.0012	0.0100
	0.855	0.0500	0.0014	0.0128
	0.855	0.0583	0.0017	0.0149
	0.916	0.0666	0.0019	0.0148
	0.855	0.0750	0.0021	0.0191
	0.807	0.0833	0.0024	0.0239
	0.843	0.0917	0.0026	0.0241
	0.807	0.1000	0.0028	0.0286
	0.916	0.1083	0.0031	0.0241
	0.867	0.1167	0.0033	0.0289
	0.795	0.1250	0.0035	0.0369
	0.759	0.1333	0.0038	0.0432
	0.892	0.1416	0.0040	0.0332
	0.638	0.1500	0.0042	0.0687
	0.627	0.1583	0.0045	0.0751
	0.674	0.1667	0.0047	0.0684
	0.650	0.1750	0.0050	0.0773
	0.578	0.1833	0.0052	0.1023
	0.590	0.1917	0.0054	0.1027
	0.566	0.2000	0.0057	0.1164
	0.566	0.2083	0.0059	0.1213

Transient Pressure Data

The pressure-time relationship for all of the data in this section is given in Figure 27. The liquid temperature for this data was 145.2°R. Table XVIII gives the measured diameters and time for bubbles No. 22-24.

TABLE XVIII

DATA FOR FIGURES 23-25

Bubble Number	Diameter Inch	Time Second	Bubble Number	Diameter Inch	Time Second
22	0.0349	0.0000	23	0.0316	0.0000
	0.0338	0.0083		0.0326	0.0083
	0.0332	0.0167		0.0372	0.0167
	0.0338	0.0250		0.0450	0.0250
	0.0383	0.0333		0.0360	0.0333
	0.0248	0.0417		0.0338	0.0417
	0.0236	0.0500		0.0400	0.0500
	0.0259	0.0583		0.0422	0.0583
	0.0282	0.0667		0.0484	0.0667
	0.0293	0.0750		0.0450	0.0750
	0.0304	0.0833		0.0507	0.0833
	0.0349	0.0917		0.0507	0.0917
	0.0394	0.1000		0.0540	0.1000
	0.0394	0.1083		0.0653	0.1083
	0.0383	0.1167		0.0653	0.1167
	0.0495	0.1250		0.0788	0.1250
	0.0495	0.1333		0.0800	0.1333
	0.0541	0.1417		0.0754	0.1417
	0.0586	0.1500		0.0834	0.1500
	0.0631	0.1583		0.0732	0.1583
	0.0686	0.1667		0.0956	0.1667
	0.0698	0.1750		0.1022	0.1750
	0.0788	0.1833		0.1281	0.1833
24	0.0298	0.0000	24	0.0653	0.1083
	0.0349	0.0083		0.0618	0.1167
	0.0343	0.0167		0.0698	0.1250
	0.0394	0.0333		0.0754	0.1333
	0.0382	0.0417		0.0720	0.1417
	0.0405	0.0500		0.0731	0.1500
	0.0338	0.0583		0.0709	0.1583
	0.0433	0.0667		0.0821	0.1667
	0.0461	0.0750		0.0832	0.1750
	0.0473	0.0833		0.1091	0.1833
	0.0507	0.0917		0.1035	0.1917
	0.0552	0.1000			